Mechanical Engineering Series

Frederick F. Ling
Series Editor

Springer
New York
Berlin
Heidelberg
Barcelona
Budapest
Hong Kong
London
Milan
Paris
Santa Clara
Singapore
Tokyo

Mechanical Engineering Series

Introductory Attitude Dynamics
F.P. Rimrott

Balancing of High-Speed Machinery
M.S. Darlow

Theory of Wire Rope
G.A. Costello

Theory of Vibration: An Introduction, 2nd ed.
A.A. Shabana

Laser Machining: Theory and Practice
G. Chryssolouris

Underconstrained Structural Systems
E.N. Kuznetsov

Principles of Heat Transfer in Porous Media, 2nd ed.
M. Kaviany

Mechatronics: Electromechanics and Contromechanics
D.K. Miu

Structural Analysis of Printed Circuit Board Systems
P.A. Engel

Kinematic and Dynamic Simulation of Multibody Systems: The Real-Time Challenge
J. García de Jalón and E. Bayo

High Sensitivity Moiré: Experimental Analysis for Mechanics and Materials
D. Post, B. Han, and P. Ifju

Principles of Convective Heat Transfer
M. Kaviany

(continued after index)

C.V. Madhusudana

Thermal Contact Conductance

With 49 Illustrations

Springer

C.V. Madhusudana
School of Mechanical and Manufacturing Engineering
University of New South Wales
Sydney, NSW
2052 Australia

Series Editor
Frederick F. Ling
Ernest F. Gloyna Regents Chair in Engineering
Department of Mechanical Engineering
The University of Texas at Austin
Austin, TX 78712-1063 USA
and
William Howard Hart Professor Emeritus
Department of Mechanical Engineering,
Aeronautical Engineering and Mechanics
Rensselaer Polytechnic Institute
Troy, NY 12180-3590 USA

Library of Congress Cataloging-in-Publication Data
Madhusudana, C.V.
Thermal contact conductance / C.V. Madhusudana.
p. cm. — (Mechanical engineering series)
Includes bibliographical references and index.

ISBN-13:978-1-4612-8457-4 e-ISBN:978-1-4612-3978-9
DOI: 10.1007/978-1-4612-3978-9

1. Heat—Conduction. 2. Surfaces (Technology) I. Title.
II. Series: Mechanical engineering series (Berlin, Germany)
TJ260.M23 1995
621.402'2—dc20 95-19291

Printed on acid-free paper.

Softcover reprint of the hardcover 2nd edition 1996

Production coordinated by Chernow Editorial Services, Inc., and managed by Natalie Johnson; manufacturing supervised by Joseph Quatela.
Typeset by Asco Trade Typesetting Ltd., Hong Kong.

9 8 7 6 5 4 3 2 1

Dedicated to my Mother
and
to the memory of my Father

Series Preface

Mechanical engineering, an engineering discipline born of the needs of the industrial revolution, is once again asked to do its substantial share in the call for industrial renewal. The general call is urgent as we face profound issues of productivity and competitiveness that require engineering solutions, among others. The Mechanical Engineering Series is a series featuring graduate texts and research monographs intended to address the need for information in contemporary areas of mechanical engineering.

The series is conceived as a comprehensive one that covers a broad range of concentrations important to mechanical engineering graduate education and research. We are fortunate to have a distinguished roster of consulting editors, each an expert in one of the areas of concentration. The names of the consulting editors are listed on the next page of this volume. The areas of concentration are applied mechanics, biomechanics, computational mechanics, dynamic systems and control, energetics, mechanics of materials, processing, thermal science, and tribology.

Professor Bergles, the consulting editor for thermal science, and I are pleased to present this volume of the series: *Thermal Contact Conductance*, by C.V. Madhusudana. The selection of this volume underscores again the interest of the Mechanical Engineering Series to provide our readers with topical monographs as well as graduate texts.

New York, New York Frederick F. Ling

Mechanical Engineering Series

Frederick F. Ling
Series Editor

Preface

Over the past fifty years a significant amount of fundamental and applied research has been carried out in the field of contact heat transfer. In this book, I have attempted to synthesize the information generated during these years and present it in a form that is, I hope, interesting to the practicing engineer, scientist, or student. For this reason, many applications are enumerated in the introduction and emphasized in later chapters. It is also hoped that the material presented is readily understandable. To this end, I have explained in some detail the steps involved in developing the basic concepts in Chapters 2 and 3. Although written mainly for the generalist engineer or physicist, I believe there is sufficient detail, especially in Chapters 4, 6, and 7, to be of interest to the specialist or the advanced student in this field. Chapter 5 should be of particular interest to those contemplating experimental determination of thermal contact conductance and associated problems.

Although more than 500 references were consulted during the preparation of the manuscript, only a few representative ones in each category have been cited, so that the actual number of references listed is approximately half the number consulted. For the sake of systematic and chronological development of each particular theme, however, early pioneering work in that area has necessarily been cited. In general, reference has not been made to internal reports, theses, or other work that is not readily available in open literature. Because of language limitations, references in English, or English translations of references in other languages, have been used.

Some graphs and diagrams from the original sources have been modified and redrawn to suit the format of the present work. These have been identified by the words "after" or "based on" followed by the reference to the source.

Since the subject of contact heat transfer has a broad range, it is likely that some topics have been omitted in a work of this size. I hope, however, that the majority of topics, both basic and applied, have received some airing.

It is a pleasure to acknowledge my debt of gratitude to Dr. Arthur Williams, who introduced me to contact heat transfer at Monash University. I sincerely appreciate the help and cooperation I received from Professor Skip Fletcher and Professor Bud Peterson during my sabbaticals at Texas A&M University. Particular mention must be made of the vast source of references I had access to during those periods. I am grateful to Professor Brian Milton and Professor Mark Wainwright of the University of New South Wales for "reassigning my duties" in lieu of a sabbatical during the first half of 1993. This helped me in gathering, collating, and updating the material for this work. Finally, my thanks go to my wife Nagu for her support and understanding.

C.V. Madhusudana

Contents

Nomenclature

The most frequently used symbols in this book are defined below; other symbols are defined in their proper contexts.

Symbol	Meaning
A	Area
a	Radius of contact spot
b	Radius of the cylinder feeding the contact spot
B	Correlation distance
c	Radius of the contact zone in a bolted joint
C_v	Specific heat at constant volume
CLA	Center Line Average
d	Diameter of specimen
e	Effectiveness of filler material
E	Modulus of elasticity
E'	Reduced modulus of elasticity $= 2[(1 - \nu_1^2)/E_1 + (1 - \nu_2^2)/E_2]^{-1}$
F	Constriction alleviation factor
f	Degrees of freedom of a gas molecule
g	Temperature jump distance; also, shape factor (Chapter 3)
h	Thermal conductance based on unit area
H	Microhardness
J	Bessel function of the first kind
k	Thermal conductivity
M	Molecular mass
n	Number of contact spots per unit area
N_{KN}	Knudsen number
P	Contact pressure
Q	Rate of heat flow
q	Heat flux

R	Thermal resistance based on unit area
r	Radial co-ordinate
R'	Thermal resistance
rms	Root mean square
s	Mean area of a contact spot
S_u	Ultimate compressive strength
T	Temperature
TCC	Thermal contact conductance
TCR	Thermal contact resistance
t	Thickness of filler material
u	Interference
w	Probability density function
W	Load (force)
x	Mass fraction
Z	Axial coordinate
α	Coefficient of thermal expansion; also, accommodation coefficient (Chapter 4)
δ	Mean thickness of gas gap; also, flatness deviation (Chapter 3)
ε	Average clearance
ϕ	Porosity
γ	Ratio of specific heats
λ	Wave length; also, mean free path (Chapter 4)
μ	Viscosity
ν	Poisson's ratio
ρ	Radius of curvature
σ	Standard deviation of asperity heights; also, stress (Chapter 7)
ξ	Waviness number
ψ	Plasticity index

Subscripts

c	Constriction
cd	Disc constriction
eff	Effective
g	Gas
L	Large; also, layer (Chapter 7)
m	Mean or average
N	Nondimensional
r	Real
s	Solid; also, small (Chapter 3)

1
Introduction

Microscopic and macroscopic irregularities are present in all practical solid surfaces. Surface roughness is a measure of the microscopic irregularity, whereas the macroscopic errors of form include flatness deviations, waviness and, for cylindrical surfaces, out-of-roundness. Two solid surfaces apparently in contact, therefore, touch each other only at a few individual spots (Fig. 1.1). Even at relatively high contact pressures of the order of 10 MPa, the actual area of contact for most metallic surfaces is only about 1 to 2% of the nominal contact area (see, e.g., Bowden and Tabor, 1950). Since the heat flow lines are constrained to flow through the sparsely spaced actual contact spots, there exists an additional resistance to heat flow at a joint. This resistance manifests itself as a sudden temperature drop at the interface.

1.1 Mechanism of Contact Heat Transfer

The heat transfer through a joint may be considered to be made up of three components:

a. Conduction through the actual contact spots.
b. Conduction through the interstitial medium, such as air.
c. Radiation.

The interfacial gap thickness, generally of the order of 1 μm, is too small for convection currents to be set up. Radiation can be neglected unless the temperatures at the joint are in excess of 300 °C. Radiation may also be significant if the temperature difference across the interface is large; this implies that the fraction of heat transmitted by radiation is also dependent on the contact resistance. It is often considered that the heat conduction through the actual contact spots is the only significant component. However, the area available for heat

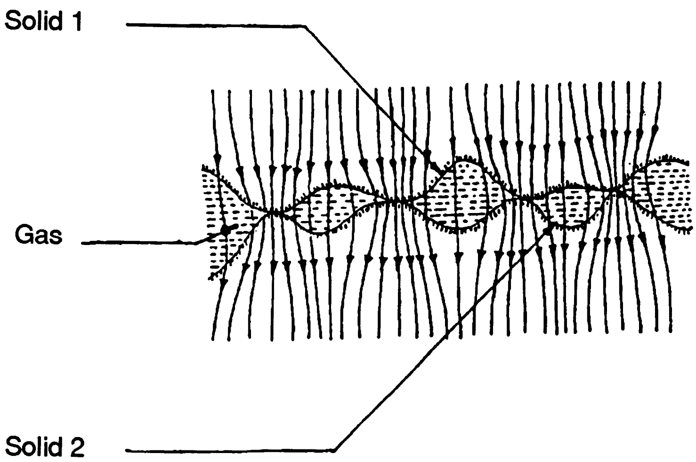

FIGURE 1.1. Heat flow through a joint.

flow through the interstitial gaps is frequently 2 to 4 orders of magnitudes greater than the actual contact area. Hence the heat flow through the gaps cannot be neglected, especially if the solids are relatively poor conductors such as stainless steel, or the interface medium is a good conductor.

Thermal contact conductance, h, is defined as the ratio of the heat flux (Q/A) to the additional temperature drop (ΔT) due to the presence of the (imperfect) joint (Fig. 1.2):

$$h = Q/(A\Delta T) \tag{1.1}$$

In Eq. (1.1), Q is the total heat flow and A is the nominal contact area.

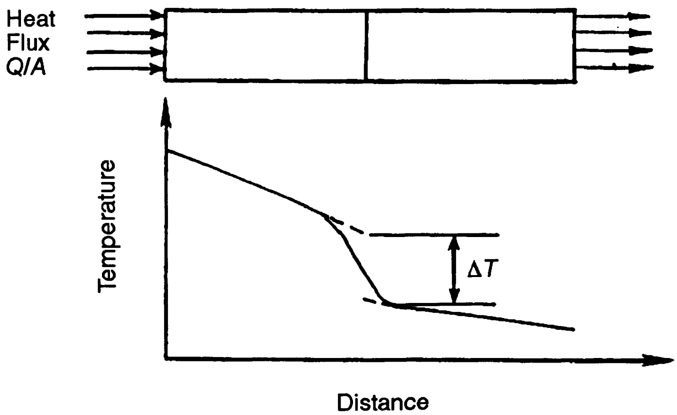

FIGURE 1.2. Temperature drop at an interface.

Thermal contact resistance, R, is the reciprocal of thermal contact conductance:

$$R = A\Delta T/Q \tag{1.2}$$

It may be noted that the conductance and resistance, as defined above, are what are usually called unit conductance and specific resistance, respectively, in heat transfer literature.

Some researchers define the thermal contact resistance as the ratio of ΔT to the total heat flow, Q. It this work, this latter definition will be represented by R', i.e.,

$$R' = \Delta T/Q \tag{1.3}$$

If it is possible to separate the heat flow through the solid spots, Q_S, from the heat flow through the fluid in the gaps, Q_g, such that

$$Q = Q_S + Q_g \tag{1.4}$$

then the solid spot conductance can be defined as

$$h_S = Q_S/(A\Delta T) \tag{1.5}$$

and the gap fluid conductance as

$$h_g = Q_g/(A\Delta T) \tag{1.6}$$

Then from Eq. (1.1),

$$h = h_S + h_g \tag{1.7}$$

The heat flow through the solid spots is usually determined by conducting the heat transfer tests in a vacuum. Q_g is then determined, if required, by conducting the tests in the desired environment and then taking the difference. It will be appreciated, however, that Q_s and Q_g are not independent. The solid spot conductance, as obtained in the vacuum test, will be somewhat less than that obtained in a conducting environment; the heat flow lines follow a less tortuous path in the second test. The effect, however, is smaller unless h_S and h_g are of comparable magnitude.

1.2 Significance of Contact Heat Transfer

Heat transfer systems need to have a high overall efficiency for a number of reasons including energy conservation, limiting maximum temperatures and accuracy of temperature measurements. Some applications, where a high value of the thermal contact conductance is necessary to obtain high system efficiencies, are listed below.

1. The fuel/can interface of a nuclear power reactor (Dean, 1962).
2. Bimetallic plain tube, and attached finned tube types of heat exchangers (Wood et al., 1987; Taborek, 1987).
3. Aircraft structural joints subjected to aerodynamic heating (Barzelay et al., 1954).
4. Cooling in electronic systems (Kraus and Bar-Cohen, 1983); for example, transistor mounted on an aluminum heat sink (Scott, 1974); the series interface resistances between the chip, the diebond epoxy, the heat spreader, and the mold compound in electronic packages (Childres and Peterson (1989); the base plate and the heat sink of a multiple chip unit of a large computer (Fitch, 1990). In IBM's 3081 Thermal Conduction Module (TCM), a spring loaded piston conducts the heat released by each chip to an aluminium hat and then to a water-cooled cold plate (Tummala and Rymaszewski, 1989). The internal resistances are minimized by hermetically sealing helium inside the module but the resistances are still significant: 3 °C between piston and chip, 3.2 °C through the metallic piston and the helium gap surrounding the housing and 1.6 °C through the housing and the cold plate. It may be noted that internal resistances account for approximately 50% of the overall resistances in a typical thermal conduction module. With the present trend toward microminiaturization and consequent increase in power densities, the interface heat transfer in electronic components, in general, is becoming an area of increasing interest.
5. Structural joints of machine tools (Attia and Kops, 1980).
6. Bolted and riveted joints in general (Madhusudana et al., 1988).
7. In manufacturing systems: for example, at the casting-mold interface (Attia and Osman, 1988); at metal–die interfaces in hot forming processes such as forging, extrusion, and rolling (Im and Altan, 1988); between the abrasive grain and workpiece in grinding (Lavine and Jen, 1989); and in injection molding (Yu et al., 1990).
8. Interface between cast iron paper dryer and the paper web in the paper drying process (Asensio et al., 1993).
9. In dry sliding contacts (Kennedy, 1984; Burton and Burton, 1991).

Other examples where a high value of thermal contact conductance is desirable include: the interface between gas turbine blades and rotor, the measurement of surface temperatures by thermocouples, cooking on a hot plate, and in reinforced multistrand overhead electric transmission lines.

On the other hand, there are several instances where a high value of the thermal contact resistance, rather than conductance, is desirable. Such applications include:

1. Low conductivity structural supports for storage and transport of cryogenic fluids (Mikesell and Scott, 1956).
2. Thermal isolation of space craft components (Fletcher, 1973).
3. Insulations made of powdered materials (Reiss, 1981).

Reference may be made to the following reviews for additional applications: Wong (1968); Williams (1968); Madhusudana and Fletcher (1986); Snaith et al. (1986); Fletcher (1988, 1990).

1.3 Scope of Present Work

This book deals with the theoretical analyses, experimental methods, experimental results, control of thermal contact conductance, special problems, and future directions of study in contact heat transfer.

For the purpose of thermal design of equipment, it is desirable to have simple correlations in order that the contact heat transfer coefficients may be estimated quickly. Such correlations are usually derived from the experimental results of several investigations. However, it is not uncommon to find simple correlations based on theoretical open-form solutions since the open-form solutions are frequently difficult to interpret and evaluate without the aid of a computer. Nondimensional correlations attempt to present thermal contact conductance data for a large variety of material combinations and a wide range of system parameters in the form of a simple formula or a graph. However, some material combinations, for example, porous metals, do not belong to the main category of metal-to-metal joints. Also, for extensively used metals and alloys such as aluminum and stainless steel, the amount of experimental data available is so large as to justify separate correlations for these materials. There are also correlations available for particular configurations, such as stacks of thin layers and finned tubes. In this book, correlations relevant to each specific topic are included at the end of the discussion of that topic.

Theoretical analyses include a consideration of the thermal constriction resistance of a single spot and the combined resistance of multiple spots; they also consider how these resistances may be combined with the variation of surface properties under load in order that the overall thermal resistance of a joint may be estimated. Analyses of the constriction resistance are presented in Chapter 2. The surface and deformation analyses of the interface are then considered in Chapter 3; these lead to the theoretical expressions, as functions of the contact pressure, the properties of the materials and the surfaces, for the solid spot conductance of a joint consisting several contact spots.

The factors influencing the gas gap conductance are described in detail in Chapter 4. These factors include the surface roughness, the properties of gas and the gas/solid interface, the gas pressure, and the contact pressure. The effects of these are then synthesized to yield usable methods for calculating the gap conductance.

In the experimental determination of thermal contact conductance, the interface is usually the junction of the flat surfaces at the ends of two bars (as shown in Fig. 1.2). The geometrical and the mechanical properties of the surfaces are determined prior to test. The contact pressure is controlled by loading the bars in the axial direction by either mechanical or hydraulic means. In cylindrical joints with radial heat flow, however, the contact pressure is mainly developed as a result of the differential expansion of the cylinders. Therefore, a different type of equipment would be needed to measure the contact conductance in such a situation. Experimental facilities are also available for the determination of conductance of periodic contacts. These and other experimental aspects will be discussed in Chapter 5.

The use of interstitial materials is a practical way of achieving thermal control, i.e., either to enhance the heat transfer rate, or, conversely, to achieve thermal isolation. Typical interstitial substances for improving conductance include foils, coatings, and heat transfer greases. On the other hand, thermal resistance may be increased by the use of screens and insulating films. The effects of interstitial materials on thermal contact conductance are considered in detail in Chapter 6.

Several special topics in contact heat transfer are treated in Chapter 7. Some of these arise because of unusual loading conditions and loading histories; examples include directional effects and hysteresis. Other problems may be due to particular geometries and specific contact configurations; bolted joints, cylindrical joints, stacks of laminations, and packed beds fall into this category. This chapter also includes a discussion of contact conductance of specific materials and the correlations of experimental data for such materials.

The final chapter reviews and summarizes possible methods for the control of thermal contact conductance. Recommendations for future work are also included in this chapter.

References

Asensio, M.C., Seyed-Yagoobi, J., and Fletcher, I.S. (1993). Thermal Contact Conductance of a Moist Paper Handsheet/Metal Interface for Paper Drying Applications. Trans ASME, Heat Transfer, 115:1051–1053.

Attia, M.H., and Kops, L. (1980). Importance of Contact Pressure Distribution on Heat Transfer in Structural Joints of Machine Tools. Trans ASME, J Eng Ind, 102:159–167.

Attia, M.H., and Osman, M.O.M. (1988). Thermal Response of Metallic Moulds to Thermoelastic Interaction at Its Mould Inner Boundary. Thermal Aspects in Manufacturing, ASME, PED, 30:63–76.

Barzelay, M.E., Tong, K.N., and Hollo, C. (1954). Thermal Conductance of Contacts in Aircraft Joints. US Natl Adv Comm Aeronautics. Washington, DC.

Bowden, F.P., and Tabor, D. (1950). The Friction and Lubrication of Solids. Oxford University Press, London, pp. 20–32.

Burton, R.A., and Burton, R.G. (1991). Cooperative Interactions of Asperities in the Thermotribology of Sliding Contacts IEEE Trans, Components, Hybrids, pp. 23–25.

Childres, W.S., and Peterson, G.P. (1989). Quantification of Thermal Contact Conductance in Electronic Packages. IEEE Trans, Components, Hybrids, pp. 717–723.

Dean, R.A. (1962). Thermal Contact Conductance Between UO_2 and Zircaloy-2 Westinghouse Electric Corporation, Report CVNA-127 Pittsburgh, PA.

Fitch, J.S. (1990). A One-Dimensional Thermal Model for the Vax 9000 Multi-Chip Units. Am Soc Mech Eng, 153:59–64.

Fletcher, L.S. (1973). Thermal Control Materials for Spacecraft Systems. 10th Int Symp Space Technol Sci, Tokyo, pp. 579–586.

Fletcher, L.S. (1988). Recent Developments in Contact Conductance Heat Transfer. Trans ASME, J Heat Transfer, 110:1059–1070.

Fletcher, L.S. (1990). A Review of Thermal Enhancement Techniques for Electronic Systems IEEE Trans, Components, Hybrids, Manuf Technol, 13(4): 1012–1021.

Im, Y.T., and Altan, T. (1988). Heat Generation and Transfer in Metal Forming: Recent Developments. Thermal Aspects in Manufacturing, ASME, PED, 30:77–88.

Kennedy, F.E., Jr. (1984). Thermal and Thermomechanical Effects in Dry Sliding. Wear, 100:453–476.

Kraus, A.D., and Bar-Cohen, A. (1983). Thermal Analysis and Control of Electronic Equipment. McGraw-Hill, New York, pp. 199–214.

Lavine, A.S., and Jen, T.-C. (1989). Thermal Aspects of Grinding: Heat Transfer to Workpiece, Wheel and Fluid, J Heat Transfer, 123:267–274.

Madhusudana, C.V., and Fletcher, L.S. (1986). Contact Heat Transfer—The Last Decade, AIAA J, 24(3):510–523.

Madhusudana, C.V., Peterson, G.P., and Fletcher, L.S. (1988). Effect of Non-Uniform Pressures on the Thermal Conductance in Bolted and Riveted Joints, Am Soc Mech Eng, 104:57–67.

Mikesell, R.P., and Scott, R.B. (1956). Heat Conduction Through Insulating Supports in Very Low Temperature Equipment. J Res, US Natl Bureau Standards, 57(6): 371–378.

Reiss, H. (1981). An Evacuated Powder Insulation for a High Temperature Na/S-Battery. AIAA Paper 81-1107, New York.

Scott, A.W. (1974). Cooling of Electronic Equipment. John Wiley, New York, pp. 1–43.
Snaith, B., Probert, S.D., and O'Callaghan, P.W. (1986). Thermal Resistance of Pressed Contacts. Appl Energy, 22:31–84.
Taborek, J. (1987). Bond Resistance and Design Temperatures for High-Finned Tubes—A Reappraisal Heat Transfer Eng, 8(2):26–34.
Tummala, R.R., and Rymaszewski, E.J. (eds.). (1989). Microelectronics Paackaging Handbook. Van Nostrand Reinhold, New York, pp. 211–213.
Williams, A. (1968). Heat Transfer Across Metallic Joints Inst Eng (Australia) Mech Chem Eng Trans, 4:247–254.
Wong, H.Y. (1968). A Survey of Thermal Conductance of Metallic Contacts. Aeronautical Research Council, CIP No. 973, London.
Wood, R.A., Sheffield, J.W., and Sauer, H.J., Jr. (1987a). Thermal Contact Conductance of Finned Tubes: The Effect of Various Parameters. ASHRAE Trans, 93(2): 798–809.
Wood, R.A., Sheffield, J.W., and Sauer, H.J., Jr. (1987b). Thermal Contact Conductance of Finned Tubes: A Generalized Correlation ASHRAE Trans, 93(2):786–796.
Yu, C.J., Sunderland, J.E., and Poli, C. (1990). Thermal Contact Resistance in Injection Molding. Polym Eng Sci, 30(24):1599–1606.

2
Thermal Constriction Resistance

It was seen in Chapter 1 that the contact interface consists of a number of discrete and small actual contact spots separated by relatively large gaps. These gaps may be either evacuated or filled with a conducting medium such as gas. In the first case, all of the heat flow lines are constrained to pass through the contact spots. If the gaps are filled with a conducting medium, however, some of the heat flow lines are allowed to pass through the gaps, that is, they are less constrained and thus the constriction is alleviated to some extent.

Constriction resistance is a measure of the additional temperature drop associated with a single constriction. Let T_0 be the temperature difference required for the passage of heat at the rate, Q, through a medium when there is no constraint, and, T, the temperature difference required when a constriction is present, other things remaining the same. Then the constriction resistance, R_c, is defined as

$$R_c = (T - T_0)/Q \tag{2.1}$$

In this chapter, the theory pertaining to the constriction resistance is derived first when the constriction is in isolation, that is, when the effect of adjacent spots is ignored. Next the constriction resistance of a contact spot when it is surrounded by similar spots is determined. The contact conductance is the sum of the conductances of the several spots existing on the interface. The average radius of these contact spots as well as their number can be determined by means of surface and deformation analyses so that the contact conductance can be finally determined as a function of the surface parameters, material properties and the contact pressure.

2.1 Circular Disc in Half Space

The logical starting point for the discussion of constriction resistance would be a consideration of the resistance associated with a circular area located on the boundary of a semi-infinite medium. This is equivalent to assuming that:

a. The constriction is small compared to the other dimensions of the medium in which heat flow occurs;
b. The constriction of heat flow lines is not affected by the presence of other contact spots;
c. There is no conduction of heat through the gap surrounding the contact spot.

The problem is illustrated in Fig. 2.1. Many solutions to this problem are available (see, e.g., Llewellyn-Jones, 1957; Holm, 1967). We will describe here, in some detail, the method used by Carslaw and Jaeger (1959). It is believed that such detail is necessary in order to appreciate fully the mathematical complexities involved in the analytical solutions of even the simplest configurations. In what follows, frequent reference is made to the work by Gradshteyn and Ryzhik (1980). The formulas in this reference will be indicated by G–R followed by the formula number.

The equation of heat conduction in cylindrical coordinates, with no heat generation is:

$$(\partial^2 T/\partial r^2) + (1/r)(\partial T/\partial r) + (\partial^2 T/\partial z^2) = 0 \qquad (2.2)$$

Using the method of separation of variables, we seek a solution of the form:

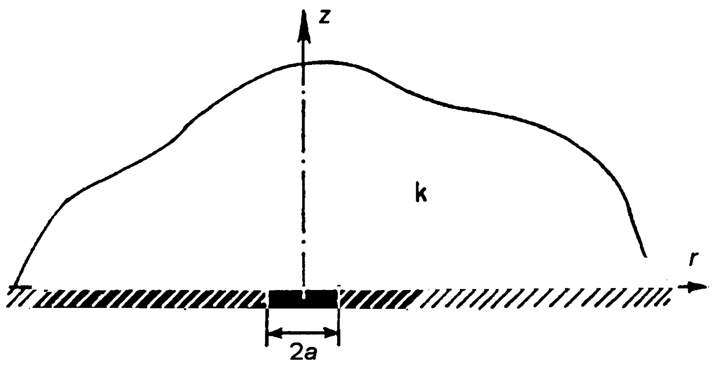

FIGURE 2.1. Circular constriction in half space.

$$T(r,z) = R(r)Z(z) \tag{2.3}$$

so that Eq. (2.2) may be written as

$$R''Z + (Z/r)R' = -Z''R$$

or,

$$(1/R)(R'' + R'/r) = -Z''/Z = -\lambda^2$$

Thus Eq. (2.2) is reduced to two ordinary differential equations:

$$(d^2R/dr^2) + (1/r)(dR/dr) + \lambda^2 R = 0 \tag{2.4a}$$

and

$$(d^2Z/dz^2) - \lambda^2 Z = 0 \tag{2.4b}$$

Equation (2.4a) is a form of Bessel's differential equation of order zero and a solution of this is $J_0(\lambda r)$ and a solution of Eq. (24b) is $e^{-\lambda z}$. Therefore, Eq. (2.2) is satisfied by $e^{-\lambda z}J_0(\lambda r)$ for any λ. Hence

$$\int_0^\infty e^{-\lambda z}J_0(\lambda r)f(\lambda)\,d\lambda \tag{2.5}$$

will also be a solution if $f(\lambda)$ can be chosen to satisfy the boundary conditions at $z = 0$. At $z = 0$, the solution reduces to

$$T_c = \int_0^\infty J_0(\lambda r)f(\lambda)\,d\lambda \tag{2.6}$$

In the problem being considered, at $z = 0$, there is no heat flow over the region $r > a$; also in the same plane, the region $r < a$ could be, for example, at constant temperature or uniform heat flux. These two cases are considered below.

1. The contact area is maintained at constant temperature, T_c, over $0 < r < a$.

According to G–R 6.693.1,

$$\begin{aligned}\mathrm{Int}_\nu &= \int_0^\infty J_\nu(\alpha x)\sin(\beta x)\,dx/x = (1/\nu)\sin[\nu \arcsin(\beta/\alpha)], && \beta \le \alpha\\ &= [\alpha^\nu \sin(\nu\pi/2)]/[\nu(\beta + \sqrt{\beta^2 - \alpha^2})^\nu], && \beta > \alpha\end{aligned}$$

Taking the limit as $\nu \to 0$, (applying L'Hôpital's rule), these integrals turn out to be

$$\begin{aligned}\mathrm{Int}_0 &= \arcsin(\beta/\alpha), && \text{for } \beta \le \alpha\\ &= \pi/2, && \text{for } \beta > \alpha\end{aligned}$$

Hence, if we take

$$f(\lambda) = (2T_c/\pi)\sin(\lambda a)/\lambda$$

in (2.6), we get, for the temperature at $z = 0$,

$$\begin{aligned}(2T_c/\pi)\int_0^\infty \mathrm{J}_0(\lambda r)[\sin(\lambda a)/\lambda]\,d\lambda &= (2T_c/\pi)(\pi/2) = T_c, \quad \text{for } r \le a\\ &= (2T_c/\pi)\arcsin(a/r), \quad \text{for } r > a\end{aligned}$$

Since the temperature is independent of z for $r > a$, this satisfies the other boundary condition, namely, no heat flow over the rest of the plane at $z = 0$.

Substituting for $f(\lambda)$ in Eq. (2.5),

$$T = (2T_c/\pi)\int_0^\infty e^{-\lambda z}\mathrm{J}_0(\lambda r)[\sin(\lambda a)/\lambda]\,d\lambda \tag{2.7}$$

Then, from G–R 6.752.1,

$$T = (2T_c/\pi)\sin^{-1}[2a/[\{(r-a)^2 + z^2\}^{1/2} + \{(r+a)^2 + z^2\}^{1/2}]] \tag{2.8}$$

Note that

$$\begin{aligned}-(\partial T/\partial z)_{z=0} &= (2T_c/\pi)\int_0^\infty \mathrm{J}_0(\lambda r)\sin(\lambda a)\,d\lambda\\ &= (2T_c/\pi)/(a^2 - r^2)^{1/2}, \quad \text{for } 0 < r \le a\end{aligned} \tag{2.9}$$

from G–R 6.671.7.

The heat flow rate over the circle $0 < r \le a$ is

$$\begin{aligned}Q &= -2\pi k\int_0^a (\partial T/\partial z)_{z=0} r\,dr\\ &= -2\pi k(2T_c/\pi)\int_0^a\left[\int_0^\infty -\lambda e^{-\lambda z}\mathrm{J}_0(\lambda r)\{\sin(\lambda a)/\lambda\}\,d\lambda\right]_{z=0} r\,dr\\ &= 4kT_c\int_0^a\left[\int_0^\infty \lambda\mathrm{J}_0(\lambda r)\{\sin(\lambda a)/\lambda\}\,d\lambda\right] r\,dr\\ &= 4kT_c\int_0^\infty\left[\int_0^a \mathrm{J}_0(\lambda r)\sin(\lambda a) r\,dr\right] d\lambda\\ &= 4kT_c\int_0^\infty \sin(\lambda a)\left[\int_0^a \mathrm{J}_0(\lambda r) r\,dr\right] d\lambda\end{aligned}$$

$$= 4kT_c \int_0^\infty \sin(\lambda a)[aJ_1(\lambda a)/\lambda]\, d\lambda \quad \text{(G–R 6.561.5)}$$

$$= 4kT_c a \int_0^\infty [J_1(\lambda a)\sin(\lambda a)/\lambda]\, d\lambda$$

$$= 4kT_c a(1) \quad \text{(G–R 6.693.1)}$$

The constriction resistance is, therefore,

$$R_{cd1} = (T_c - 0)/Q = T_c/(4kT_c a) = 1/(4ka) \tag{2.10}$$

2. *The contact area is subjected to uniform heat flux.*

In this case, the boundary conditions at $z = 0$ are,

$$\left.\begin{aligned} -k(\partial T/\partial z)z = 0 &= q, \quad 0 < r \leq a \\ &= 0, \quad r > a \end{aligned}\right\} \tag{2.11}$$

where q is the heat flux.

The problem is again one of finding a suitable $f(\lambda)$ in Eq. (2.5) to satisfy the above boundary conditions.

Differentiating Eq. (2.5) with respect to z,

$$(\partial T/\partial z) = \int_0^\infty -\lambda e^{-\lambda z} J_0(\lambda r) f(\lambda)\, d\lambda$$

Applying the first of the boundary conditions (at $z = 0$) of (2.11),

$$-(\partial T/\partial z) = \int_0^\infty \lambda J_0(\lambda r) f(\lambda)\, d\lambda = q/k$$

Consider the integral (G–R, 6.512.3)

$$\int_0^\infty J_0(\lambda r)J_1(\lambda a)\, d\lambda \begin{cases} = 0, & \text{for } r > a \\ = 1/2a, & \text{for } r = a \\ = 1/a, & \text{for } r < a \end{cases} \tag{2.12}$$

Hence we see that

$$f(\lambda) = (qa/k)[J_1(\lambda a)/\lambda]$$

so that the solution is

$$T = (qa/k) \int_0^\infty e^{-\lambda z} J_0(\lambda r) J_1(\lambda a)\, d\lambda/\lambda \tag{2.13}$$

The average temperature, T_{av}, over $0 < r \leq a$ and $z = 0$ is,

$$
\begin{aligned}
T_{av} &= (1/\pi a^2) \int_0^a T(2\pi r)\, dr \\
&= (2q/ak) \int_0^\infty (\mathrm{J}_1(\lambda a)/\lambda) \left\{ \int_0^a \mathrm{J}_0(\lambda r) r\, dr \right\} d\lambda \\
&= (2q/ak) \int_0^\infty (\mathrm{J}_1(\lambda a)/\lambda) \{ (a\mathrm{J}_1(\lambda a)/\lambda) \}\, d\lambda \quad \text{G–R 6.561.5} \\
&= (2q/ak) \int_0^\infty a\{\mathrm{J}_1^2(\lambda a)/\lambda^2)\}\, d\lambda \\
&= (2q/k)(4a/3\pi) \qquad \text{G–R 6.574.2}
\end{aligned}
$$

Hence

$$T_{av} = 8qa/(3\pi k) \tag{2.14}$$

The heat flow rate is

$$Q = \pi a^2 q$$

Hence the constriction resistance, in this case, is

$$R_{cd2} = T_{av}/Q = 8/(3\pi^2 ka) = 0.27/(ka) \tag{2.15}$$

This is about 8% larger than the constriction resistance obtained for the case of uniform temperature.

2.2 Resistance of a Constriction Bounded by a Semi-Infinite Cylinder

In a real joint there will be several contact spots. Each contact spot, of radius a_i, may be imagined to be fed by a cylinder of larger radius, b_i, as shown in Fig. 2.2. Note that the sum of areas of all of the contact spots is equal to the real contact area, A_r, while the sum of cross-sectional areas of all of the cylinders is taken to be equal to the (nominal) apparent area of contact, A_n.

It is further assumed that there is no cross flow of heat between the adjacent cylinders. There also is no heat flow across the gap between the adjacent contact spots; that is, the contact spot is surrounded by a vacuum in the contact plane.

There are several solutions available to this problem. The following analysis is based on the solution described by Mikic and Rohsenow (1966) and Cooper et al. (1969).

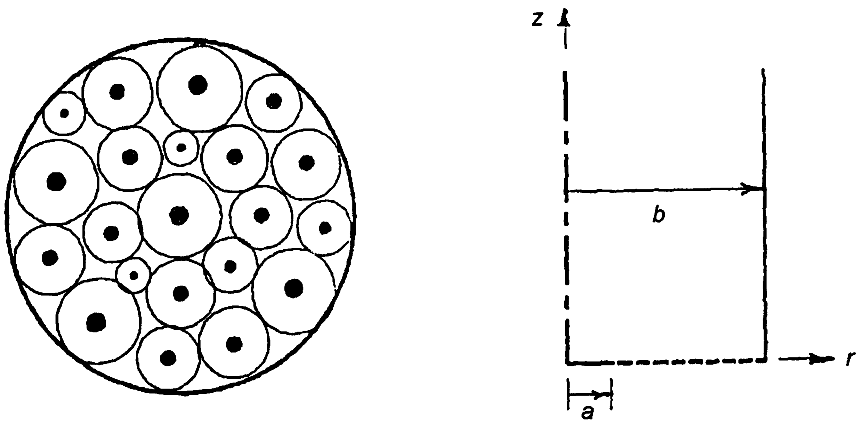

Idealized View of Contact Plane

Constriction Bounded by Semi-Infinite Cylinder

FIGURE 2.2. Modeling of a single contact spot in a cluster of spots.

The boundary conditions are:

$$T = \text{constant};\ z = 0, 0 < r \leq a \tag{2.16a}$$

$$-k(\partial T/\partial z) = 0;\ z = 0, r > a \tag{2.16b}$$

$$-k(\partial T/\partial z) = Q/(\pi b^2);\ z \to \infty \tag{2.16c}$$

$$-k(\partial T/\partial r) = 0;\ r = b \tag{2.16d}$$

$$-k(\partial T/\partial r) = 0;\ r = 0 \tag{2.16e}$$

To satisfy conditions in Eq. (2.16c) and Eq. (2.16e), the solution of Eq. (2.2) should be in the form:

$$T = -[Q/(\pi b^2 k)]z + \sum_{n=1}^{\infty} C_n e^{-\lambda z} \mathrm{J}_0(\lambda_n r) + T_0 \tag{2.17}$$

From boundary condition in Eq. (2.16d),

$$\mathrm{J}_1(\lambda_n b) = 0 \tag{2.18}$$

Hence, $b = 3.83171$, 7.01559, 10.17347, etc. (Abramovitz and Segun, 1968a) Also by integrating Eq. (2.17) over the *whole of the interfacial area* ($0 < r < b$) at $z = 0$ and using Eq. (2.18), we see that the average temperature for this area is T_0.

In Eq. (2.17), the C_ns are to be determined from boundary conditions in Eq. (2.16a) and Eq. (2.16b) at $z = 0$. These boundary conditions are mixed, however, and to overcome the this problem, the

Dirichlet boundary condition in Eq. (2.16a) is replaced by a heat flux boundary condition based on the exact temperature distribution for the circular disc in half space:

$$-k(\partial T/\partial z) = Q/(2\pi a\sqrt{a^2 - r^2});\ 0 < r < a,\ z = 0 \qquad (2.19)$$

[see Eq. (2.9)].

This approximation would lead to a nearly constant temperature distribution over the area $0 < r \leq a$, especially for small values of a/b.

However, from Eq. (2.17), at $z = 0$

$$-k(\partial T/\partial z) = k[Q/(\pi kb^2) + \sum C_n\lambda_n J_0(\lambda_n r)] \qquad (2.20)$$

From (2.19) and (2.20),

$$Q/(\pi kb^2) + \sum_{n=1}^{\infty} C_n\lambda_n J_0(\lambda_n r) = Q/(2\pi ka\sqrt{a^2 - r^2})$$

To utilize the orthogonality property of the Bessel function, both sides of the above equation are multiplied by $rJ_0(\lambda_n r)$ and integrated over $0 < r < b$ to yield

$$Q/(\pi kb^2)\int_0^b rJ_0(\lambda_n r)\,dr + C_n\lambda_n\int_0^b rJ_0^2(\lambda_n r)\,dr$$

$$= Q/(2\pi ka)\int_0^a [rJ_0(\lambda_n r)/\sqrt{a^2 - r^2}]\,dr$$

see (G–R 6.521.1).

However,

$$\int_0^b rJ_0(\lambda_n r)\,dr = (b/\lambda_n)J_1(\lambda_n b);$$

this is equal to zero by virtue of Eq. (2.18).

From the orthogonality property (Abramovitz and Segun, 1968b),

$$\int_0^b rJ_0^2(\lambda_n r)\,dr = (b^2/2)J_0^2(\lambda_n b);$$

and

$$\int_0^a [rJ_0(\lambda_n r)/\sqrt{a^2 - r^2}]\,dr = \sin(\lambda_n a)/\lambda_n \quad \text{(G–R 6.554.2)}$$

Therefore,

$$C_n = (Q/\pi ka)\sin(\lambda_n a)/[(\lambda_n b)^2 J_0^2(\lambda_n b)]$$

Substituting for C_n in Eq. (2.17),

$$T = -[Q/(\pi b^2 k)]z + (Q/\pi ka) \sum_{n=1}^{\infty} e^{-\lambda z} \sin(\lambda_n a) \mathrm{J}_0(\lambda_n r)/[(\lambda_n b)^2 \mathrm{J}_0^2(\lambda_n b)] + T_0 \tag{2.21}$$

The mean temperature over the contact area is then obtained from:

$$T_m = [1/(\pi a^2)]\left[\int_0^a T(2\pi r\,dr)\right]_{z=0} + [1/(\pi b^2)]\left[\int_0^b T_0(2\pi r\,dr)\right]$$

$$= (2/a^2) \int_0^a (Q/\pi ka) \sum_{n=1}^{\infty} [\sin(\lambda_n a) \mathrm{J}_0(\lambda_n r)/\{(\lambda_n b)^2 \mathrm{J}_0^2(\lambda_n b)\}] r\,dr + T_0$$

$$= [Q/(4ka)][8/(\pi a^2)] \sum_{n=1}^{\infty} \left[[\sin(\lambda_n a)/\{(\lambda_n b)^2 \mathrm{J}_0^2(\lambda_n b)\}] \cdot \int_0^a r \mathrm{J}_0(\lambda_n r)\,dr\right] + T_0$$

$$= [Q/(4ka)][8/(\pi a^2)]ab \sum_{n=1}^{\infty} [\sin(\lambda_n a) \mathrm{J}_1(\lambda_n a)/\{(\lambda_n b)^3 \mathrm{J}_0^2(\lambda_n b)\}] + T_0$$

$$= [Q/(4ka)][8/\pi](b/a) \sum_{n=1}^{\infty} [\sin(\lambda_n a) \mathrm{J}_1(\lambda_n a)/\{(\lambda_n b)^3 \mathrm{J}_0^2(\lambda_n b)\}] + T_0 \tag{2.22}$$

Note that the factor $1/(4ka)$ represents the disc constriction resistance of Eq. (2.10). The thermal resistance between $z = 0$ and $z = L$ (for large L) is given by

$$R_t = (T_m - T_{z=L})/Q = (T_m/Q) + [L/(\pi k b^2)] - T_0/Q$$

Hence the *additional* resistance due to constriction is

$$R = R_t - [L/(\pi k b^2)] = (T_m - T_0)/Q$$

$$= [1/(4ka)](8/\pi)(b/a) \sum_{n=1}^{\infty} [\sin\{\lambda_n b(a/b)\} \mathrm{J}_1\{\lambda_n b(a/b)\}/\{(\lambda_n b)^3 \mathrm{J}_0^2(\lambda_n b)\}]$$

$$= R_{cd1} F(a/b) \tag{2.23}$$

where

$$F(a/b) = (8\pi)(b/a) \sum_{n=1}^{\infty} [\sin\{\lambda_n b(a/b)\} \mathrm{J}_1\{\lambda_n b(a/b)\}/\{(\lambda_n b)^3 \mathrm{J}_0^2(\lambda_n b)\}] \tag{2.24}$$

is called the *constriction alleviation factor*.

TABLE 2.1. Comparison of constriction alleviation factors.

a/b	Roess	Mikic	Gibson	Negus and Yovanovich
0.1	0.8594	0.8584	0.8594	0.8594
0.2	0.7205	0.7202	0.7209	0.7208
0.3	0.5853	0.5851	0.5865	0.5865
0.4	0.4558	0.4557	0.4586	0.4586
0.5	0.3340	0.3341	0.3398	0.3395
0.6	0.2230	0.2231	0.2328	0.2318

Yovanovich (1975) obtained expressions for the constriction alleviation factor for heat flux functions of the form

$$[1 - (r/a)^2]^m; \ z = 0, 0 < r \leq a$$

His results for $m = -0.5$, as expected, were identical to that of Mikic. Other solutions to the above problem include those of Roess (as presented by Weills and Ryder, 1949); Hunter and Williams (1969); Gibson (1976); and Negus and Yovanovich (1984). The algebraic expressions derived for the constriction alleviation factor by Roess, Gibson, and Negus and Yovanovich are somewhat similar:

$$F_{\text{Roess}} = 1 - 1.4093(a/b) + 0.2959(a/b)^3 + 0.05254(a/b)^5 + \cdots \tag{2.25}$$

$$F_{\text{Gibson}} = 1 - 1.4092(a/b) + 0.3380(a/b)^3 + 0.0679(a/b)^5 + \cdots \tag{2.26}$$

$$F_{\text{N-Y}} = 1 - 1.4098(a/b) + 0.3441(a/b)^3 + 0.0435(a/b)^5 + \cdots \tag{2.27}$$

The constriction alleviation factors obtained by Eq. (2.24), (2.25), (2.26), and (2.27) are compared in Table 2.1. The first 120 terms were used in evaluating the series of Eq. (2.24).

2.3 Constriction in a Fluid Environment

Here the boundary conditions at the contact plane ($z = 0$) are as shown in Fig. 2.3:

$$T = \text{constant} = T_c, \text{ for } 0 < r < a$$

$$-k(\partial T/\partial z) = k_f(T_c - T)/\delta, \text{ for } a < r < b$$

where k_f is the thermal conductivity of the fluid and δ is the effective gap thickness (taking into account the gas/solid interactions at the interface).

Approximate solutions to the above problem have been obtained by estimating the radius b_1, which defines that part of the cylinder

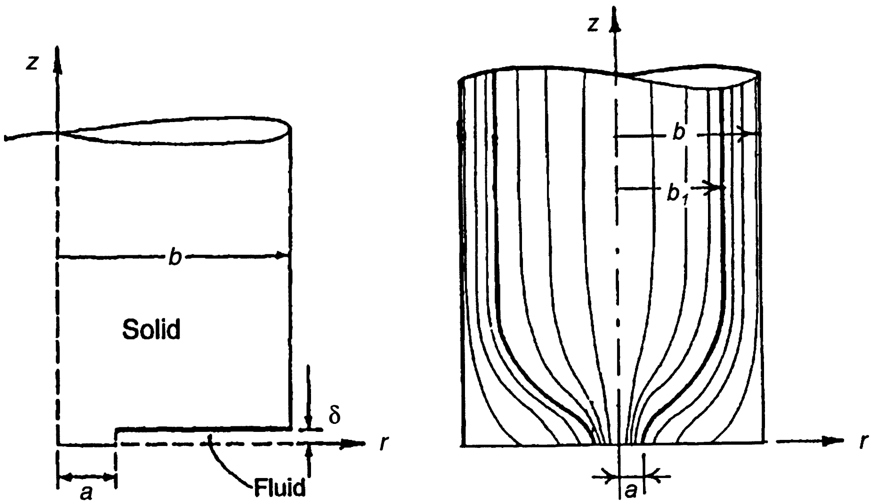

FIGURE 2.3. Constriction in a fluid environment.

feeding the solid contact spot (Cetinkale and Fishenden, 1951; Mikic and Rohsenow, 1966). The total resistance is then expressed as:

$$R = 1/[(1/R_s) + (1/R_f)] \tag{2.28}$$

where

$R_s = R_{cd1} F(a/b_1)$
$F(a/b_1)$ is the constriction alleviation factor

and

$R_f = \delta/(\pi b^2 k_f)$

Other approximate solutions to this problem have also been presented by Fenech and Rohsenow (1963) and Tsukizoe and Hisakado (1972). An "exact" solution has been presented by Sanokawa (1968); the results of this work, however, are not in a readily usable form. In any case, it can be seen that the model used for deriving these solutions is somewhat artificial because, in reality, the gap does not abruptly change from zero thickness at $r = a$ to a finite thickness at the same radius. The thickness is expected to increase gradually. Any analytical solution is, therefore, likely to be complicated and a recourse to a digital computer would be still required to evaluate the results. For this reason, it would appear that a numerical solution is perhaps more appropriate for the solution of this type of problem. The references for this and other types of constrictions are summarized in the table at the end of this section.

TABLE 2.2. Representative works.

No.	Reference	Configuration	Approach
1	Mikic and Rohsenow, 1966	Strip of constant width in vacuum	Analytical
2	Mikic and Rohsenow, 1966	Rectangle in vacuum	Analytical
3	Yip and Venart, 1968	Single and multiple disc constrictions in vacuum	Analog
4	Veziroglu and Chandra, 1969	Two dimensional, symmetric and eccentric, in vacuum	Analytical and analog
5	Sexl and Burkhard, 1969	Two dimensional, symmetric and eccentric, in vacuum	Analytical
6	Strong et al., 1974	Disc constriction in half space, vacuum	Numerical
7	Williams, 1975	Conical constriction in vacuum	Experimental and analytical
8	Yovanovich, 1976	Circular annular contact at the end of a semi-infinite cylinder in vacuum	Analytical
9	Yovanovich and Schneider, 1976	Annular constriction in half space in vacuum	Analytical
10	Gibson and Bush, 1977	Disc constriction in half space in conducting environment	Analytical
11	Major and Williams, 1977	Conical constriction in vacuum	Analog
12	Schneider, 1978	Rectangular and annular contacts in half space in vacuum	Numerical
13	Yovanovich et al., 1979	Doubly connected areas bounded by circles, squares, and triangles in vacuum	Numerical
14	Madhusudana, 1979, 1980	Conical constrictions at the end of a cylinder; in vacuum or in conducting environment	Numerical and experimental
15	Major, 1980	Conical constrictions in vacuum	Numerical
16	Negus et al., 1988	Circular contact on coated surfaces in vacuum	Analytical
17	Gladwell and Lemczyk, 1988	Circular contact at the end of a finite cylinder; insulated, isothermal or convective boundaries	Analytical
18	Das and Sadhal, 1992	Two dimensional gaps at the interface of two semi-infinite solids in conducting environment	Analytical
19	Madhusudana and Chen, 1994	Annular constriction at the end of a semi-infinite cylinder in vacuum	Analytical and analog

In a large number of cases, the heat flow through the gap is small compared to the heat flow through the contact spot. In such cases the fluid conductance may be estimated by dividing the fluid conductivity by the effective gap thickness. This may then be added to the solid spot conductance to obtain the total contact conductance. Factors affecting the fluid conductance are discussed in detail in Chapter 4.

2.4 Other Types of Constrictions

Apart from the solutions discussed above, the problems pertaining to constrictions of other shapes and boundary conditions have been analyzed by various investigators as shown in Table 2.2.

References

Abramovitz, M., and Segun, I.A. (1968a). Handbook of Mathematical Functions. Dover, New York, p. 409.

Abramovitz, M., and Segun, I.A. (1968b). Handbook of Mathematical Functions. Dover, New York, p. 48.

Çarslaw, H.S., and Jaeger, J.C. (1959). Conduction of Heat in Solids, 2nd ed. Clarendon Press, Oxford, pp. 214–217.

Cetinkale, T.N., and Fishenden, M. (1951). Thermal Conductance of Metal Surfaces in Contact. Proc Gen Disc Heat Transfer. Institute of Mechanical Engineers, London, pp. 271–275.

Cooper, M.G., Mikic, B.B., and Yovanovich, M.M. (1969). Thermal Contact Conductance. Int J Heat Mass Transfer, 12:279–300.

Das, A.K., and Sadhal, S.S. (1992). The Effect of Interstitial Fluid on Thermal Constriction Resistance. Trans ASME, J Heat Transfer, 114:1045–1048.

Fenech, H., and Rohsenow, W.M. (1963). Prediction of Thermal Conductance of Metallic Surfaces in Contact. Trans ASME, J Heat Transfer, 85:15–24.

Gibson, R.D. (1976). The Contact Resistance for a Semi-Infinite Cylinder in a Vacuum. Appl Energy, 2:57–65.

Gibson, R.D., and Bush, A.W. (1977). The Flow of Heat Between Bodies in Gas-Filled Contact. Appl Energy, 3:189–195.

Gladwell, G.M.L., and Lemczyk, T.F. (1988). Thermal Constriction Resistance of A Contact on A Circular Cylinder with Mixed Convective Boundaries. Proc R Soc (London), Ser. A, 323–354.

Gradshteyn, I.S., and Ryzhik, M. (1980). Tables of Integrals, Series, and Products. Academic Press, New York.

Holm, R. (1967). Electric Contacts—Theory and Application, 4th ed. Springer-Verlag, New York, pp. 11–16.

Hunter, A., and Williams, A. (1969). Heat Flow Across Metallic Joints—The Constriction Alleviation Factor. Int J Heat Mass Transfer, 12:524–526.

Llewellyn-Jones, F. (1957). The Physics of Electrical Contacts. Oxford University Press, New York, pp. 13–15.

Madhusudana, C.V. (1979). Heat Flow Through Conical Constrictions in Vacuum and in Conducting Media. AIAA Paper 79-1071. American Institute of Aeronautics and Astronautics, New York.

Madhusudana, C.V. (1980). Heat Flow Through Conical Constrictions. AIAA J, 18(10):1261–1262.

Madhusudana, C.V., and Chen, P.Y.P. (1994). Heat Flow Through Concentric Annular Constrictions. Proc. 10th Intl Heat Transfer Conf. Paper 3-Nt 18. Institute of Chemical Engineers, Rugby, UK.

Major, S.J. (1980). The Finite Difference Solution of Conduction Problems in Cylindrical Coordinates. Inst Eng (Australia), Mech Eng Trans, Paper M1049. Institute of Engineers (Australia), Canberra.

Major, S.J., and Williams, A. (1977). The Solution of a Steady Conduction Heat Transfer Problem Using an Electrolytic Tank Analogue. Inst Eng (Australia), Mech Eng Trans, pp. 7–11.

Mikic, B.B., and Rohsenow, W.M. (1966). Thermal Contact Resistance. Mech Eng Depart Report No. DSR 74542-41, MIT, Cambridge, MA.

Negus, K.J., and Yovanovich, M.M. (1984). Constriction Resistance of Circular Flux Tubes with Mixed Boundary Conditions by Superposition of Neumann Solutions. ASME Paper 84-HT-84, 6 pp. American Society of Mechanical Engineers, New York.

Negus, K.J., Yovanovich, M.M., and Thompson, J.C. (1988). Constriction Resistance of Circular Contacts on Coated Surfaces: Effect of Boundary Conditions. J Therm Heat Transfer, 12(2):158–164.

Sanokawa, K. (1968). Heat Transfer Between Metallic Surfaces. Bull JSME, 11:253–293.

Schneider, G.E. (1978). Thermal Constriction Resistance Due to Arbitrary Contacts on a Half Space—Numerical Solution. AIAA Paper 78-870. American Institute of Aeronautics and Astronautics, New York.

Sexl, R.U., and Burkhard, D.G. (1969). An Exact Solution for Thermal Conduction Through a Two-Dimensional Eccentric Constriction. Prog Astro Aero, 21:617–620.

Strong, A., Schneider, G., and Yovanovich, M.M. (1974). Thermal Constriction Resistance of a Disc with Arbitrary Heat Flux Prog Astro Aero, 39:65–78.

Tsukizoe, T., and Hisakado, T. (1972). On the Mechanism of Heat Transfer Between Metal Surfaces in Contact. Part 1 Heat Transfer—Japanese Res, 1(1):104–112.

Veziroglu, T.N., and Chandra, S. (1969). Thermal Conductance of Two-Dimensional Constrictions. Prog Astro Aero, 21:591–615.

Weills, N.D., and Ryder, E.A. (1949). Thermal Resistance of Joints Formed by Stationary Metal Surfaces. Trans ASME, 71:259–267.

Williams, A. (1975). Heat Flow Through Single Points of Metallic Contacts of Simple Shapes. Prog Astro Aero, 39:129–142.

Yip, F.C., and Venart, J.E.S. (1968). Surface Topography Effects in the Estimation of Thermal and Electrical Contact Resistance. Proc I Mech Eng, 182(3):81–91.

Yovanovich, M.M. (1975). General Expressions for Constriction Resistances Due to Arbitrary Flux Distributions. AIAA Paper 75-188. American Institute of Aeronautics and Astronautics, New York.

Yovanovich, M.M. (1976). General Thermal Constriction Parameter for Annular Contacts on Circular Flux Tubes. AIAA J, 14(6):822–824.

Yovanovich, M.M., and Schneider, G.E. (1976). Thermal Constriction Resistance Due to a Circular Annular Contact. AIAA Paper 76-142. American Institute of Aeronautics and Astronautics, New York.

Yovanovich, M.M., and Martin, K.A., and Schneider, G.E. (1979). Constriction Resistance of Doubly-Connected Contact Areas Under Uniform Flux. AIAA Paper 79-1070. American Institute of Aeronautics and Astronautics, New York.

3
Solid Spot Thermal Conductance of a Joint

3.1 Multiple Spot Contact Conductance

When both sides of the contact spot are considered (Fig. 3.1), the total resistance is simply the sum of the resistances for each side of the contact. Therefore, if k_1 and k_2 are the thermal conductivities of the two solids in contact, then the resistance associated with a single contact spot is given by:

$$R = F/(4ak_1) + F/(4ak_2) \tag{3.1}$$

$$= F/(2ak) \tag{3.2}$$

where F is the constriction alleviation factor defined in chapter 2 and

$$k = 2k_1k_2/(k_1 + k_2) \tag{3.3}$$

is the harmonic mean of the conductivities.

The thermal conductance of a single contact spot is, therefore:

$$h = 2ak/F \tag{3.4}$$

Hence, if there are n contact spots in the interface, the thermal conductance of the solid spots is:

$$h_s = 2k\overset{n}{\Sigma}(a_i/F_i) \tag{3.5}$$

Neglecting the variation in F_i and writing

$$a_i = na_m \tag{3.6}$$

Where a_m = average radius of the contact spots, we obtain

$$h_S = 2na_mk/F \tag{3.7}$$

It now remains to obtain n and a_m by means of surface and deformation analyses.

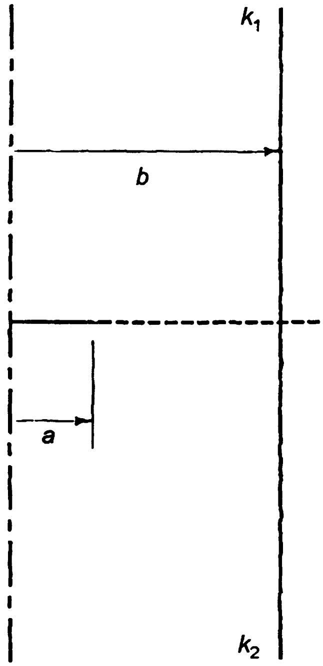

FIGURE 3.1. Two sides of a contact spot.

3.2 Estimation of the Number and Average Size of Contact Spots

Several authors have described the method of calculating the number and size of contact spots when two rough surfaces are placed in contact under specified mechanical pressure (see, e.g., Tsukizoe and Hisakado, 1965, 1968; Mikic and Rohsenow, 1966; Greenwood, 1967; Greenwood and Tripp, 1970). A bibliography of works on surface topography in general is provided by Thomas and King (1977). The following analysis is based on the method presented by Kimura (1970). In the analysis, it is assumed that the heights and slopes of the surface profiles are randomly distributed. It is also assumed that the probability densities of the height and the slope are independent. Other assumptions relate to particular cases and will be stated in their proper contexts.

We first consider the contact of a rough surface with a flat smooth surface. Let $z = f(x, y)$ be the profile height above the $x - y$ plane defined by

$$\iint_A z\,dx\,dy = 0$$

where A is the nominal contact area. This indicates that the $x - y$ plane is located at mean height of the profile.

Further, the slopes in the x- and y-directions are given by

$$z_x = (\partial z/\partial x) \quad \text{and} \quad z_y = (\partial z/\partial y)$$

Let $w(z)$ be the probability density function so that $w(z)\,dz$ is the probability that z is in the range z to $z + dz$.

If A_r is the real area of contact and ε the average clearance for a pressure, P, then

$$(A_r/A) = \text{prob}(z > \varepsilon) = \int_\varepsilon^\infty w(z)\,dz \tag{3.8}$$

See Fig. 3.2 for an illustration of this point.

Consider a *unit length* of surface profile parallel to the x-axis. In this length, let n_x be the number of sections in which the profile is in the real area of contact.

The joint probability that z is in the range z to $z + dz$ and z_x is in the range z_x to $z_x + dz_x$ is given by

$$w(z, z_x)\,dz\,dz_x$$

Note that this is also the fraction of length per unit length, in the x-direction, that the height and the slope are in the specificed ranges.

But, to cross the interval dz, a length $dz/|z_x|$ is needed in the x-direction (Fig. 3.3). Hence the expected number of crossings, per unit length, at $z = \varepsilon$ and $z_x = z_x$ is given by

$$w(\varepsilon, z_x)\,dz\,dz_x/(dz/|z_x|) = |z_x|\,w(\varepsilon, z_x)\,dz_x$$

Now z_x can have any value at $z = \varepsilon$. Hence the total number of crossings at $z = \varepsilon$ is

$$\int_{-\infty}^{\infty} |z_x|\,w(\varepsilon, z_x)\,dz_x$$

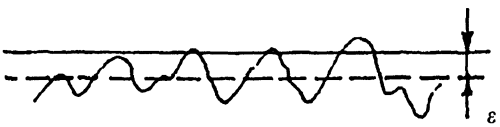

FIGURE 3.2. Clearance between a flat plane and a rough surface.

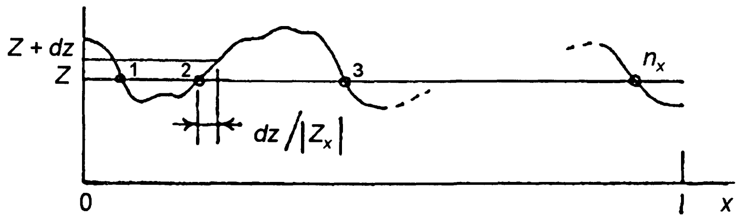

FIGURE 3.3. Number of crossings between z and $z + dz$ (after Kimura, 1970).

In the above integration, both upward and downward crossings are included. The number of *sections* will be half the above value. Further, since the probability densities of the height and the slope are independent, the joint probability is simply the product of the two probabilities. Hence

$$n_x = (1/2)w(\varepsilon)\int_{-\infty}^{\infty} |z_x|\, w(z_x)\, dz_x \tag{3.9}$$

The number of sections, n_y, per unit length in the y-direction can be found similarly.

Let a_x and a_y be the mean lengths of the contact spots in the x- and y-directions, respectively (Fig. 3.4). Then

$$\begin{aligned} a_x n_x = a_y n_y &= \int_{\varepsilon}^{\infty} w(z)\, dz \\ &= A_r/A \end{aligned} \tag{3.10}$$

from Eq. (3.8).

If s is the mean area of a contact spot, then a nondimensional shape factor, g, may be defined as

$$g = s/(a_x a_y) \tag{3.11}$$

Note that $g = 1$ for a rectangular cross section and $g = 4/\pi$ for an elliptical cross section. If n is the number of contact spots per unit area, then

$$ns = A_r/A \tag{3.12}$$

Hence

$$\begin{aligned} n &= (A_r/A)(1/s) \\ &= (A_r/A)[1/(g a_x a_y))] \\ &= (1/g)(A_r/A)(n_x n_y)/[(A_r/A)^2], \text{ from Eq. (3.10).} \end{aligned}$$

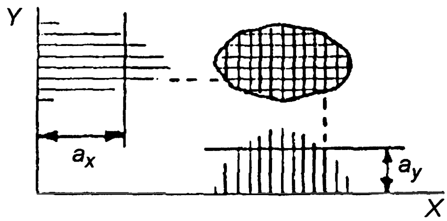

FIGURE 3.4. Mean lengths of contact spots.

Therefore,

$$n = (1/g)(A/A_r)(n_x n_y)$$

Substituting for n_x, from Eq. (3.9), and a similar one for n_y, the number of contact spots per unit area is obtained as

$$n = (1/4g)(A/A_r)\{w(\varepsilon)\}^2 \int_{-\infty}^{\infty} |z_x| w(z_x) dz_x \int_{-\infty}^{\infty} |z_y| w(z_y) dz_y \quad (3.13)$$

Then, from Equation (3.12), the average area of a contact spot is

$$s = 4g(A_r/A)^2 \Big/ \left[\{w(\varepsilon)\}^2 \int_{-\infty}^{\infty} |z_x| w(z_x) dz_x \int_{-\infty}^{\infty} |z_y| w(z_y) dz_y \right] \quad (3.14)$$

The contact between two rough surfaces may be treated as that of an "equivalent" rough surface with a flat smooth plane. The height and slopes of the equivalent surface are defined by

$$z_e = z_1 + z_2$$

$$(z_x)_e = (z_x)_1 + (z_x)_2$$

$$(z_y)_e = (z_y)_1 + (z_y)_2$$

With these definitions, the number and average area of contact spots for contact between two rough surfaces may be obtained if the slopes and heights are taken to be the equivalent ones in Eq. (3.13) and (3.14).

3.2.1 Gaussian Distribution of Heights and Slopes

Here

$$w(z) = [1/(\sqrt{2\sigma\pi})] \exp(-z^2/2\sigma^2) \quad (3.15)$$

in which σ is the standard deviation of profile heights. Similar expressions for $w(z_x)$ and $w(z_y)$ may be written by replacing σ by the standard deviations for the profile slopes, σ_x and σ_y.

Then the average clearance is given by

$$(A_r/A) = (1/2)[erfc(\varepsilon/\sigma\sqrt{2})], \quad \varepsilon \geq 0 \tag{3.16}$$

Note that the above equation is applicable for $(A_r/A) < 0.5$; ε would be negative if (A_r/A) is greater than 0.5.

Solving for the clearance,

$$\varepsilon = \sqrt{2}\sigma\, erfc^{-1}(2A_r/A) \tag{3.17}$$

From Eqs. (3.13) and (3.14)

$$n = [1/(4\pi^2 g)][\sigma_x\sigma_y/\sigma^2](A/A_r)\exp[-2\{erfc^{-1}(2A_r/A)\}^2] \tag{3.18}$$

$$s = (4\pi^2 g)][\sigma^2/(\sigma_x\sigma_y)](A_r/A)^2\exp[2\{erfc^{-1}(2A_r/A)\}^2] \tag{3.19}$$

In Eqs. (3.16) to (3.19), $erfc(x) = 1 - erf(x)$, and $erfc^{-1}(x)$ denotes the inverse of $erfc(x)$. Also, for Gaussian distribution, note that the standard deviation of the heights of the equivalent surface is given by

$$(\sigma_e)^2 = (\sigma_1)^2 + (\sigma_2)^2 \tag{3.20}$$

and by similar expressions for the equivalent slopes.

3.3 Deformation Analysis

The purpose of this section is to present the means of estimating (A_r/A), which is required to evaluate the number and size of the contact spots in Eqs. (3.18) and (3.19). In order to do this, we have to first determine whether the deformation will be plastic or elastic in a given situation. The concept of a "plasticity index" is useful in this connection.

3.3.1 The Plasticity Index

The deformation of an asperity will be elastic up to some given load above which some plastic flow will occur. If w_p is the compliance of the asperity at the onset of plastic flow, then the deformation will be entirely elastic for compliances less than this value.

For a sphere in contact with a smooth plane, this compliance is given by (Tabor, 1951)

$$w_p = r(H/E')^2 \tag{3.21}$$

in which r is the radius of the spherical asperities, H is the hardness of the asperity material, and E' is the reduced elastic modulus for the two materials in contact.

If σ is the standard deviation of asperity heights, then the value of w_p/σ could be used as the criterion for whether the contact is elastic, plastic, or lies within the load-dependent range. For Gaussian distribution of profile heights, Greenwood (1967), proposed a plasticity index

$$\psi_G = (E'/H)\sqrt{(\sigma/r)} \tag{3.22}$$

Greenwood showed that the surfaces with the plasticity index values greater than 1, representing many freshy made surfaces, will have plastic contact at the lightest loads. Values below 0.7, which can be obtained by careful polishing, give elastic contact even at heavy loads.

The random surface model of Whitehouse and Archard (1970), also results in a somewhat similar plasticity index (Tabor, 1975):

$$\psi_A = (E'/H)(\sigma/B) \tag{3.23}$$

in which B is the correlation distance corresponding roughly to the spacing between asperities of equal heights.

Tabor (1975) demonstrated that, in each case:

a. Plastic deformation occurred when the plasticity index attained the value of 1.
b. The coefficient of (E'/H) represented the mean slope of the asperities.

Mikic (1974) has also shown that it is the slope of the asperities that controls the mode of deformation for a given pair of materials in contact.

Another version of the plasticity index using the first three moments of the power spectral density of the surface profile, rather than the radius of curvature and standard deviation, has been proposed by Bush and Gibson (1979).

Chang et al. (1987) presented a general elastic-plastic model for the contact of rough surfaces. Their results agreed, as far as the real area of contact was concerned, with the results of the elastic model of Greenwood and Williamson (1966), and the plastic model of Pullen and Williamson (1972), for a wide range of the plasticity index.

3.3.2 *Ratio of Real to Apparent Area of Contact*

In the following discussion, P is the load (mechanical pressure) between the contact surfaces.

(i) Purely Plastic Deformation

Here it is assumed that all asperities in contact are deforming at the same flow pressure, H, which is the microhardness of the softer of the two materials. Hence,

$$A_r H = AP$$

or

$$A_r/A = P/H \tag{3.24}$$

In the above equation, it is implicitly assumed that the displaced material simply disappears; that is, conservation of volume is not observed. This will not introduce serious errors for low contact pressures (large separations). For larger loads, Mikic (1974) proposed that the above equation be modified as

$$A_r/A = P/(H + P) \tag{3.25}$$

Both Eqs. (3.24) and (3.25) assume that there is no work-hardening of the surfaces in contact.

(ii) Elastic Deformation

For elastic deformations, the contact area can be related to the displacement and, hence, the load by Hertzian theory. For spherically shaped asperities whose heights follow a Gaussian distribution, Roca and Mikic (1971) proved that

$$A_r/A = P\sqrt{2}/(E' \tan\theta) \tag{3.26}$$

where $\tan\theta$ is the mean absolute slope of the surface profile.

Note that, even for elastic deformation, the real area of contact is proportional to the contact pressure.

3.4 Theoretical Expressions for Thermal Contact Conductance

We are now in a position to combine the results of the thermal, the surface, and the deformation analyses so as to obtain usable expressions for the solid spot thermal conductance.

For circular contact spots the shape factor, g, in Eq. (3.11) is $4/\pi$ and $s = \pi a_m^2$, so that $a_m^2 = s/\pi$. Hence, from Eq. (3.19)

$$a_m^2 = (1/\pi)4\pi^2(4/\pi)(\sigma/\tan\theta)^2(A_r/A)^2 \exp[2\{erfc^{-1}(2A_r/A)\}^2]$$
$$= 16(\sigma/\tan\theta)^2(A_r/A)^2 \exp[2\{erfc^{-1}(2A_r/A)\}^2]$$

where

$(\tan\theta)^2 = \sigma_x\sigma_y$

Hence

$$a_m = 4(\sigma/\tan\theta)(A_r/A)\exp\{erfc^{-1}(2A_r/A)\}^2 \tag{3.27}$$

Similarly the Eq. (3.18) for the number of contact spots may be written as

$$n = [1/(16\pi)](\tan\theta/\sigma)^2(A/A_r)\exp[-2\{erfc^{-1}(2A_r/A)\}^2] \tag{3.28}$$

Multiplying (3.27) and (3.28),

$$na_m = [1/(4\pi)](\tan\theta/\sigma)\exp[-\{erfc^{-1}(2A_r/A)\}^2] \tag{3.29}$$

Substituting for na_m in Eq. (3.7), we obtain

$$h_S = [1/(2\pi)](k\tan\theta/\sigma)\exp(-X)/F \tag{3.30}$$

where

$$X = \{erfc^{-1}(2A_r/A)\}^2 \tag{3.31}$$

It may be noted that until this point no assumption has been made regarding the mode of deformation.

3.4.1 Solid Spot Conductance for Fully Plastic Deformation

Here we use Eq. (3.24) for calculating the true contact area so that

$$X = \{erfc^{-1}(2P/H)\}^2 \tag{3.32}$$

Hence the solid spot conductance may be calculated for any contact pressure. The analysis of Mikic (1974) yielded a similar result

$$h_S = (1.13k\tan\theta/\sigma)(P/H)^{0.94} \tag{3.33}$$

However, note that in Eq. (3.33), $\tan\theta$ is the mean of absolute slope of the profiles, in Eq. (3.30), $\tan\theta$ is the standard deviation of the slopes.

If the displaced volume of material is taken into account, then Eq. (3.25) is used to determine the area ratio in Eq. (3.32). Similarly (P/H) is replaced by $[P/(P+H)]$ in Eq. (3.33).

3.4.2 Solid Spot Conductance for Elastic Deformation

Here the value of (A_r/A) s given by Eq. (3.26). The equation derived by Mikic for the elastic deformation of asperities is

$$h_S = 1.55(k \tan\theta/\sigma)[P\sqrt{2}/(E' \tan\theta)]^{0.94} \tag{3.34}$$

Here the numerical coefficient is different from 1.13 of Eq. (3.33). This may be explained by observing that, for a given separation, the contact area in an elastic deformation is twice that in purely plastic deformation. This implies that, for a given area ratio, the sum of contact radii, in elastic deformation, is approximately $\sqrt{2}$ times the value in pure plastic deformation. Also note that the conductance is only a weak function of $\tan\theta$ indicating that variations in $\tan\theta$ will not significantly alter the conductance.

3.5 Effect of Macroscopic Irregularities

The analyses presented so far assume that the surfaces are rough, but flat. In practice, many manufactured surfaces possess some degree of deviation from flatness. It is also likely that some waviness would be present as a result of the machining process, such as grinding or turning, by which the surfaces were produced. It would be necessary to correct the expression for thermal contact conductance (or resistance) to account for such departures from flatness.

Clausing and Chao (1965) suggested that the flatness deviations may be accounted for by means of the "spherical cap" model (Fig. 3.5). The apparent contact area is then divided into two regions:

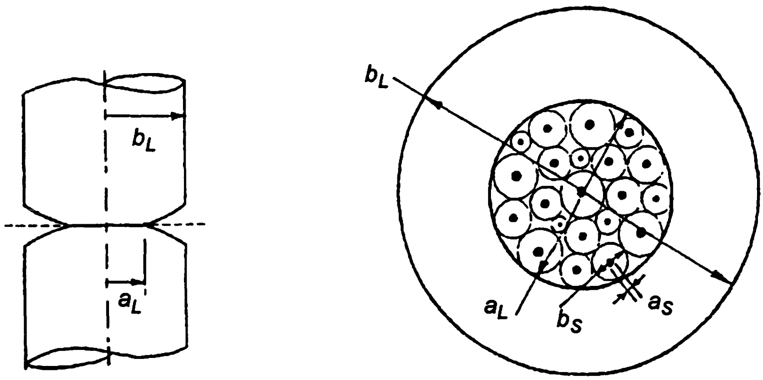

FIGURE 3.5. Macroscopic and microscopic contact areas.

a. The noncontact region, which contains few or no microscopic contact areas.
b. The contact region, where the density of microcontacts is high.

The flow of heat is first constrained to the large scale contact areas and then further constricted to the microscopic contacts within this macroscopic area. The total resistance, R_t, is then given by

$$R_t = R_L + R_s \tag{3.35}$$

in which R_L and R_s represent the macroscopic and microscopic constriction resistances, respectively. A film resistance may also need to be added for oxidized surfaces.

Since the resistance is the reciprocal of conductance, we get, using Eq. (3.7),

$$R_t = F_L/(2a_L k) + F_s/(2na_s k) \tag{3.36a}$$

As an example, consider two identical cylinders in contact, each with a flatness deviation δ. Then, from geometry, the radius of curvature of the spherical caps is given by

$$\rho \approx b_L^2/2\delta$$

By Herzian equation for elastic deformation of spheres, the radius of macroscopic contact area for a contact force W is (Timoshenko and Goodier, 1970),

$$a_L = 1.109[W\rho/(2E)]^{1/3} = 1.109[Wb_L^2/(4\delta E)]^{1/3} \tag{3.36b}$$

In this expression E is the elastic modulus and the Poisson's ratio is taken to be 0.3.

Substituting for a_L in Eq. (3.36a), we see that the macroscopic resistance varies as $W^{-1/3}$.

Yovanovich (1969) demonstrated that the theory of Clausing and Chao may be extended to predict the resistance of rough, wavy surfaces. In this case, the macroscopic contact areas, called "contour areas," are formed due to the waviness of the contacting surfaces.

Thomas and Sayles (1975) considered that a vertical section through a surface contained a continuous spectrum of wavelengths (Fig. 3.6). The largest wavelengths with the largest amplitudes correspond to large scale errors of form; the shorter and smaller wavelengths constitute the waviness; the shortest and smallest waviness represent the roughness. Therefore, waviness and roughness should be discussed in terms of bandwidths of this spectrum rather than of fixed wavelengths.

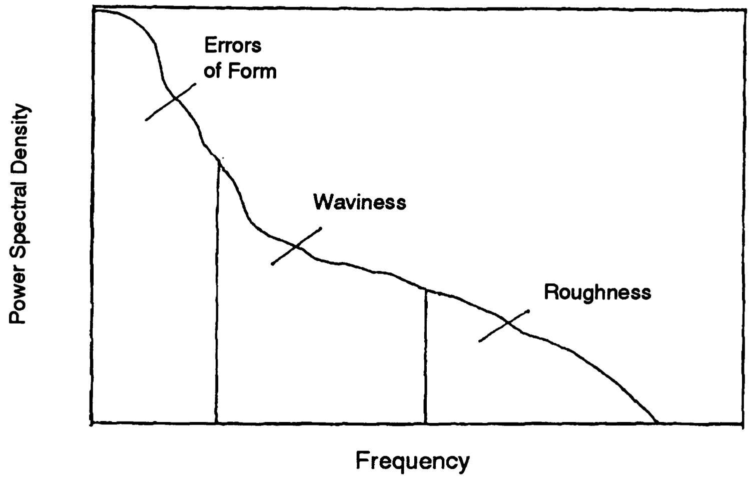

FIGURE 3.6. Power spectrum of surface profile (after Thomas and Sayles, 1975).

In their analysis, it was assumed that:

a. One of the contacting surfaces is smooth and flat, whereas the other surface is randomly and isotropically rough.
b. The cutoff wavelength is $2d$ where d is the diameter of the specimen.
c. Initially, the surfaces touch each other at three points (the summits), so that there will be three macroscopic contact areas.
d. All three summits have the same height and the same radius of curvature, r_0.
e. The radius of the contour areas is given by Hertzian relation for the elastic area of contact between a sphere of radius, r_0, and a flat.

The analysis showed that

$$r_0 = 4.2(10^{-3})d^2/\sigma \tag{3.37}$$

Hence the contour area radius was shown to be given by

$$(a_L/b_L) = 0.44\xi^{1/3} \tag{3.38}$$

where

$$\xi = W/(E'd\sigma) \tag{3.39}$$

is the waviness number and W is the load (force).

It was also shown that σ was proportional to $d^{1/2}$. Hence, if σ_m was the measured roughness at a cutoff length of L, then

$$\sigma = \sigma_m(d/L)^{1/2} \tag{3.40}$$

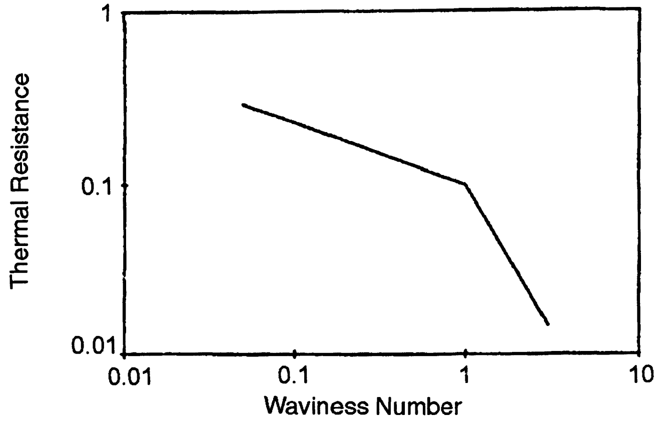

FIGURE 3.7. Thermal resistance and the waviness number (after Thomas and Sayles, 1975).

From Eq. (3.38), when $\xi = 1$, the value of (a_L/b_L) is 0.44 and, using a constriction factor such as that given by Eq. (2.25), we can see that the macroscopic resistance is less than half the value of the disc constriction resistance. Hence Thomas and Sayles suggested that the effect of waviness be neglected for $\xi > 1$. For higher values of ξ, the effect of roughness only need to be considered (Fig. 3.7). However, most of the available experimental data indicated that this condition is not satisfied. This implies that for the range of conditions of engineering interest, the effect of waviness can never be neglected. Furthermore, if the resistance is entirely due to waviness, then the resistance would be proportional to $W^{-1/3}$. This is the same result that we obtained for the resistance due to flatness deviation. On the other hand, we have seen that, if roughness was the only consideration, the resistance would be proportional to $W^{-0.94}$. As will be seen in the next section and also in later chapters, the majority of experimental data show an index that is in between these two extremes indicating that, in practice, the resistance is due to the combined effect of roughness and waviness or flatness deviation.

3.6 Correlations for Solid Spot Conductance

Over the past forty years, several different correlations have been proposed for the solid spot conductance. In what follows, only a few *representative* correlations will be discussed.

In general, experimental results for solid spot conductance are obtained from tests conducted under vacuum conditions. It is clear, from the theoretical analysis just presented, that the parameters of significance to solid spot conductance should include:

a. The harmonic mean of the thermal conductivities of the two solids.
b. The contact pressure.
c. The surface roughness.
d. The "flow pressure" or similar property of the softer material.
e. The mean junction temperature.

In addition, the effects of flatness deviation and the mean slope of surface profile should also be included. However, these parameters, in general, are less readily measured and, therefore, many of the proposed correlations do not take them into account. It may be noted that the information about the mean junction temperature is also not available in some early work.

One of the early correlations for solid spot conductance was that presented by Laming (1961):

$$(h_S/k) = 2[\{1/(\pi\lambda_1\lambda_2)\}(P/H)]^{0.5}/(1-F) \tag{3.41}$$

in which F is the Roess constriction alleviation factor.

It should be noted that the above formula was based on the theoretical and experimental results for joints composed of crossed ridges of wavelengths, λ_1 and λ_2, respectively, and hence, *the number of contact spots remained constant with load.* For randomly rough surfaces, the number of contact spots increases with contact pressure. The above correlation, therefore, is applicable only to joints such as those composed of crossed wedges or pyramids contacting a flat smooth surface.

Based on 92 experimental data points generated by seven different investigators, Mal'kov (1970) proposed the following correlation:

$$h_s\bar{a}/k = 0.118(PC_1/3S_u)^{0.66} \tag{3.42}$$

Here $\bar{a}$ is the average contact spot radius which was taken by Mal'kov to be $4\,(10^{-5})$ m, and use was made of the result that the flow pressure is approximately equal to three times the ultimate compressive strength, S_u. C_1 is a factor that depends on the mean height of microprojections, H_{av}, of the surfaces, as given by the following relations:

$$C_1 = 1 \qquad \text{for } H_{av1} + H_{av2} > 30\,\mu\text{m}$$

$$C_1 = \{30/(H_{av1} + H_{av2})\}^{1/3} \qquad \text{for } 10\,\mu\text{m} < H_{av1} + H_{av2} < 30\,\mu\text{m}$$

$$C_1 = 15/(H_{av1} + H_{av2}) \qquad \text{for } H_{av1} + H_{av2} < 10\,\mu\text{m}$$

TABLE 3.1. Average heights of microprojections.

Material	Maching method	Surface finish	H_{av}, μm
Stainless steel	Turned	∇_4	23.5
Stainless steel	Turned	∇_5	14.0
Stainless steel	Turned	∇_8	2.4
Stainless steel	Ground	∇_8	2.2
Stainless steel	Ground	∇_9	1.2
Stainless steel	Turned and lapped	∇_{10}	0.6–0.8
Molybdenum	Ground	∇_9	1.0
Molybdenum	Ground	∇_9	1.07

The average heights of microprojections for different kinds of machining are presented in Table 3.1.

The correlation, indicated by line II in Fig. 3.8, appeared to agree well with the data of seven independent investigators. It was, however, seen that at high contact pressures the data seemed to be better approximated by line I, which has a slope of 0.86. Although the effect of temperature was not directly included, it was suggested that correlations such as this should not be applied to contact zone temperatures exceeding 0.3 times the melting point of the (softer) material. The author also pointed out that, because of lack of data, the feasibility of extrapolating the correlation to *low* contact pressures must be checked experimentally.

Fletcher and Gyorog (1971) obtained a correlation which was of a different form than the ones just listed. In particular, they represented the material property by the Young's Modulus E and also took the effects of the mean junction temperature, T, the gap thickness and the flatness deviation, FD, into account. The result was expressed as:

$$h_S = (k_s/\delta_o)\delta[5.22(10^{-6})\delta_o^* + 0.036P^*T^*]^{0.56} \tag{3.43}$$

where

$$\delta = \delta_o \exp(-170P^*T^*/\delta_o^*)$$
$$P^* = P/E$$
$$T^* = \alpha T_m$$
α = coefficient of thermal expansion
T_m = mean temperature
δ_o = initial gap thickness
$$\delta_o^* = \delta_o/b$$
b = specimen radius

δ_9 depended on the contact surface parameter, d, which was defined by

$$d = (FD + 2RD)_{\text{rough surface}} - 0.5(FD + 2RD)_{\text{smooth surface}},$$

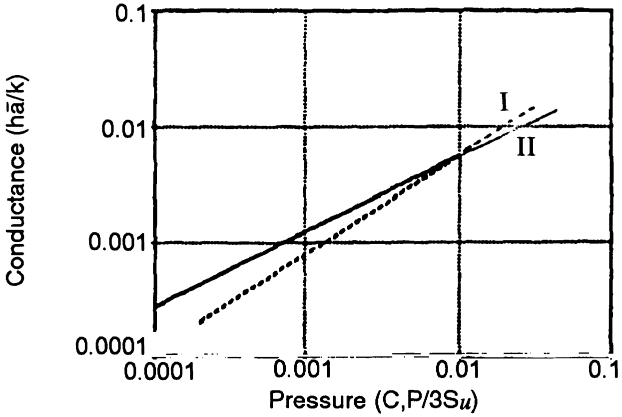

FIGURE 3.8. Mal'kov's correlation of experimental data.

FD and *RD* being flatness and roughness deviations, respectively. The relation between δ_o and d was presented in the form of a graph (see Fig. 3.9).

The correlation predicted the contact conductance, within an error of 24%, the test results of Fletcher and Gyorog, and those of nine other independent investigations. However, care should be taken in the use of correct units in applying Eq. (3.43) with h is expressed in BTU/(hr ft^2 °F); FD, RD, d, and δ_o in micro inches; k in BTU/(hr ft °F); P and E in psi; T in °F; T_m in °R; α in 1/°F, b in ft.

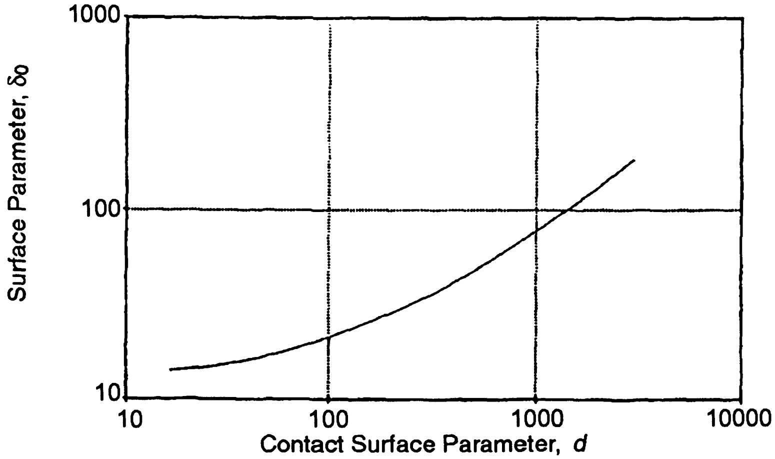

FIGURE 3.9. Variation of surface parameter, δ_o, with contact surface parameter, d (Fletcher and Gyorog, 1971).

Yovanovich (1981), based on theoretical considerations of plastically deforming asperities whose heights followed a Gaussian distribution, proposed the following correlation:

$$h_S\sigma/(k\tan\theta) = 1.25(P/H)^{0.95} \tag{3.44}$$

This correlation applies to conforming rough surfaces, for example neither surface having any appreciable flatness deviation. This correlation agreed to within an rms error of 6.4%, with the experimental results of three different investigations using similar equipment and techniques. This correlation is very similar to that derived by Mikic (1974). See also Eq. (3.33).

It may also be noted that the correlations for flat surfaces derived by Popov (1976) and Antonetti et al. (1993), also yielded similar indices, 0.956 and 0.95, respectively, for the nondimensional pressure. The dimensional analysis of Tien (1967) also yielded a correlation similar to Eq. (3.33). The index of the pressure term, however, was found to be 0.85.

In summary, correlations for solid spot conductance seem to fit into two categories in general: those in which the exponent of the contact pressure is about 0.95 and those in which the exponent is in the range 0.6 to 0.75. The results for nominally flat surfaces appear to fit the first category. On the other hand, correlations (e.g., those of Mal'kov or Fletcher and Gyorog), which collate the works of a large number of investigators generally yield much lower exponents reflecting that practical surfaces contain waviness, flatness deviation, or other macroscopic errors of form. This fact will be confirmed when we consider the correlations for specific materials in a later chapter.

3.7 Numerical Example: Solid Spot Conductance

The numerical example given below illustrates the steps in estimating the solid spot thermal conductance for a joint formed between two nominally flat surfaces. The data used are given in Table 3.2. Compu-

TABLE 3.2. Data used in calculations.

Property	Aluminium alloy	Stainless steel
Thermal conductivity, k	200 W/(m K)	16.5 W/(m K)
Hardness, H	1400 MPa	3800 MPa
Modulus of elasticity, E	$70(10^3)$ MPa	$190(10^3)$ MPa
Poisson's ratio, ν	0.33	0.29

TABLE 3.3. Surface combinations used in computations.

	Aluminium		Stainless steel	
Combination number	CLA roughness	Slope	CLA roughness	Slope
A	1 μm	0.18 rad	1 μm	0.18 rad
B	0.1 μm	0.03 rad	0.1 μm	0.03 rad
C	1 μm	0.18 rad	0.1 μm	0.03 rad

tations will be performed for three separate surface combinations—both surfaces rough, both surfaces smooth, and one surface rough and the other smooth (see Table 3.3). For Gaussian surfaces, rms surface roughness is $\sigma \approx 1.25$ (CLA Roughness). The effective values are first calculated as follows:

Effective modulus of elasticity,

$$E = 2[\{(1 - \nu_1^2)/E_1\} + \{(1 - \nu_2^2)/E_2\}]^{-1}$$
$$= 114(10^3)\,\text{MPa}$$

Effective thermal conductivity,

$$k = 2k_1k_2/(k_1 + k_2) = 30.48\ \text{W/(m K)}$$

Effective or combined roughness:

$$\sigma = (\sigma_1^2 + \sigma_2^2)^{0.5}$$

Thus,

$$\sigma_A = 1.25(1^2 + 1^2)^{0.5} = 1.77\,\mu\text{m}$$

Similarly,

$$\sigma_B = 0.177\,\mu\text{m};\quad \sigma_C = 1.256\,\mu\text{m}$$

The effective or combined slope is, $\tan\theta \approx (\text{slope}_1^2 + \text{slope}_1^2)^{0.5}$. Thus

$$\tan\theta_A = 0.254$$

$$\tan\theta_B = 0.0424$$

$$\tan\theta_C = 0.182$$

The plasticity index, as defined in Eq. 3.23, may be calculated as

$$\psi = (E'/H)\tan\theta$$

TABLE 3.4. Results of solid spot conductance estimation.

	Solid spot conductance, W/(m² K)		
Contact pressure MPa	Rough/rough	Smooth/smooth	Rough/smooth
0.1	626	1045	632
0.5	2842	4744	2870
1.0	5453	9102	5506
5.0	24755	41321	24996
10	47494	79275	47955
50	215610	359890	217700
100	413650	690460	417670

where, H is the hardness of the softer material. In this example,

$$H = 1400\,\text{MPa}$$

so that,

$$\psi_A = 20.7; \quad \psi_B = 3.45; \quad \psi_C = 14.82$$

Thus the plasticity index is greater than 1 for all three combinations indicating that the formula, Eq. (3.33), for plastic deformation needs to be used in calculating the solid spot conductance.

$$h_s = 1.13(k/H^{0.94})(\tan\theta/\sigma)P^{0.94}$$

For the givn pair of materials, $k = 30.48$ W/(m K) and $H = 1400$ MPa, so that

$$h_s = 0.038(\tan\theta/\sigma)P^{0.94}$$

Thus, the conductance versus pressure relationships which are shown in Table 3.4, for the three combinations, would be:

A. (Rough/Rough): $h_s = 5453P^{0.94}$
B. (Smooth/Smooth): $h_s = 9102P^{0.94}$
C. (Rough/Smooth): $h_s = 5506P^{0.94}$

Note

1. The solid spot conductance would, in fact, be the joint thermal conductance in vacuum if radiation is not significant. For heat transfer in nonvacuum conditions, the gas gap conductance needs to be added. See Chapter 4 for additional information.

2. It is immediately clear that little enhancement in conductance can be obtained if only one of the surfaces is made smooth; the roughness of BOTH surfaces needs to be reduced if a significant increase in conductance is required.

References

Antonetti, V.W., Whittle, T.D., and Simons, R.E. (1993). An Approximate Thermal Contact Conductance Correlation. ASME, Electronic Packaging, 115:131–134.

Bush, A.W., and Gibson, R.D. (1979). A Theoretical Investigation of Thermal Contact Conductance. Appl Energy, 5:11–22.

Chang, W.R., Etsion, I., and Bogy, D.B. (1987). An Elastic-Plastic Model for the Contact of Rough Surfaces. J Tribol, 109:257–263.

Clausing, A.M., and Chao, B.T. (1965). Thermal Contact Resistance in a Vacuum Environment. Trans ASME, J Heat Transfer, 87:243–251.

Fletcher, L.S., and Gyorog, D.A. (1971). Prediction of Thermal Contact Conductance Between Similar Metal Surfaces. Prog Astro Aero, 24:273–288.

Greenwood, J.A. (1967). The Area of Contact Between Rough Surfaces and Flats. Trans ASME, J Lub Technol, 89:81–91.

Greenwood, J.A., and Tripp, J.H. (1970). The Contact of Two Nominally Flat Rough Surfaces. Proc I Mech Eng, 185:625–633.

Greenwood, J.A., and Williamson, J.B.P. (1966). Contact of Nominally Flat Surfaces. Proc R Soc (London), Ser. A, 295:299–319.

Kimura, Y. (1970). Estimation of the Number and the Mean Area of Real Contact Points on the Basis of Surface Profiles. Wear 15:47–55.

Laming, L.C. (1961). Thermal Conductance of Machined Metal Contacts. Proc Int Conf Devel Heat Transfer. American Society of Mechanical Engineers, New York, pp. 65–76.

Mal'kov, V.A. (1970). Thermal Contact Resistance of Machined Metal Surfaces in a Vacuum Environment. Heat Transfer—Soviet Res, 2(4):24–33.

Mikic, B.B. (1974). Thermal Contact Conductance: Theoretical Considerations. Int J Heat Mass Transfer, 17:205–214.

Mikic, B.B., and Rohsenow, W.M. (1966). Thermal Contact Resistance. Mech Eng Dept Report No. DSR 74542-41, MIT, Cambridge, MA.

Popov, V.M. (1976). Concerning the Problem of Investigating Thermal Contact Resistance. Power Eng (NY), 14:158–163.

Pullen, J., and Williamson, J.B.P. (1972). On the Plastic Contact of Rough Surfaces. Proc R Soc (London), Ser. A., 327:159–173.

Roca, R.T., and Mikic, B.B. (1971). Thermal Contact Resistance in a Non-Ideal Joint. Mech Eng Dept Report No DSR 71821-77, MIT, Cambridge, MA.

Tabor, D. (1951). The Hardness of Metals. Oxford University Press, London.

Tabor, D. (1975). A Simplfied Account of Surface Topography and the Contact Between Solids. Wear, 32(2):269–271.

Thomas, T.R., and King, M. (1977). Surface Topography in Engineering: A State of the Art Review and Bibliography. BHRA Fluid Eng Ser, Vol. 3, 130 pp.

Thomas, T.R., and Sayles, R.S. (1975). Random Process Analysis of the Effect of Waviness on Thermal Contact Resistance. Prog Astro Aero, 39:3–20.

Tien, C.L. (1968). A Correlation for Thermal Contact Conductance of Nominally-Flat Surfaces in Vacuum. Proc. 7th Conf on Thermal Conductivity, U.S. National Bureau of Standards, Gaithersburg, MD.

Timoshenko, S.P., and Goodier, J.N. (1970). Theory of Elasticity, 3d ed. McGraw-Hill, New York.

Tsukizoe, T., and Hisakado, T. (1965). On the Mechanism of Contact Between Metal Surfaces—The Penetrating Depth and the Average Clearance. Trans ASME, J Basic Eng, 87:666–674.

Tsukizoe, T., and Hisakado, T. (1968). On the Mechanism of Contact Between Metal Surfaces. Part 2—The Real Area and the Number of Contact Points. Trans ASME, J Lub Technol., 90:81–88.

Whitehouse, D.J., and Archard, J.F. (1970). The Properties of Random Surfaces of Significance in Their Contact. Proc R Soc (London), Ser. A., 316:97–121.

Yovanovich, M.M. (1969). Overall Constriction Resistance Between Contacting Rough, Wavy Surfaces. Int J Heat Mass Transfer, 12:1517–1520.

Yovanovich, M.M. (1981). New Contact and Gap Conductance Correlations for Conforming Rough Surfaces. AIAA Paper 81K-1164, 6 pp.

4
Gas Gap Conductance

At low contact pressures (of the order of 10^{-4} H or less), it can be shown that the heat transfer across a joint occurs mainly through the gas gap (Madhusudana, 1993). Boeschoten and van der Held (1957) had also made the qualitative observation that heat transfer was predominantly through the gas gap for "low (up to several kg/sq cm)" contact pressures. Furthermore, Lang (1962) pointed out that the convective heat transfer is usually negligible for gap widths of up to about 6 mm (corresponding to Grashof numbers of 2000 for air at atmospheric pressure of 101 kPa and temperature of 300 K). Since the mean separation between contacting engineering surfaces is some three orders of magnitude less than this dimension, it is clear that convection cannot be the mode of the heat transfer across the gas gap. Thus, the mode of heat transfer across the gas filling the voids between the actual contact spots, as also noted earlier, is principally by conduction.

4.1 Factors Affecting Gas Gap Conductance

The following is a brief discussion of the factors affecting the heat transfer across the thin gas gap by conduction. A review summarizing the state of knowledge on gas gap conductance, to 1980, was published by Madhusudana and Fletcher (1981).

If the gas layer can be considered as a continuum, then Fourier's law of heat conduction applies, and the heat transfer coefficient, h_g, for the gas gap may simply be written:

$$h_g = k_g/\delta \tag{4.1}$$

where

k_g = thermal conductivity of the gas
δ = mean thickness of the gas gap

The effective thickness of the gap would be of the same order of magnitude as the surface roughness heights. For most practical surfaces in contact, the surface roughness heights have a range between 0.1 and 10 μm. Therefore, the mean gap thickness of smooth surfaces would be similar in magnitude to the mean free path, λ, of the gas molecules at atmospheric pressure. Under these circumstances, the phenomenon of "temperature jump" becomes important. Since λ increases as the gas pressure is reduced, this effect becomes important for rough surfaces also if the pressure is subatmospheric. The temperature jump accounts for the inefficiency in energy transfer between the gas molecules and the solid surfaces during a single collision (Smoluchowski Effect). Thus, when heat is conducted across two parallel plates separated by a distance similar to λ, the temperature distribution within the gas layer would be as shown in Fig. 4.1. It is clear from the figure that the effect of temperature jump at each of the surfaces is to increase the length of the heat transfer path by an amount that can be called the *temperature jump distance*, g. Kennard (1938) gives the following equation for the temperature jump distance:

$$g = [(2 - \alpha)/\alpha][2/(\gamma + 1)][(k_g/(\mu C_v)]\lambda \tag{4.2}$$

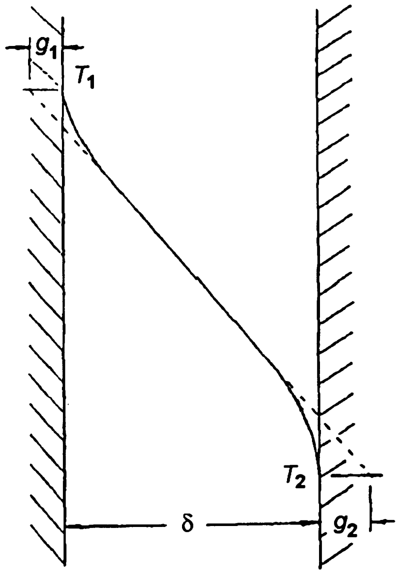

FIGURE 4.1. Temperature jump distance.

where,

α = accommodation coefficient
γ = ratio of specific heats
k_g = thermal conductivity of the gas
μ = viscosity
C_v = specific heat at constant volume
λ = mean free path of gas molecules

Eq. (4.2) applies to a single gas. The temperature jump distance, g_m, for a *mixture of gases* was determined by Vickerman and Harris (1975) to be

$$g_m = \Sigma(x_i g_i / M_i^{0.5}) / \Sigma(x_i / M_i^{0.5}) \tag{4.3}$$

where

x_i = mass fraction of constituent gas i
M_i = molecular mass of constituent gas i
g_i = temperature jump distance of constituent gas i

Table 4.1 lists the above properties for several gases. The values refer to atmospheric pressure and temperatures of approximately 101 kPa and 300 K, respectively. Since the accommodation coefficient is a complex parameter, which depends on the nature of the gas as well as the solid surfaces with which the gas is in contact, it is discussed separately in the next subsection.

Eq. (4.1) may now be modified, as follows, to take the temperature jump distance into account:

$$h_g = k_g / (\delta + g_1 + g_2) \tag{4.4}$$

Thus the problem of determining the gas gap thermal conductance reduces to one of determining the mean gap thickness and the temperature jump distances.

TABLE 4.1. Thermophysical properties of selected gases.

Gas	k_g, (W/m K)	γ	μ [10^{-6} kg/(m s)]	C_v, (J/kg K)	λ, (10^{-6} m)
Hydrogen	0.180	1.41	8.9	10120	0.118
Helium	0.149	1.66	19.8	3150	0.186
Neon	0.048	1.64	31.6	635	0.132
Nitrogen	0.026	1.40	17.8	741	0.063
Oxygen	0.0267	1.40	20.7	657	0.068
Argon	0.0167	1.67	22.4	310	0.067
Carbon dioxide	0.0167	1.30	14.9	648	0.042
Air	0.0262	1.40	18.5	718	0.064

In this connection, a nondimensional parameter called the Knudsen number, N_{Kn} is defined as follows:

$$N_{\mathrm{Kn}} = \lambda/\delta \tag{4.5}$$

For convenience, we can then identify three regimes of gas gap conduction:

1. Continuum: $N_{\mathrm{Kn}} \ll 1$; Fourier's law of heat conduction may be applied.
2. Temperature Jump: $0.01 < N_{\mathrm{Kn}} < 10$; Eq. (4.4) is applicable.
3. Free Molecular Conduction: $N_{\mathrm{Kn}} > 10$; in this case, the mean gap thickness would be much smaller than the temperature jump distances, and the Eq. (4.4) may be approximated as

$$h_g \cong k_g/(g_1 + g_2) \tag{4.6}$$

In other words, the heat transfer rate would be independent of the physical distance between the surfaces.

4.2 The Accommodation Coefficient

It is clear from Eq. (4.2) that the accommodation coefficient plays an important role in controlling the temperature jump distance and hence the gas gap conductance. Accommodation coefficient stands for the fractional extent to which the molecules that fall on the surface and are reflected or reemitted from it, have their energy adjusted or accommodated toward what the energy would have been if the returning molecules were issuing as a stream of gas at the temperature of the wall. In other words, accommodation coefficient characterizes the extent of gas–surface energy exchange. It is, therefore, defined as

$$\alpha = [T_f - T_g]/[T_s - T_g] \tag{4.7}$$

in which

T_s = temperature of the surface
T_g = temperature of the incident gas
T_f = effective temperature of the scattered gas

It is evident that the accommodation coefficient, at a given temperature, must depend upon the nature of both the gas and the (solid) surface. There exists a large number of works dealing with experimental and theoretical determination of α for various "gases" in contact with specific solid materials (see, e.g., Wiedmann and Trumpler, 1946; Wachman, 1962; and Semyonov et al., 1984). The following discussion should provide some insights to the nature and behavior of the accommodation coefficient (see Dharmadurai, 1983). Based on phonon energy transmission theory, the following approximate expression was derived for the accommodation coefficient of a *monatomic* gas

$$\alpha \cong [2n(A_e/A)M_g/M_s]/[1 + n(A_e/A)M_g/M_s] \tag{4.8}$$

at ambient temperatures in contact with a *clean* solid surface.

In Eq. (4.8),

n = atomicity (valency) of the solid
A_e = effective surface area available for gas–surface energy exchange
A = macroscopic interfacial area
M_g = molecular mass of gas
M_s = molecular mass of solid

For smooth surfaces, in general, $A_e/A = 1$; for rough surfaces, this ratio can be significantly larger than 1. (Even for smooth surfaces, A_e/A may be greater than 1 if the atomic diameter of the gas is much smaller than that of the solid surface.) If can be seen that for monatomic and clean solid surfaces in contact with a light gas ($M_g/M_s < 1$), Eq. (4.8) yields a value of $2(M_g/M_s)$ for the accommodation coefficient. This is in accordance with the rigorous gas-scattering theories for monatomic solids.

For contaminated surfaces, the above equation is modified as

$$\alpha \cong [2(M_g/A)\{fC_a n_a A_{ea}/M_a + (1-f)n_s A_{es}/M_s\}]/[1 + (M_g/A) \cdot \{fC_a n_a A_{ea}/M_a + (1-f)n_s A_{es}/M_s\}] \tag{4.9}$$

In this expression, C_a, is a constant characterizing the condensed phase of the adsorbed molecules, f, is the fraction of occupied surface sites and the subscripts, a, and, s, refer to the absorbed and surface molecules respectively. If the condensed phase is solid-like, then $C_a = 1$, while if it is fluid-like, then $C_a \cong 1/2$. For clean surfaces, $f = 0$. As the temperature of an initially totally covered ($f = 1$) surface rises, desorption increases leading to a gradual decrease in f. It follows that for systems with $M_s/A_{es} > M_a/(C_a A_{ea})$, the accommodation coefficient should decrease as the temperature increases.

Song and Yovanovich (1987) developed a correlation for the accommodation coefficient for "engineering" surfaces (i.e., surfaces with adsorbed layers of gases and oxides). This correlation was based on the experimental results of several previous investigators, for monatomic gases. The resulting relation was extended, by the use of a "monatomic equivalent molecular weight," to apply for diatomic/polyatomic gases. The final correlation was as follows:

$$\alpha = \exp(C_0 T)[M_g/(C_1 + M_g) + \{1 - \exp(C_0 T)\}\{2.4\mu/(1 + \mu)^2\}] \tag{4.10}$$

where

C_0 = dimensionless constant equal to -0.57
$T = (T_s - T_o)/T_o$
$M_g = M_g$ for monatomic gases
$= 1.4M_g$ for diatomic/polyatomic gases
$C_1 = 6.8$, units of M_g [g/mole]
$\mu = M_g/M_s$

The agreement between the published experimental data for diatomic and polyatomic gases and the predictions according to the above equations was generally within $\pm 25\%$.

Table 4.2 summarizes the accommodation coefficients for single gases in contact with various metals, as determined experimentally by various investigators. Table 4.3 lists the accommodation coefficients *for air* determined by Wiedmann and Trumpler (1946). Unless other-

TABLE 4.2. Accommodation coefficients for single gases.

	He	Ne	Ar	H_2	O_2	N_2	CO_2	Reference
Platinum	0.38	0.75	0.80	0.24	0.62	0.68	0.52	Smoluchowski, 1898
Platinum (bright)	0.44			0.32				Knudsen, 1934
Platinum (blackened)	0.91			0.72				Knudsen, 1934
Platinum (uncleaned)	0.446	0.816	1.01			0.975	1.00	Semyonov et al., 1984
Platinum			0.644					Thomas and Brown, 1950
Tungsten (clean 1000 °C)				0.54				Blodgett and Langmuir, 1932
Tungsten (clean fresh)	.06–.07							Roberts, 1932
Tungsten (uncleaned)	0.393	0.796	1.00			0.975	1.00	Semyonov et al., 1984
Tantalum (uncleaned)	0.493	0.848	0.974			0.991	1.00	Semyonov et al., 1984
Uranium dioxide	0.55		0.75					Hall et al., 1990
Nickel (uncleaned)	0.457	0.831	1.02			0.978	1.02	Semyonov et al., 1984

TABLE 4.3. Accommodation coefficients for air.

Solid Surface	Accommodation coefficient
Flat black lacquer on bronze	0.881–0.894
Bronze, polished	0.91–0.94
Bronze, machined	0.89–0.93
Bronze, etched	0.93–0.95
Cast iron, polished	0.87–0.93
Cast iron, machined	0.87–0.88
Cast iron, etched	0.89–0.96
Aluminum, polished	0.87–0.95
Aluminum, machined	0.95–0.97
Aluminum	0.89–0.97

Note: The apparatus employed by Wiedmann and Trumpler for determining the accommodation coefficients for air required the calculation of heat transfer by radiation and rarefied gas conduction between two long, concentric cylinders. They noted that the emissivity of etched aluminum dropped from 0.833 to 0.753 during the tests. Hence it was suggested that the accommodation coefficient data for etched aluminum was not reliable.

wise noted, the values in both tables pertain to ambient temperatures of about 300 K.

4.2.1 *Effect of Temperature on Accommodation Coefficient*

The experimental results of Ullman et al. (1974) for helium and xenon in contact with stainless steel and uranium dioxide surfaces indicated that, in all cases, the accommodation coefficient decreased with temperature. The temperature range of solid surfaces during their tests was 500 to 1000 K and no attempt had been made to clean or polish either of the surfaces. Their data for helium is approximated by the correlation, (Thomas and Loyalka, 1982):

$$\alpha_{He} = 0.425 - 2.3(10^{-4})T$$

This is in agreement with the conclusion reached earlier in this section, namely, that the accommodation coefficient for unclean surfaces should decrease as the temperature increases. On the other hand, the results reported by Kharitonov et al. (1973) indicate that, for helium and neon gases in contact with *pure* tungsten, the accommodation coefficient increases with temperature for temperatures greater than 300 K. A comparison of the two sets of data further shows that the accommodation coefficients for helium in contact with an unclean surface is at least an order of magnitude greater than those obtained with clean surfaces.

Before we leave this section on accommodation coefficients, it is interesting to consider the experimental observation of Cohen et al. (1960) that the conductance between the fuel and jacket in a nuclear power reactor was independent of the gas composition. An explanation for this unexpected behavior was offered by Kharitonov et al. (1973) based on the fact (see Eqs. (5.5) and (5.6)), that the accommodation coefficient depends on the molecular mass of the gas. Thus, for a gas such as helium with low molecular mass, the accommodation coefficient would also be small, as seen in Table 4.2. For such a case one can write

$$g \cong \lambda/\alpha \tag{4.11}$$

Furthermore, the mean free path for helium is large (see Table 4.2) and for small gap thicknesses and/or low contact pressures the assumption of free molecule conduction, Eq. (4.6), is valid so that

$$h_g \cong k_g/2g \cong k_g\alpha/2\lambda \tag{4.12}$$

In Eqs. (4.11) and (4.12), it is assumed that the accommodation coefficients and, therefore, the temperature jump distances are the same for the two surfaces with which the gas is in contact.

From Eq. (4.12) we see that it would be wrong to assume that the gap conductance would be proportional to the gas conductivity alone; gap conductance is also affected by the ratio (α/λ), which is comparatively small for helium. Indeed it can be shown that, for pure surfaces of heavy metals, the gap conductance with xenon would be greater than that with helium in contact with a similar pair of surfaces although the conductivity of helium is about thirty times that of xenon.

4.2.2 *Summary of Observations*

The following general conclusions may be made in view of the above discussion of previous experimental and theoretical investigations on accommodation coefficient.

Accommodation coefficients usually range in values from 0.01 to 1.0, although values higher than 1 are possible.

In general, lighter, monatomic gases have low accommodation coefficients.

Clean surfaces result in lower accommodation coefficients compared to contaminated surfaces.

For unclean surfaces, accommodation coefficient decreases as the temperature increases.

The accommodation coefficient appears to be inversely proportional to the thermal conductivity of the gas.
The accommodation coefficient is essentially independent of the gas pressure.

4.3 Effect of Gas Pressure on Gas Gap Conductance

From kinetic theory of gases, it can be shown that the thermal conductivity of a gas is given by, Hardee and Green (1968),

$$k_g = (4f/3d^2)[k^2 T/(\pi^2 M)]^{0.5} \tag{4.13}$$

where

f = degrees of freedom of the gas molecule
d = diameter of the gas molecule, m
T = absolute temperature of the gas, K
k = Bolzman constant, $1.381(10^{-23})$ J/K
M = mass of gas molecules, kg

It can be seen that the thermal conductivity of a gas is independent of its pressure. Therefore, Aaron (1963) considered that the conductance of a gas gap should be insensitive to decreases in gas pressure until a certain "threshold pressure" is reached when the mean free path of the gas molecules became comparable in magnitude to the average gap thickness, and Eq. (4.4) became applicable. For Aaron's experiments in air with a gap thickness of 9.6 μm, this threshold pressure was found to be equal to 21 mm Hg (2.79 kPa) at a temperature of 300 K. Thus, for this set of conditions, the decrease in the gas conductance would not be noticeable until a pressure of 2.79 kPa is reached. For further decreases in gas pressure, the conductance will decrease as the mean free path and, therefore, the temperature jump distance increase.

A similar conclusion can be drawn from the results of Shlykov and Ganin's (1964) tests on stainless steel contacts in air (see Fig. 4.2). It can be seen that, for a given contact pressure, in this case 20 kg/cm^2 ($\cong$19.6 MPa), there was noticeable increase in resistance only when the pressure dropped below 100 mm Hg. In other words, the threshold pressure applicable for this situation was 100 mm Hg ($\cong$13 kPa). The experimental results of Madhusudana (1975) on stainless steel/Nilo surfaces in air confirm the existence of a threshold pressure of similar magnitude.

At the other end of the spectrum, Shlykov and Ganin's results show that, for a given contact pressure, there is very little increase in the

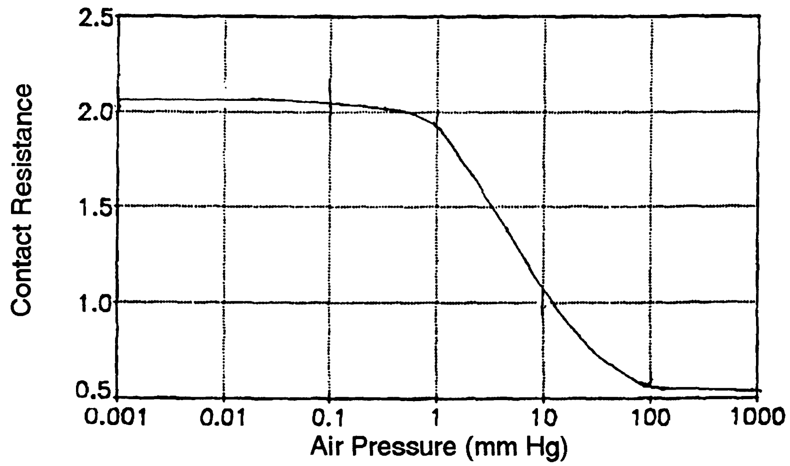

FIGURE 4.2. Effect of gas pressure on contact resistance (after Shlykov and Ganin, 1964).

total contact resistance for gas gap pressures below, approximately, 1 mm Hg (see Fig. 4.2). They therefore concluded that the gas conductance became practically zero at a pressure of 0.1 mm Hg. Hence it was recommended that tests in a vacuum of the order of 0.1 mm Hg would be sufficient to determine the solid spot contact conductance. Cassidy and Mark (1969) experimentally measured thermal contact resistance of stainless steel (type AISI 416) joints in air as the ambient pressure was decreased from one atmosphere down to $3(10^{-12})$ mm Hg. They confirmed that the assumption of zero thermal conductivity was valid for gas pressures below 1 mm Hg. The recent theoretical and experimental results of Nishino and Torii (1994) also confirm that the thermal contact conductance is insensitive to air pressures below 10 Pa.

4.4 Correlations for Gas Gap Conductance

From Eq. (4.4), it would appear that in order to estimate the gap conductance for a given gas, it is desirable to correlate the mean gap width, δ, with some physically measured surface parameters and the applicable temperature jump distances. Several correlations have been proposed of the form

$$Y = f(X) \tag{4.14}$$

where

$Y = b_t/\delta_{\text{eff}}$
$X = b_t/(g_1 + g_2)$
b_t = total peak-to-peak surface roughness
δ_{eff} = effective gap thickness $= \delta + g_1 + g_2$

It is frequently assumed that $g_1 = g_2 = g$, so that, $Y = b_t/(\delta + 2g)$ and $X = b_t/2g$.

The earliest and the simplest correlation is the one proposed by Cetinkale and Fishenden (1951). As quoted by Rapier et al. (1963), this correlation is equivalent to:

$$Y = 1/[0.305 + (1/X)] \tag{4.15}$$

The experimental results of Cetinkale and Fishenden pertained to large values of X and in fact only confirm that $Y \cong 1/0.305$ in this region.

The correlation developed by Rapier et al. (1963), based on the experimental results of several investigators, and their own results for helium, neon, and argon in contact with uranium dioxide–stainless steel surfaces, is

$$Y = 0.6/[1 + (1/2X)] + 0.4 \ln(1 + 2X) \tag{4.16}$$

Correlations in Eqs. (5.11) and (5.12) do not take into account the effect of variation of gap thickness with contact pressure. Dutkiewicz (1966) conducted a numerical analysis of surfaces taking into account the variation of contact area, and therefore the gap thickness, with contact load, assuming that asperity heights were normally distributed. His results, presented in tabular form, gave values of the gap thickness variable, $D^* = \sigma'/(\delta + 2g)$, for arbitrary values of the temperature jump distance variable $C^* = \sigma'/2g$, and the ratio, B, of real to apparent area of contact. In the expressions for C^* and D^*, σ' is the standard deviation of the profile height distribution. His results also showed that $b_t \cong 6\sigma'$ which indicates that $C^* = X/6$ and $D^* = Y/6$ according to the nomenclature used in the present section. Table 4.4 lists the values obtained by Dutkiewicz for the case when the standard deviations of both surfaces are the same.

Another correlation, which takes the variation of gap thickness with the load, is that due to Popov and Krasnoborod'ko (1975). This follows along the lines of Rapier et al. with X_1 and Y_1 defined as follows:

$$\left.\begin{aligned} X_1 &= \delta_{\max}(1 - \zeta)/(g_1 + g_2) \\ Y_1 &= \delta_{\max}(1 - \zeta)/\delta_{\text{eff}} \end{aligned}\right\} \tag{4.17}$$

TABLE 4.4. Variation of gap thickness variable D^* with contact area.

	B				
C^*	0	0.01	0.025	0.050	0.100
200	0.290	0.435	0.531	0.713	2.593
20	0.279	0.410	0.499	0.653	1.178
2	0.237	0.315	0.367	0.431	0.531
0.2	0.111	0.124	0.131	0.138	0.147
0.02	0.019	0.019	0.020	0.020	0.020

where ζ is the *relative* approach of the two surfaces due to mechanical loading. δ_{max} is defined as the maximum thickness of the interface layer. A careful study of their analysis indicates that δ_{max} could be taken to be the same as b_t. Hence we see that, for zero load, X_1 and Y_1 correspond to X and Y, respectively, of this section. Popov and Krasnoborod'ko provided empirical correlations for determining $(1 - \zeta)$ and empirical relations between Y_1 and X_1 for steel and Duralumin for different classes of surface finish.

Figure 4.3 below compares the different correlations for zero mechanical loading. Curve 3, representing the prediction of Popov and Krasnoborod'ko, is actually a composite graph. This represents the average of the values for four different types of surface finish and has been plotted from the expressions given by Popov and Krasnoborod'ko for steel surfaces. From an examination of this figure, it is clear that

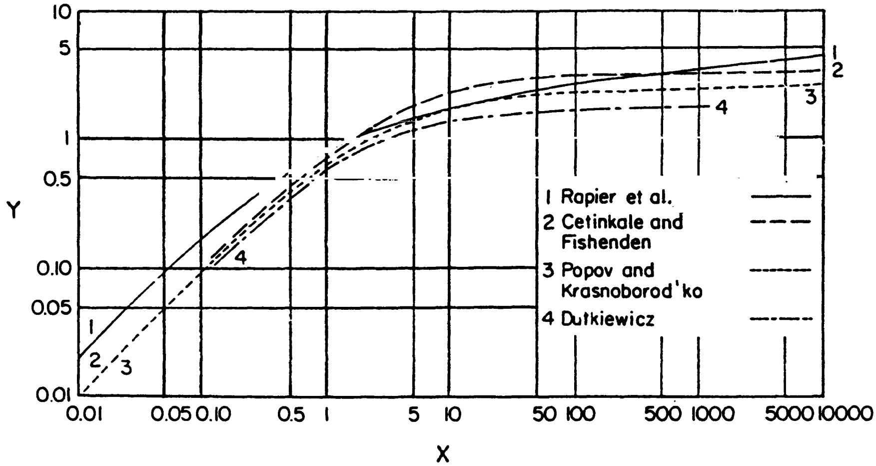

FIGURE 4.3. Comparisons of correlations for gas gap conductance (Madhusudana and Fletcher, 1981, used with permission).

there is not a great deal of difference between the predictions; any one of them is probably just as good as the others. It should be emphasized, however, that the correlations of Cetinkale and Fishenden, and Rapier et al., do not allow for the variation of the gap thickness with the contact pressure, and one of the other three correlations has to be used if such variation is significant. Of course, whatever correlation is used, it is first of all necessary to establish the surface parameters and the temperature jump distances before proceeding to determine the effective gap thickness.

For conforming rough surfaces with a Gaussian height distribution, the mean separation between the surfaces is given by (see Antonetti, 1992),

$$\delta = 1.53\sigma(P/H)^{-0.097} \tag{4.18}$$

The gap conductance at any mechanical load may be simply estimated using this equation in conjunction with Eq. (4.4).

Yovanovich and his co-workers (see Yovanovich, 1981, 1986; Yovanovich et al. 1982; Song et al. 1989; and Song et al., 1993) also took into account the variation of gap thickness with contact load. It was assumed that the surfaces were conforming and had Gaussian surface height distributions. The correlation, proposed by Negus and Yovanovich (1988), for example, is expressed as

$$h_f = (k_f/\sigma)I_g \tag{4.19}$$

where

$$\begin{aligned}
\sigma &= \text{rms roughness} = (\sigma_1^2 + \sigma_2^2)^{0.5} \\
I_g &= \text{"gap conductance integral"} \\
&= f_g/(\delta/\sigma + G/\sigma) \\
f_g &= \text{correlation factor} \\
&= 1.063 + 0.0471[4 - (Y/\sigma)]^{1.68}(\ln \sigma/G)^{0.84}, \text{ for } 0.01 \le (G/\sigma) \le 1 \\
&= 1 + 0.66(\sigma/G)^{0.8}, \text{ for } 1 \le (G/\sigma) < \infty \\
\delta &= \text{Mean plane separation} \\
\delta/\sigma &= 1.184[-\ln(3.132(P/H)]^{0.547} \\
G &= \alpha\beta\lambda \\
\alpha &= (2 - \alpha_1)/\alpha_1 + (2 - \alpha_2)/\alpha_2 \\
\beta &= 2\gamma/[(\gamma + 1)Pr] \\
\lambda &= \lambda_0(T_g/T_0)(p_g/p_0)
\end{aligned}$$

T and p refer respectively to the gas temperature and pressure; the subscript 0 refer to standard conditions, the subscript g refers to actual conditions; λ is the mean free path. It is readily seen that G is the sum of the temperature distances for the two surfaces.

Negus and Yovanovich (1988) verified that the joint conductances, obtained by adding the gap conductance calculated by the above correlation to the solid spot conductance, showed good agreement with the experimental results of Hegazy (1985).

Real surfaces have a finite maximum height whereas the normal distribution assumes an infinite maximum height. Therefore, Majumdar and Williamson (1990) suggested that inverted chi-square (ICS), rather than Gaussian, distribution should be used for surface heights. The use of ICS distribution results in higher values for the gap conductances.

4.5 Gas Gap Conductance: Conclusions

The following general conclusions follow as a result of the discussion in this section.

1. The gas gap conductance depends on the mean gap thickness, which is a function of the surface finishes of the bodies in contact, and the gas thermal conductivity. However, as listed below, there are other factors, which might significantly affect the gas conductance.
2. The gas gap conductance increases with contact pressure due to the reduction of gap thickness with contact pressure. Such a reduction would be noticeable, however, only if the surfaces are relatively coarse.
3. The gap conductance depends on the temperature jump distance which depends not only on the thermophysical properties of the gas but also on the accommodation coefficient. At any given temperature, the accommodation coefficient depends on the gas, the solids in contact and the condition of the solid surfaces.
4. For a given pair of surfaces and temperature, there is a threshold gas pressure (typically, 100 mm Hg or 13 kPa) above which the increase of the conductance with gas pressure is insignificant.
5. If the gas pressure is below 1 mm Hg (0.13 kPa), the gas conduction contribution to heat transfer is negligible.
6. For intermediate pressures and/or when the physical gap thickness is small, free molecular heat conduction may be important.
7. Gap conductance can be calculated by correlations such as those produced by Rapier et al. although these need the peak-to-peak roughness values for the evaluation of gap conductance. It was pointed out that correlations are available relating the rms or CLA roughnesses with the peak-to-peak values.

8. For flat surfaces with Gaussian distribution of asperity heights, the correlation (4.18) proposed by Negus and Yovanovich could be used. Alternatively, the mean separation and the temperature jump distance may be calculated by Eqs. (4.19) and (4.2), respectively, and then substituted in Eq. (4.4) to calculate the gap conductance.
9. Both methods also account for the variation of gap thickness with mechanical load for the specified surfaces.
10. The method proposed by Popov and Krasnoborod'ko also account for the variation of gap thickness with load for different classes of surface finish for specific materials.

4.6 Numerical Example: Gas Gap Conductance

For the stainless steel/aluminium rough/rough surfaces (pair A of the Numerical Example in Chapter 3), the gap conductance is calculated below for two cases (see Table 4.5).

From Eq. (4.18), the mean physical gap at any contact pressure P is,

$$\begin{aligned}\delta &= 1.53\sigma(P/H)^{-0.097}\\ &= 1.53(1.77)(P/1400)^{-0.097}\\ &= 5.468(P^{-0.097});\ \delta \text{ will be in } \mu\text{m if } P \text{ is expressed in MPa.}\end{aligned}$$

From Eq. (4.2), the temperature jump distance is

$$g = [(2 - \alpha)/\alpha][2/(\gamma + 1)][k_g/(\mu C_v)]\lambda$$

so that,

$$g_{air} = [1.1/(0.9)][2/(2.4)][0.0262/(18.5 \times 718)]0.064 = 0.1286\,\mu\text{m}$$

and

TABLE 4.5. Data for gas gap conductance calculation.

Property	Gas	
	Air	Helium
Thermal conductivity, k_g	0.0262 W/(m K)	0.149 W/(m K)
Ratio of sp heats, γ	1.40	1.66
Viscosity, μ	$18.5(10^{-6})$ kg/(m s)	$19.8(10^{-6})$ kg/(m s)
Sp heat at const vol, C_v	718 J/(kg K)	3150 J/(kg K)
Mean free path, λ	$0.064(10^{-6})$ m	$0.186(10^{-6})$ m
Accom coefficient, α	0.90	0.45

TABLE 4.6. Gas gap and solid spot conductances.*

P, MPa	0.1	0.5	1	5	10	50	100
δ, μm	1.675	1.433	1.34	1.15	1.07	0.92	0.86
$h_{g,\mathrm{air}}$, W/(m² K)	3693	4291	4576	5307	5659	6555	6977
$h_{g,\mathrm{He}}$, W/(m² K)	17160	19370	20377	22839	23960	26680	27890
h_s, W/(m² K)	626	2842	5453	24755	47493	215610	413650

* See Numerical Example in Chapter 3.

$$g_{\mathrm{He}} = [1.55/(0.45))][2/(3.32)][0.149/(19.8 \times 3150)]0.186 = 0.922\,\mu\mathrm{m}$$

The gap conductance is then given by

$$h_g = k_g/(\delta + 2g)$$

Hence Table 4.6 is generated. The solid spot conductance, h_s, from the Numerical Example in Chapter 3 is given for the sake of comparison.

The calculations emphasize that:

1. The gas gap conduction is the predominant mode of heat transfer at low to moderate contact pressures of up to 1 MPa. It could be significant at higher pressures too depending on the solid/gas combination.
2. The variation in gas gap conductance with contact pressure is relatively small; for a thousandfold increase in contact pressure, the gap conductance increases by less than twofold.
3. The gas gap conductance is not directly proportional to the gas thermal conductivity.

It is interesting to compare the above results with those obtained by using the correlation Eq. (4.16) of Rapier Jones and McIntosh:

$$Y = 0.6/[1 + \{1/(2X)\}] + 0.4\ln(1 + 2X)$$

where $Y = b_t/\delta_{\mathrm{eff}}$, $X = b_t/2g$, and $b_t = 6\sigma$.

In this example, therefore,

$$X_{\mathrm{air}} = 6(1.77)/[2(0.1286)] = 41.3$$

Hence

$$Y_{\mathrm{air}} = 2.36$$

giving

$$\delta_{\mathrm{eff}} = 4.5\,\mu\mathrm{m},$$

and

$$h_{g,\mathrm{air}} = (k_g/\delta_{\mathrm{eff}})_{\mathrm{air}} = 0.0262/[4.5(10^{-6})] = 5882\,\mathrm{W/(m^2\,K)}$$

Similarly

$$X_{\mathrm{He}} = 6(1.77)/[2(0.922)] = 5.76$$

Hence

$$Y_{\mathrm{He}} = 1.563$$

giving

$$\delta_{\mathrm{eff}} = 6.79\,\mu\mathrm{m},$$

and

$$h_{g,\mathrm{He}} = (k_g/\delta_{\mathrm{eff}})_{\mathrm{He}} = 0.149/[6.79(10^{-6})] = 21944\,\mathrm{W/(m^2\,K)}$$

Inasmuch as we do not know the range of contact pressures covered by the correlation of Rapier, Jones and McIntosh, it is, perhaps, coincidental that both of these figures are within 10% of the results, corresponding to a contact pressure of 10 MPa, listed in the above table which was obtained by using a more recent correlation for the mean gap.

References

Aaron, R.L. (1963). A Theoretical Study of the Thermal Conductance of Joints with Varying Ambient Pressure. MS Thesis, Southern Methodist University, Dallas.

Antonetti, V.W. (1992). Statistical Variability of Thermal Interface Conductance. NSF/DITAC Workshop, Melbourne, Australia, pp. 37–45.

Blodgett, K.B., and Langmuir, I. (1932). The Accommodation Coefficient of Hydrogen: A Sensitive Detector of Surface Films. Phys Rev, 40:78–104.

Boeschoten, F., and Van der Held, E.F.M. (1957). The Thermal Conductance of Contacts Between Aluminium and Other Metals. Physica, 23:37–44.

Cassidy, J.F., and Mark, H. (1969). Thermal Contact Resistance Measurements at Ambient Pressures to 3×10^{-12} Mm Hg and Comparison with Theoretical Predictions. NASA, Technical Memorandum X-52566.

Cetinkale, T.N., and Fishenden, M. (1951). Thermal Conductance of Metal Surfaces in Contact. Proc Gen Disc Heat Transfer. Institute of Mechanical Engineers, London, pp. 271–275.

Cohen, I., Lustman, B., and Eichenberg, J.D. (1960). Measurement of Thermal Conductivity of Metal-Clad Uranium Oxide Rods During Irradiation. Report Wapd-288. Bettis Atomic Power Laboratory, Washington, DC.

Dharmadurai, G., (1983). Estimation of Thermal Accommodation Coefficients for Inert Gases on Nuclear Materials. J App Phys, 54(10):5990–5992.

Dutkiewicz, R.K. (1966). Interfacial Gas Gap for Heat Transfer Between Two Randomly Rough Surfaces. 3rd Int Heat Transfer Conf, 4:118–126.

Hall, R.O.A., Martin, D.G., and Mortimer, M.J. (1990). The Thermal Conductivity of UO_2 Sphere-Pac Beds. J Nucl Mat, 173:130–141.

Hardee, H.C., and Green, W.R. (1968). Thermal Conductivity in Small Air Gaps at Very Low Pressures. Sc-Tm-68-309, Sandia Laboratory, Albuquerque, NM.

Hegazy, A.H. (1985). Thermal Joint Conductance of Conforming Rough Surfaces: Effect of Surface Micro-Hardness Variation. Ph.D. Thesis, University of Waterloo, Canada [Cited In Negus and Yovanovich (1988)].

Kennard, E.H. (1938). Kinetic Theory of Gases. McGraw-Hill, New York, pp. 311–327.

Kharitonov, V.V., Kokorev, L.S., and Del'vin, N.N. (1973). On the Role of the Accommodation Coefficient in Contact Heat Exchange. Atomnaya Energiya, 35(5):360–361.

Knudsen, M. (1934). The Kinetic Theory of Gases. Methuen, London, pp. 46–61.

Lang, P.M. (1962). Calculating Heat Transfer Across Small Gas-Filled Gaps. Nucleonics, 20(1):62–63.

Madhusudana, C.V. (1975). The Effect of Interface Fluid on Thermal Contact Conductance. Int J Heat Mass Transfer, 18:989–991.

Madhusudana, C.V. (1993). Thermal Contact Conductance and Rectification at Low Joint Pressures. Int Comm Heat Mass Transfer, 20:123–132.

Madhusudana, C.V., and Fletcher, L.S. (1981). Gas Conductance Contribution to Contact Heat Transfer. AIAA Paper 81-1163. American Institute of Aeronautics and Astronautics, New York.

Majumdar, A., and Williamson, M. (1990). Effect of Interstitial Media on Contact Conductance: A Fractal Approach. ASME HTD, 153:49–57.

Negus, K.J., and Yovanovich, M.M. (1988). Correlation of the Gap Conductance Integral for Conforming Rough Surfaces. J Thermophy Heat Transfer, 2:279–281.

Nishino, K., and Torii, K. (1994). Thermal Contact Conductance of Wavy Metal Surfaces Under Arbitrary Ambient Pressure. Proc 10th Intl Heat Transfer Conf, Paper No. 15 C-118. Institution of Chemical Engineers, Rugby, UK.

Popov, V.M., and Krasnoborod'ko, A.I. (1975). Thermal Contact Resistance in a Gaseous Medium. Inzhenerno-Fizicheski Zhurnal, 28(5):875–883.

Rapier, A.C., Jones, T.M., and McIntosh, J.E. (1963). The Thermal Conductance of Uranium Dioxide/Stainless Steel Interfaces. Int J Heat Mass Transfer, 6:397–416.

Roberts, J.K. (1932). The Exchange of Energy Between Gas Atoms and Solid Surfaces II: The Temperature Variation of Accommodation Coefficient of Helium. Proc R Soc (London), Ser. A, 135:192–205.

Semyonov, Yu.G., Borisov, S.E., and Suetin, P.E. (1984). Investigation of Heat Transfer in Rarefied Gases Over a Wide Range of Knudsen Numbers. Int J Heat Mass Transfer, 27:1789–1799.

Shlykov, Yu.P., and Ganin, Ye.A. (1964). Thermal Resistance of Metallic Contacts. Int J Heat Mass Transfer, 7:921–929.

Smoluchowski, M.S. (1898). On Conduction of Heat in Rarefied Gases. Phil Mag J Sci, Ser. 5, 192–206.

Song, S., and Yovanovich, M.M. (1987). Correlation of Thermal Accommodation Coefficient for Engineering Surfaces. ASME HTD, 69:107–116.

Song, S., Yovanovich, M.M., and Nho, K. (1989). Thermal Gap Conductance: Effect of Gas Pressure and Mechanical Load. AIAA Paper 89-0429. American Institute of Aeronautics and Astronautics, Washington, DC.

Song, S., Yovanovich, M.M., and Goodman, F.O. (1993). Thermal Gap Conductance of Conforming Rough Surfaces in Contact. Trans ASME, J Heat Transfer, 115: 533–540.

Thomas, L.B., and Brown, R.E. (1950). The Accommodation Coefficient of Gases on Platinum as a Function of Pressure. J Chem Phys, 18:1367–1372.

Thomas, L.B., and Loyalka, S.K. (1982). Determination of Thermal Accommodation Coefficients of Inert Gases on a Surface of Vitreous UO_2 at 35 °C. Nucl Technol, 59:63–69.

Ullman, A., Acharya, R., and Olander, D.R. (1974). Thermal Accommodation Coefficients of Inert Gases on Stainless Steel and UO_2. J Nucl Mat. 51:277–279.

Vickerman, R.H., and Harris, R. (1975). The Thermal Conductivity and Temp Jump Distance of Gas Mixtures. Am Nucl Soc, Winter Meeting. American Nuclear Society, San Francisco.

Wachman, H.Y. (1962). The Thermal Accommodation Coefficient: A Critical Survey. ARS J, 32:2–12.

Wiedmann, M.L., and Trumpler, P.R. (1946). Thermal Accommodation Coefficients. Trans ASME, 68:57–64.

Yovanovich, M.M. (1981). New Contact and Gap Conductance Correlations for Conforming Rough Surfaces. AIAA Paper 81-1164. American Institute of Aeronautics and Astronautics, New York.

Yovanovich, M.M. (1986). Recent Developments in Thermal Contact, Gap and Joint Conductance Theories and Experiments. 8th Int Heat Transfer Conf, 1:35–45.

Yovanovich, M.M., DeVaal, J.W., and Hegazy, A.A. (1982). A Statistical Model to Predict Thermal Gap Conductance Between Conforming Rough Surfaces. AIAA Paper 82-0888. American Institute of Aeronautics and Astronautics, New York.

5 Experimental Aspects

Thermal conductance of joints may be determined experimentally in several ways. However, by far the most common method uses the axial flow apparatus in which two cylinders of similar or dissimilar materials are placed end to end as illustrated in Fig. 1.2 (Chapter 1). There have been other apparatus built for specific needs, for example, to determine contact conductance in concentric cylinders when the heat flow is radial; in periodic contacts; and in transient situations. In every case, before the heat transfer experiments are performed, it is necessary that profilometric measurements are made to characterize the surfaces. It is also necessary to determine the microhardness of the surfaces prior to the heat transfer tests.

Apart from heat transfer apparatus, conducting sheet and electrolytic tank analogues have been constructed and used, mainly to determine the resistance of various shapes of constrictions. Some of this equipment will also be briefly described in this chapter.

5.1 Axial Heat Flow Apparatus

Several investigators have used this type of experimental rig for contact conductance measurements, for example, Cetinkale and Fishenden (1951); Williams (1966); Mikic and Rohsenow (1966); Fletcher et al. (1969); and O'Callaghan and Probert (1972).

The schematic of a typical axial heat flow apparatus is shown in Fig. 5.1. Essentially, the rig consists of two cylinders, placed end to end, and loaded in the axial direction either mechanically or by hydraulic means. If the loading is achieved by other than mechanical means, then the contact load needs to be measured by the use of a calibrated load cell. Axial heat flow is achieved by providing a heat source at the top end and a heat sink at the bottom end. Frequently,

1 Vacuum Chamber
2 Lever Arm
3 Bellows
4 Heating elements
5 Cooling Coils
6 Specimens
7 Thermocouples
8 Insulators
9 Flexible Tubing

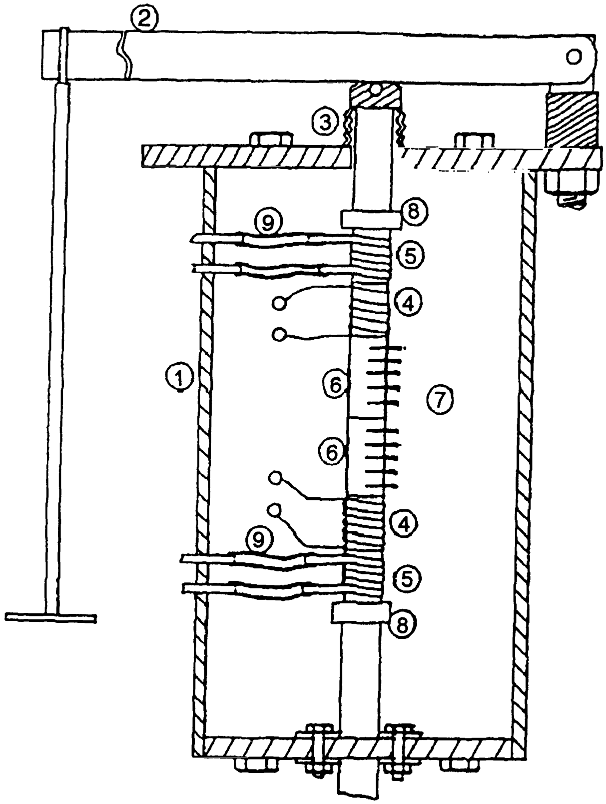

FIGURE 5.1. Axial heat flow apparatus.

however, provision for heating as well as cooling of either end is made so that the effect of reversing the direction of heat flow may be studied, without dismantling and reassembling the specimens. Generally, the assembly is placed in a chamber that can be evacuated in order that the solid spot conductance may be isolated and determined. To transmit the mechanical load to the assembly inside the chamber, a bellows or similar device would be required. A rotary vane-type vacuum pump is satisfactory for pressures down to 10^{-3} Torr; a vacuum diffusion pump is also needed if lower pressures (of the order of 10^{-6} Torr) are required. The preferred method of heating seems to be by the use of electrical resistance coils, for example, Nichrome, and cooling by water circulating in a coil and supplied from a constant head tank. Constant temperature circulating baths, however, have also been used to provide both heating and cooling.

To minimize heat losses, a guard heater or a thermal shield should be placed around the test section. This is especially important if the tests are done in a conducting environment such as air. In addition, insulators need to be placed at either end of the assembly to prevent heat losses in the axial direction.

The usual method of measuring temperatures in the specimens is by means of calibrated thermocouples. These thermocouples are inserted in holes drilled normal to the axis and extending to the axis; that is, the length of the holes is equal to the radius of the specimens. Use of a conducting cement or a soft foil at the bottom of the hole is desirable to provide good thermal contact between the thermocouple and the specimen. The output from the thermocouples is read in a potentiometer, digital voltmeter, multichannel recorder, or a personal computer-based data takers, the last method having the advantage that the experimental data can be processed as the experiment is being performed.

5.2 Radial Heat Flow Apparatus

In a cylindrical joint transmitting heat radially, the contact pressure is developed as a result of the differential expansion of the two cylinders. As will be seen in a later chapter, for a given pair of cylinders, the differential expansion and, hence, the contact pressure and contact conductance are functions, mainly, of the heat flux. To test these types of joints, therefore, no provision needs to be made for mechanical loading (see Cohen et al., 1960; Williams and Madhusudana, 1970; Hsu and Tam, 1979; and Madhusudana and Litvak, 1990). On the other hand, it is important to be able to measure the heat flux accurately.

The essentials of a typical radial heat flow apparatus is shown in Fig. 5.2. A major problem in testing of this type of joint appears to be the difficulty in obtaining a truly axisymmetric temperature distribution in the specimens if the inner cylinder is heated by radiation by means of a central noncontacting rod. The use of a preheated liquid to heat the inner surface of the inner specimen may alleviate this difficulty to some extent; however, this method is going to cause additional complexities when testing in vacuum is required. A second source of problems arises because of the need to make the cylinders sufficiently long to avoid the end-effects: firstly, very accurate machining to close tolerances is required to ensure the ends are straight and parallel with negligible taper; secondly, extra care is required in the assembly of long cylinders to produce a shrink fit; thirdly, it will

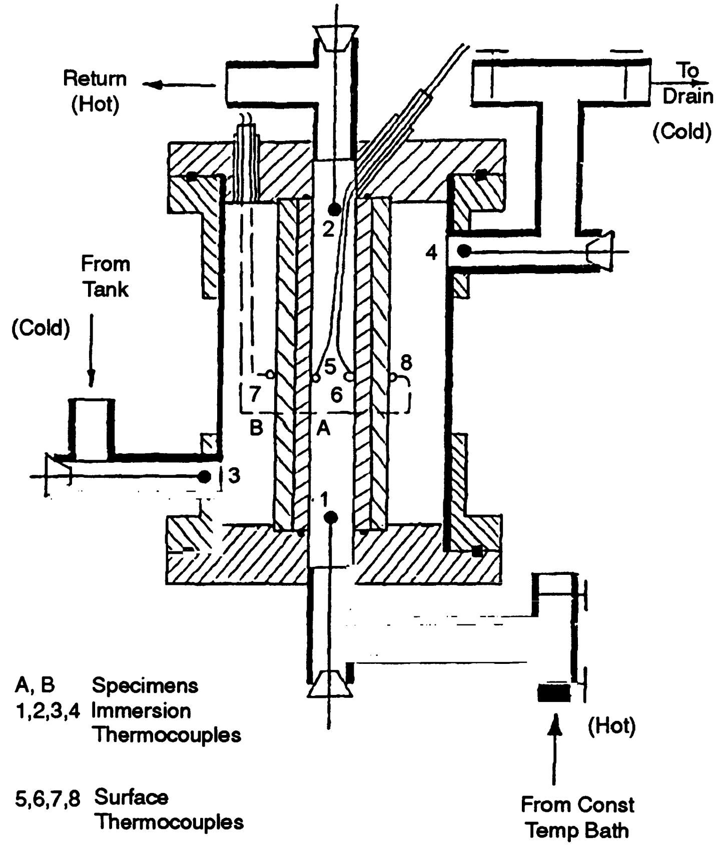

FIGURE 5.2. Radial heat flow apparatus (Madhusudana and Litvak, 1990).

be necessary to drill deep holes of very small diameter to locate the thermocouples in the specimen. Another problem results from the, usually, small thickness of the cylinders used; it would not be possible to locate sufficient number of thermocouples along the radial coordinate to measure radial temperature distribution reliably. It is also necessary to ensure that the specimens do not possess any significant degree of out-of-roundness at the interface. Perhaps because of these difficulties, there have been comparatively small number of reports dealing with experimental investigations of radial heat flow in cylindrical joints.

An associated problem is the determination of the thermal contact resistance in finned tubes. Experimental apparatus specially devised for this application have been described by, for example, Gardner and Carnavos (1960) and Sheffield et al. (1987).

5.3 Periodic Contacts

There are several applications in which the heat transfer occurs between surfaces that are undergoing a regular cycle of contact and separation. Examples include the heat transfer between the exhaust valve and its seat in an internal combustion engine; the heat transfer between the die and the workpiece in a repetitive hot metal deformation process.

The experimental apparatus used to test periodic contacts is similar to the axial heat flow rig described earlier. The facility used to make and break the contact in two such apparatuses will be briefly described.

The equipment used by Howard (1976) is shown in Fig. 5.3. In this device, compressed air was supplied to the pneumatic cylinder at the

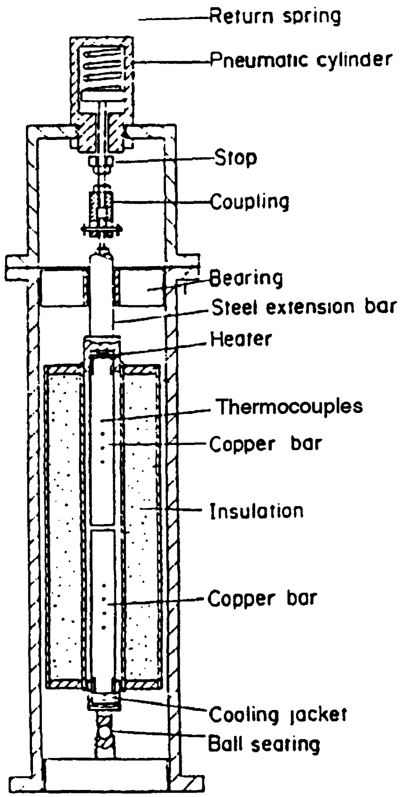

FIGURE 5.3. Experimental apparatus for periodic contacts (Howard, 1976). Copyright 1976. Reprinted by permission from Elsevier Science Ltd, The Boulevard, Kidlington, OX5 1GB, UK.

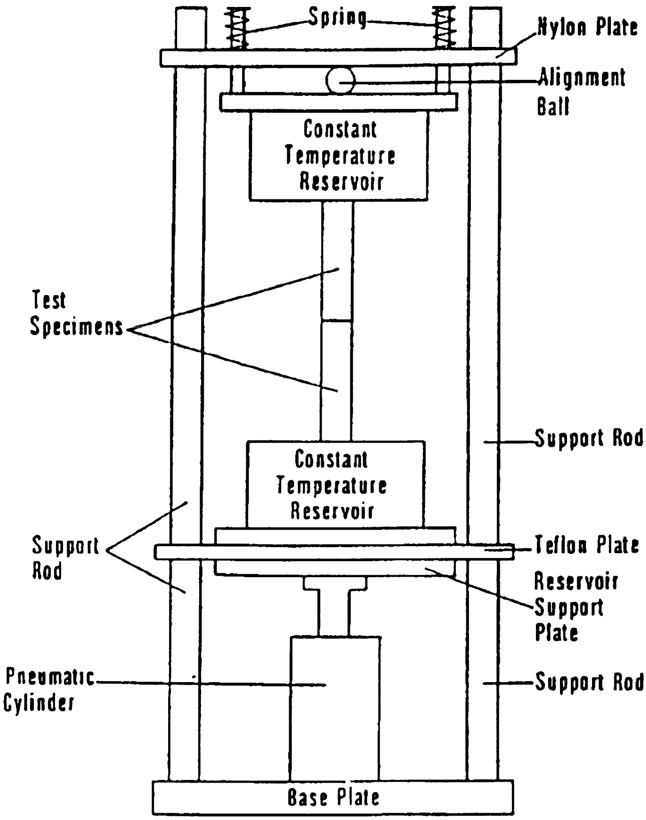

FIGURE 5.4. Experimental apparatus for periodic contacts (Dodd and Moses, 1988, used with permission).

top of the rig to lift the upper bar specimen out of contact with the lower. When the air pressure was released, the upper bar fell under the action of gravity and the return spring force to reestablish the contact. The frequency and proportion of the cycle time spent in contact could be controlled by the automatic opening and closing of valves in the inlet and exhaust lines.

In the apparatus described by Dodd and Moses (1988) (Fig. 5.4), the contact mechanism consists of two main plates, one located directly above the other. The upper plate, made of nylon, is rigidly attached to the support frame. Suspended below the plate, by means of a spring-loaded mechanism, is a smaller nylon plate to which one of the thermal reservoirs is attached. A nylon ball is sandwiched between the two plates. In conjunction with the spring-loaded mechanism, the ball requires the contact force to be transmitted through a single point, thus allowing the entire reservoir assembly and the attached test specimen to pivot about that point, bringing the surfaces of the specimens into contact in their entirety. The second test specimen and its associated thermal reservoir is attached to the lower plate, made of Teflon, which is free to slide along the four PVC rods forming the supporting frame.

The test specimens were caused to contact and separate by driving the lower plate with a pneumatic cylinder. The airflow to the cylinder was controlled by a dual-acting solenoid valve, with one airstream used to drive the test specimen into contact and the other to separate specimens at the end of the contact portion of the cycle. The valves were microprocessor controlled and the data was processed by means of a Data Acquisition/Control unit.

Both apparatus, described above, allowed tests to be conducted in ambient atmosphere only; there was no provision for evacuating the test section.

5.4 Transient Measurements

The facility used by Moore and Blum (1969), for transient measurements of the joint resistance is also an axial flow apparatus in which the test chamber could be evacuated to about 10^{-3} Torr. The test procedure was as follows: After initial assembly, the module consisting of the specimens and the heat sink was lowered so that they no longer made contact with the heat source. After the chamber was evacuated and the source temperature brought up to the desired value, the specimen/sink module was raised to make contact with the heat source. The force control system was a closed loop electrohydraulic servomechanism. The data was continually recorded on an oscillograph.

5.5 Analog Methods

The analog method is often a quick and inexpensive way of obtaining solutions to potential flow problems. In the current context, this method depends on the similarity between the electric voltage and the temperature, since both these potentials obey the same (e.g., Laplace) equation. In contact resistance work, this method has been used mainly to determine constriction resistances of various shapes.

For two-dimensional problems in the x-y plane, the problem is easily simulated. The heat flow region is simulated by an electrical conducting sheet ("teledeltos" paper). Prescribed voltages are applied

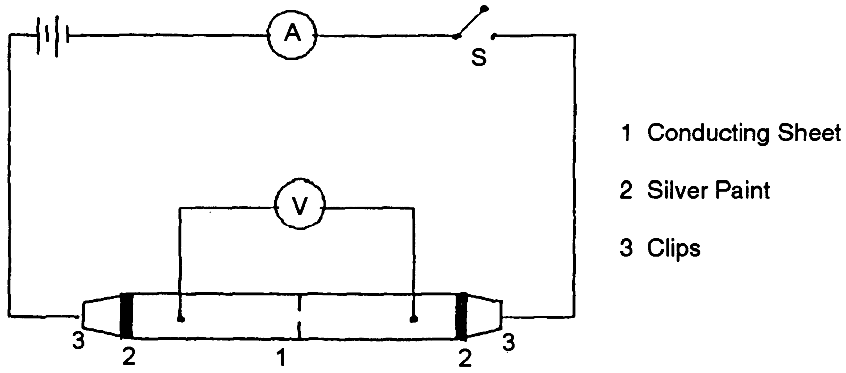

FIGURE 5.5. Conducting sheet analog for two-dimensional constrictions.

to the silver plated ends of this paper to simulate the isothermal boundary conditions (see, e.g., Veziroglu and Chandra, 1969). The schematic of the apparatus is shown in Fig. 5.5. A cut is made in the middle of the sheet to simulate the constriction. A mica insulating sheet is placed in the cut to avoid any electrical contact across the cut. The resistance with and without the cut is measured from which the additional resistance due to constriction is calculated by difference. Note that, in this method, it is also easy to obtain the lines of equipotential. Standard equipment such as the Servomex field plotter, are available for this purpose. This analogy has also been used in the determination of fin conduction shape factors required in the heat transfer analysis of finned tube heat exchangers (Sheffield et al., 1987).

For three-dimensional problems, it is necessary to use an electrolytic tank analogue (Karplus, 1958). This type of equipment has been used to measure the resistance of:

1. Single constrictions of various shapes (Major and Williams, 1977; Madhusudana, 1992).
2. Single and multiple constrictions of circular shape (Yip and Venart, 1968; Jeng, 1967; Cooper, 1969).
3. Macroscopic resistance of a bolted joint (Fletcher et al., 1989).

A diagram of the electrolytic cell used to determine the resistance of a single constriction is shown in Fig. 5.6. The following points must be noted in the design and use of an electrolytic tank analog:

1. A container is fabricated in such a way that the shape of the electrolyte within the container is a scale model of the field configuration under study. Boundaries, which are equipotential, are made

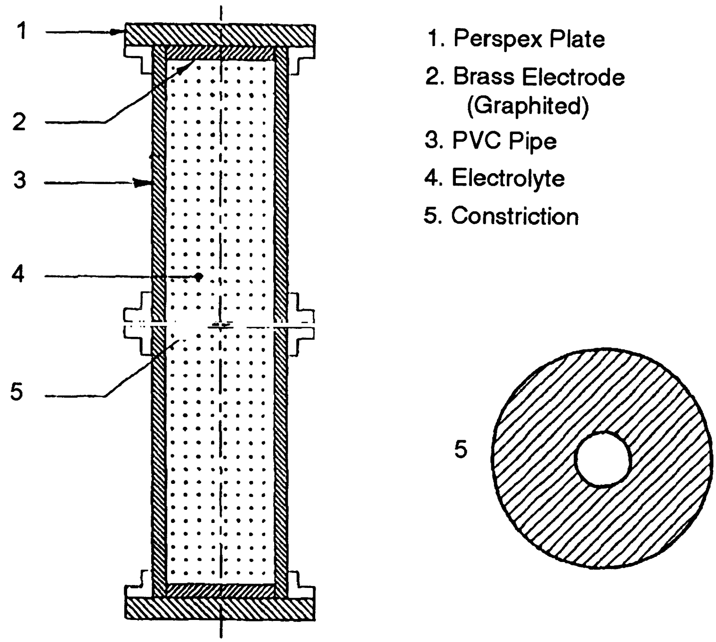

FIGURE 5.6. Electrolytic tank analog for three-dimensional constrictions.

of metal while insulating materials are employed for streamline boundaries.

2. To avoid polarization, AC voltages (frequency range 50 to 1500 Hz) should be used.
3. The electrolyte must be purely resistive.
4. To minimize error, the resistivity of the electrodes must be small compared to the resistivity of the electrolyte.
5. The surface impedance of the electrodes should be minimized by the use of graphite or platinum black coatings.

If the measurement of resistance is the only requirement, then the method is quite simple. The constriction is simulated by a plastic sheet cut to the required shape. Two measurements of the conductivity of the cell are made—one, with the constriction in place and the other, without the constriction—by means of an AC conductivity meter. Alternatively, the resistance may be measured in a universal bridge. Knowing the dimensions of the tank, the additional resistance due to the constriction may be calculated.

If the temperature profile is also required then a device such as the electronic-analogue field mapper as described by Karplus (1958) may be used. However, since we are mainly interested in determining the resistances, the additional complexities involved will defeat the purpose of obtaining quick and simple solutions. Furthermore, if an accurate temperature profile is indeed required, then it is desirable to perform a numerical analysis.

5.6 Accuracy

The contact heat transfer measurements, in general, are subject to error because of various uncertainties, including those in thermocouple calibration and location, and in thermal conductivity values required to calculate the heat flux. The experimental values are also affected by the heat transfer between the specimens and the surroundings.

In the axial heat flow apparatus, with careful design and experimentation, an experimental uncertainty of less than 10% is achievable for tests conducted in vacuum. For the tests conducted in a conducting medium, such as air, an uncertainty of 15% is probably more representative of the accuracy to be expected. It is possible to reduce this uncertainty by the provision of carefully controlled guard heaters.

In the radial heat flow apparatus, because of the difficulties in obtaining a truly axially symmetric heat distribution, in locating thermocouples accurately, and because of end effects, it is unrealistic to expect an accuracy better than about 20% when tests are done in a conducting medium. A higher accuracy could be obtained when test are carried out in vacuum conditions.

With analog methods, the uncertainty is controlled mainly by the accuracy of manufacture of the apparatus and the specimens, and the voltage measurement. With careful experimentation, uncertainties of less than 5% may be reasonably expected both in the conducting sheet and the three dimensional electrolytic tank analogs. The analog methods, however, have been mainly useful in the analysis of single constrictions.

It is worth noting that the very nature of contact resistance, depending as it does on the surface topography, introduces an uncertainty that requires that tests be performed on several pairs of similarly prepared specimens to obtain reliable estimates. No such requirement is necessary for surfaces that are random and isotropic (e.g., lapped and bead-blasted flat surfaces) or for surfaces in which the surface projections are uniformly distributed (e.g., crossed wedges or pyramids against flats). Finally, it should be pointed out that the theoretically predicted values are also subject to error due to their dependency on the measured values of microhardness and the surface profiles.

5.7 Summary

The foregoing is just a brief description of the main features of the more common types of equipment used in the experimental determination of the thermal contact resistance (and associated problems) in different situations. Space does not permit a fuller discussion of the design considerations, details of instrumentation, and the sources of error. Because of the rapid progress in technology and, in particular, microprocessor-based measurement and control, it is felt that any such information would have limited value. Readers interested in detailed information, however, may consult the references listed at the end of this chapter.

References

Cetinkale, T.N., and Fishenden, M. (1951). Thermal Conductance of Metal Surfaces in Contact. Proc Gen Disc Heat Transfer. Institute of Mechanical Engineers, London, pp. 271–275.

Cohen, I., Lustman, B., and Eichenberg, J.D. (1960). Measurement of Thermal Conductivity of Metal-Clad Uranium Oxide Rods During Irradiation. Report Wapd-228, Bettis Atomic Power Laboratory, 49 pp.

Cooper, M.G. (1969). A Note on Electrolytic Tank Analogue Experiments for Thermal Contact Resistance. Int J Heat Mass Transfer, 12:1715–1717.

Dodd, N.C., and Moses, W.M. (1988). Heat Transfer Across Aluminum/Stainless Steel Surfaces in Periodic Contact. AIAA Paper 88-2646. American Institute of Aeronautics and Astronautics, Washington, DC.

Fletcher, L.S., Peterson, G.P., Madhusudana, C.V., and Groll, E. (1989). Heat Transfer Through Bolted and Riveted Joints. ASME HTD, 123:107–115.

Fletcher, L.S., Smuda, P.A., and Gyorog, D.A. (1969). Thermal Contact Resistance of Selected Low-Conductance Interstitial Materials. AIAA J, 7:1302–1309.

Gardner, K.A. and Carnavos, T.C. (1960). Thermal Contact Resistance in Finned Tubing. Trans ASME, J Heat Transfer, 82:279–293.

Howard, J.R. (1976). An Experimental Study of Heat Transfer Through Periodically Contacting Surfaces. Int J Heat Mass Transfer, 19:367–372.

Hsu, T.R., and Tam, W.K. (1979). On Thermal Contact Resistance of Compound Cylinders. AIAA 14th Thermophysics Conf. Paper 79-1069. American Institute of Aeronautics and Astronautics, New York.

Jeng, D.R. (1967). Thermal Contact Resistance in Vacuum. Trans ASME, J Heat Transfer, 89:275–276.

Karplus, W.J. (1958). Analog Simulation (Solution of Field Problems). McGraw-Hill, New York, pp. 140–170.

Madhusudana, C.V. (1992). The Use of Electrolytic Tank for Solving Some Problems in Heat Conduction. J Energy, Heat, Mass Transfer, 14:59–64.
Madhusudana, C.V., and Litvak, A. (1990). Thermal Contact Conductance of Composite Cylinders: An Experimental Study. J Thermophys Heat Transfer, 4:79–85.
Major, S.J., and Williams, A. (1977). The Solution of a Steady Conduction Heat Transfer Problem Using an Electrolytic Tank Analogue. Inst Eng (Australia), Mech Eng Trans, pp. 7–11.
Mikic, B.B., and Rohsenow, W.M. (1966). Thermal Contact Resistance, Mech Eng Depart Report No. DSR 74542-41, MIT, Cambridge, MA.
Moore, C.J., Jr., and Blum, H.A. (1969). Effects of Transient Pressure Environments on Heat Transfer in One-Dimensional Composite Slabs with Contact Resistance. Prog Aero Astro, 21:621–636.
O'Callaghan, P.W., and Probert, S.D. (1972). An Improved Thermal Contact Resistance Rig. Meas. Control, 5(5):311–315.
Sheffield, J.W., Sauer, H.J., Jr., Wood, R.A. (1987). An Experimental Method for Measuring the Thermal Contact Resistance of Plate Finned Tube Heat Exchangers. ASHRAE Trans, 93(2): 776–785.
Veziroglu, T.N., and Chandra, S. (1969). Thermal Conductance of Two Dimensional Constrictions. Prog Astro Aero, 21:591–615.
Williams, A. (1966). Heat Transfer Through Metal to Metal Joints. 3rd Int. Heat Transfer Conf, American Institute of Chemical Engineers, New York, pp. 109–117.
Williams, A., and Madhusudana, C.V. (1970). Heat Flow Across Cylindrical Metallic Joints. 4th Int Heat Transfer Conf, Paper Cu 3.6.
Yip, F.C., and Venart, J.E.S. (1968). Surface Topography Effects in the Estimation of Thermal and Electrical Contact Resistance. Proc I Mech Eng, 182(3):81–91.

6
Control of Thermal Contact Conductance Using Interstitial Materials

As noted in Chapter 1, the actual solid-to-solid contact area, in most mechanical joints, is only a small fraction of the apparent area. The voids between the actual contact spots are usually occupied by some conducting substance such as air. Other interstitial materials may be deliberately introduced to control, that is, either to enhance or lessen, the thermal contact conductance: examples include foils, powders, wire screens, and epoxies. To enhance the conductance, the bare metal surfaces may also be coated with metals of higher thermal conductivity by electroplating or vacuum deposition. Greases and other lubricants also provide alternative means of enhancing thermal conductance of a joint.

In this chapter, interstitial materials will be grouped into the following categories for a discussion of their effect on thermal contact conductance:

Foils
Wire screens
Metallic and other coatings
Greases and lubricant films
Insulating interstitial materials

6.1 Solid Interstitial Materials

Filler materials may be used either to increase or to decrease the thermal contact conductance and, therefore, provide a means of thermal control. Futhermore, a joint with an interstitial material is less sensitive to mechanical loading and surface conditions and thus offers predictability of heat transfer behavior. Comprehensive reviews of the general role of interstitial materials in controlling the contact conductance have been published from time to time (see, e.g., Snaith et al., 1984; and Sauer, 1992). Some reviews have dealt with specific applications, for example, for spacecraft thermal control (Fletcher, 1973), or thermal enhancement for electronic systems (Fletcher, 1990).

When interstitial materials are used for the control of thermal conductance, it is desirable to have some means of comparing their effectiveness. Two parameters have been proposed for this purpose (Fletcher, 1973). The first of these parameters is, simply, the ratio of the logarithms of the conductances with and without the filler:

$$\varepsilon = \ln(h_{\mathrm{cm}})/\ln(h_{\mathrm{bj}})$$

in which the subscripts, cm, and, bj, refer to control material and bare junction, respectively. The second parameter takes the thickness of the filler material into account and is defined as

$$\eta = (ht)_{\mathrm{cm}}/(h\delta)_{\mathrm{bj}} \tag{6.1}$$

in which t is the thickness of the filler material and δ is the equivalent gap thickness calculated from (Fletcher and Gyorog, 1971)

$$\delta = 20.45 + 8.06(10^{-2})d - 1.58(10^{-5})d^2 + 1.36(10^{-9})d^3 - \cdots$$

$$d = (FD + 2RD)_{\mathrm{rs}} - 1/[2(FD + 2RD)_{\mathrm{ss}}]$$

in which FD is the flatness deviation and RD is the roughness. FD, RD, and δ are all specified in microinches (1 microinch = .0254 μm), rs and ss refer to the rough and the smooth surfaces, respectively.

In the present work the effectiveness as defined by Eq. (6.1) is not used because of the different units used and the fact that not all of the investigators report the flatness deviations. It seems more simple and direct to define the effectiveness as

$$e = h_{\mathrm{cm}}/h_{\mathrm{bj}} \tag{6.2}$$

This definition will be used in the following discussion. However, it must be emphasized that Eq. (6.1) highlights the important point that the relative thickness of the interstitial material is a significant parameter in controlling the conductance.

It this section, because of the different ways they control the contact conductance and their use in different applications, we will cosider metal foils, wire screens, insulation sheets, lubricant films, epoxies, and powders separately. For those categories in which a significant amount of experimental data generated by different investigators is available, tables are presented summarizing their results. It must be noted that the data presented is by no means exhaustive; only representative values are tabulated. It should also be noted that the figures given in these tables are approximate for the following reasons: In some cases they are extracted from graphs, in some cases they have been converted from imperial units, and in some instances the pressure and conductance per unit area have been calculated from the contact force, total conductance, and size of test specimens as published in literature.

6.2 Metallic Foils

In situations where the mechanical load on the joint has to be limited and/or when the joint is in vacuum, metal foils may be sandwiched between the bare metal surfaces. It would be then expected that the foil flows into the gaps between the surfaces thus increasing the actual contact area and enhancing the conductance.

One of the earliest experimental investigations into the effect of interfacial metal foils on thermal contact conductance was conducted by Fried and Costello (1962). Foils of lead and aluminum were used as interstitial materials between aluminum 2024-T3 surfaces.

On the other hand, Cunnington's (1964) experiments compared the conductance of the bare aluminum (6061-T4) junction with the conductance of the joint into which an indium foil had been inserted. Typical results (recast into SI units) of both these investigations are summarized below, in Table 6.1, in order to highlight the effect of the surface structure of the contacting surfaces. In each case, the bare junction conductances were measured in vacuums of less than 10^{-4} Torr. It may be noted that both of these investigations also dealt with interstitial materials other than foils. The effect of these other materials will be discussed at the appropriate sections.

TABLE 6.1. Effect of surface texture on contact conductance with a filler material.

Reference	Foil and foil thickness (μm)	Contact pressure (kPa)	Surface roughness (μm) rms	Flatness deviation (μm)	Contact conductance (W/m^2 K) bare junction	Contact conductance (W/m^2 K) with foil
Fried and	Lead	69	1.50 to 2.00	1125	190	730
Costello, 1962	(200)	207			300	830
Fried and	Aluminum	69	12 to 16	425	265	390
Costello, 1962	(50)	207			465	665
Cunnington,	Indium	276	0.30 to 0.45	0.875	2270	13060
1964	(25)		1.15 to 1.25	0.625	2780	21580
		552	0.30 to 0.45	0.875	3520	18740
			1.15 to 1.25	0.625	4540	27260

An inspection of this table reveals that:

1. The thermal contact conductance of the bare joint in vacuum is significantly increased by the insertion of a metallic foil.
2. Softer materials such as lead or indium were more effective as shims in enhancing the contact conductance.
3. Cunnington's tests show that the foil was more effective in enhancing the conductance of the rougher surfaces indicating that the optimum thickness depends on the roughness of surfaces. In these tests, it appears that the thickness of the foil used was closer to the optimum required for the rougher of the two pairs of surfaces.

Another early experimental investigation on the effect of interfacial metal foils was that undertaken by Koh and John (1965). In their tests, foils of copper, aluminum, lead, and indium were separately tested as interstitial materials between a pair of mild steel surfaces. Although copper and aluminum have high thermal conductivities, it was found that the insertion of these foils actually reduced the thermal contact conductance, whereas lead and indium foils contributed toward an increase in conductance. It was therefore confirmed that the foil softness was more significant in increasing the conductance than the foil conductivity. In another series of tests, the same authors found that there was an optimum thickness of foil, which would result in maximum enhancement of joint conductance. Apparently, thick foils are not pliable enough to fill the voids in the joint, while too thin a foil may not provide sufficient conduction material to fill the gaps in the interface. For the surface roughnesses range 4 μm to 5 μm rms encountered in the tests, the optimum thickness was found to be about 25 μm; at this thickness, the value of the conductance was about three times that for the bare junction. It was also found, for the specimens tested, a foil thickness greater than 100 μm produced no improvement in the contact conductance.

The enhancement of the contact conductance by the use of aluminum foil was also reported by Sauer et al. (1971), and Sauer (1992). The bare junction was of 2024-T4 aluminum surfaces (surface roughness of 0.77 μm), the contact pressure range was 1 to 4 Mpa, the foil thickness was 640 μm. The conductance increased by a factor of approximately 3 over the complete range of pressures. However, the bare junction was tested in air rather than in vacuum.

Yovanovich (1972) conducted a detailed experimental study of the effect of lead, tin, aluminum, and copper foils on the conductance of Armco iron joints. The contact pressure ranged from 2 to 10 MPa and the foil thicknesses from 10 to 500 μm. Unlike the tests of Fried and

Costello and those of Cunnington, the tests were conducted in atmospheric conditions. It was found that an optimum thickness, corresponding to minimum joint resistance, existed in all cases. The ratio of the optimum thickness to the surface roughness (rms) was found to be about 2 for lead, between 0.48 and 0.58 for aluminum, and 0.68 for copper. It was proposed that a foil material may be ranked by the ratio of its thermal conductivity to hardness; the larger the ratio the greater will be the increase in contact conductance.

The investigations of O'Callaghan et al. (1983, 1988) led them to conclude that, in the absence of macroscopic constrictions, the optimum film thickness should be of approximately the same magnitude as the separation between mean planes of the solid surfaces. Thus, for nominally flat surfaces, a relatively thin foil would be appropriate in enhancing the conductance. For surfaces with macroscopic errors of form or when macroscopic thermal distortions are expected, the thickness should be larger in order to bridge any gaps that would otherwise be formed. This second conclusion confirms the results of Fried and Costello (see Table 6.1), who used a very thick lead foil to maximize the conductance of a pair of surfaces with large flatness deviation.

An example of the results of the extensive experimental work of Peterson and Fletcher (1988) on the thermal contact conductance in the presence of foils is shown plotted in Fig. 6.1a. In each case, the thickness of the foil used corresponded to the optimum value suggested by Yovanovich (1972). These tests also indicated that enhancement of the conductance can be accurately ranked using the ratio of the foil thermal conductivity to hardness; the higher the value, the greater the enhancement. Indeed, Madhusudana (1994) showed that the four separate graphs showing the conductance versus contact pressure results for lead, tin, aluminum, and copper may be reduced to virtually a single line if the conductance and the contact pressure values are normalized by dividing them by foil conductivity and foil hardness respectively (see Fig. 6.1b). As can be seen, the results for tin are a slight exception and he suggested, in line with Eq. (6.1), that the ratio of surface roughness to the foil thickness should be another parameter to be considered in normalizing such data. Peterson and Fletcher also noted that foils, which were very thin (corresponding to optimum thickness required for nominally flat surfaces), were difficult to handle. Consequently, if they were not able to be applied properly, an actual decrease in conductance resulted due to the unintentional creation of folds and wrinkles.

Table 6.2 gives a summary of some representative experimental

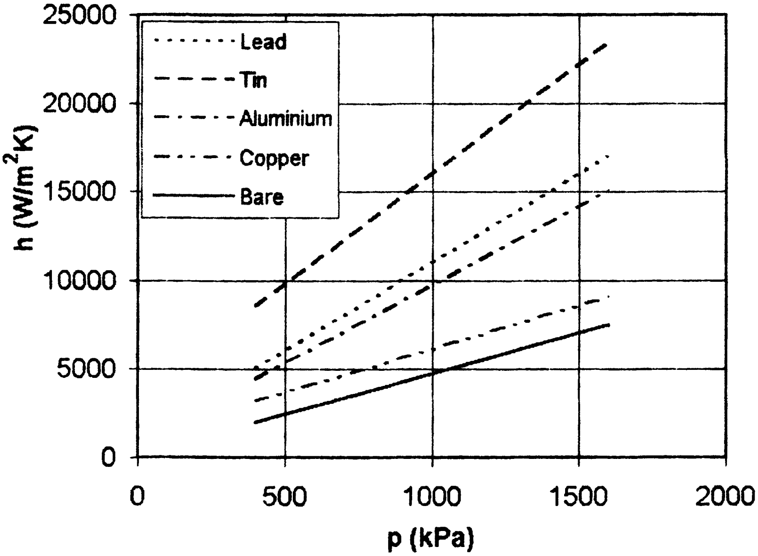

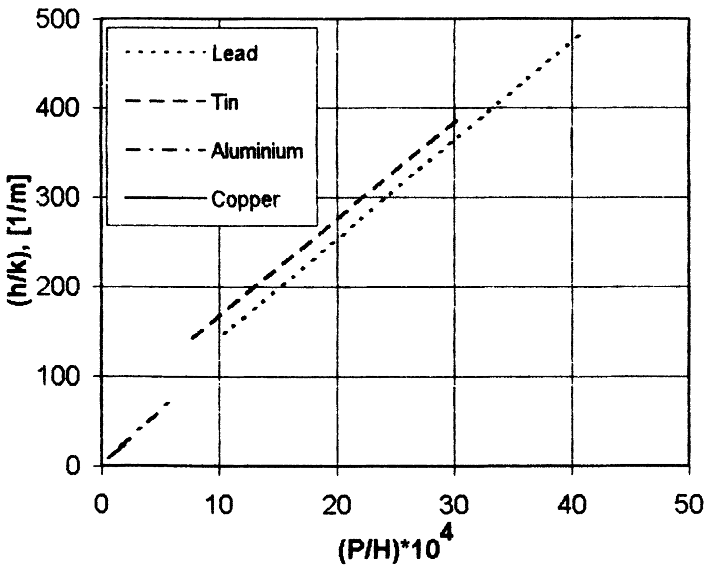

FIGURE 6.1. Thermal contact conductance in the presence of foils. (a) Data of Peterson and Fletcher, 1990. (b) "Normalized" data.

TABLE 6.2. Thermal contact conductance in the presence of foils.

Details	Cunnington, 1964	Fried and Costello, 1962	Sauer, 1992	O'Callaghan and Probert, 1988	Peterson and Fletcher, 1988
Substrate material	Aluminum 6061-T4	Aluminum 2024-T3	Aluminum 2024-T4	Duralumin/ titanium alloy	Aluminum 6061-T6
Conductivity	177	206	206	141/5.6	177
Hardness	1080	1600	1600	430 (Duralumin)	1080
Roughness	a. 0.30–0.45 b. 1.15–1.25	a. 0.15–0.20 b. 1.2–1.6	0.77	8.91/3.19	1.15/8.57
Flatness	a. 0.875 b. 0.625	a. 112.5 b. 42.5			
Foil material	Indium	a. Lead b. Aluminum	Aluminum	Aluminum	a. Copper b. Aluminum c. Lead d. Tin
Conductivity	80	a. 33 b. 206	206	206	a. 380 b. 206 c. 33 d. 60
Hardness	10	a. 40 b. 270	270	270	a. 800 b. 270 c. 40 d. 53
Thickness	25	a. 200 b. 50	640	25	a. 40 b. 30 c. 75 d. 100
Pressure	0.276–0.552	a. .069–.207 b. .069–.207	0.69–3.45	0.160–0.382	0.10–1.60
$h_{\mathrm{bare,vac}}$	a. 2270–3520 b. 3780–4540	a. 190–300 b. 265–465		178–382	800–7500
$h_{\mathrm{bare,air}}$			2960–4750		
h_{foil}	a. 13060–18740 b. 21580–27260	a. 730–830 b. 390–665	8520–13060	764–3972	a. 1800–10000 b. 2200–16000 c. 2200–18000 d. 4000–25000
$\frac{h_{\mathrm{foil}}}{h_{\mathrm{bare,vac}}}$	a. 5.75–5.32 b. 7.76–6.00	a. 3.84–2.77 b. 1.47–1.43		4.29–10.39	a. 2.25–1.33 b. 2.75–2.13 c. 2.75–2.4 d. 5–3.33
$\frac{h_{\mathrm{foil}}}{h_{\mathrm{bare,air}}}$			2.88–2.75		

Note: Conductivity in (W/mK), hardness and pressure in (MPa), surface roughness, flatness and foil thickness in (μm), and conductance in (W/m^2K).

results for the thermal conductance enhancement in the presence of foils.

6.3 Wire Screens

Fried and Costello (1962) considered that the contact conductance of poorly matching surfaces could be increased by the introduction of a copper wire screen, which would conform to the (large scale) surface irregularities and, therefore, would assure a large but finite number of contact spots. Their experiments, however, showed that the conductance, in fact, decreased due to the introduction of the wire cloth. It was concluded that the increase in resistance caused by the reduced effective contact area more than offset any reductions in individual contact spot resistance. In subsequent literature, therefore, wire screens have also been considered as a means of decreasing the contact conductance, that is, as thermal isolation materials, especially for those applications where mechanical strength is important.

The detailed experimental investigations of Gyorog (1971), using stainless steel and titanium wire mesh screens, also confirmed their use as thermal isolation materials. It was noted that coarse meshes, because of the fewer contact spots and the large wire diameter, gave rise to much lower conductances than fine meshes did. He also found that the insulation of aluminum surfaces with wire screens can be measurably improved by separating the screen from the surface with a stainless steel shim.

Experimental studies of stainless steel wire screens as the interstitial material were also carried out by Sauer et al. (1971). It was found that the TCC increased with increasing mesh number; the finer the mesh, the larger the number of contact points and hence, the larger the conductance. These results thus confirm those of Gyorog.

A theoretical model for the prediction of the contact conductance of a joint containing a wire screen was proposed by Cividino et al. (1975). Among other things, this model assumed elastic deformation of smooth, clean wires, and equal loading at all nodes. The theory was found to consistently overestimate the conductance when a comparison was made with the measured values.

The thermal behavior of copper wire gauzes inserted between stainless steel surfaces was the subject of an experimental study by O'Callaghan et al. (1975). They found that the presence of the gauze increased the conductance in vacuum but decreased it in air. Further experimental and theoretical work on the effect of copper wire gauzes was carried out by Al-Astrabadi et al. (1979). They observed that macroscopic constriction effects, due either to thermal distortions or to badly mating surfaces, may be reduced or even eliminated by the insertion of a copper gauze between the surfaces. The resulting reduction in constriction resistance may more than compensate for the greater bulk resistance because of the insert. Thus one might conclude that insertion of wire screens would decrease the resistance if there are large scale surface irregularities; the resistance is likely to increase if the surfaces are flat and conforming. In any case, the direction of change in the TCR would depend ultimately on the parent metal/wire material combination. Al-Astrabadi et al. also noted that the method of weaving the screens results in the weft being a series of almost straight wires, all in one plane, with the warp interlaced. Contact, therefore, occurs only between the warp and the solid surfaces, that is, only at *every other* crossing. This would be one of the reasons (Madhusudana and Fletcher, 1986) why the theory of Cividino et al., which assumed that contact occurred at *every* crossing, overestimated the conductance.

Table 6.3 summarizes the results of experimental investigations of thermal contact resistance in the presence of screens.

6.4 Surface Coatings

One way of reducing the TCR of a joint would be to plate or coat the surfaces with a material of high thermal conductivity. Whenever coatings are contemplated, the mechanical strength, stability, or durability with respect to operating conditions and time and adhesion to the parent surface are also important considerations. Plating would also result in a change in the contact geometry for a given load, since the plating material might have a different flow pressure from that of the bare material. For maximum benefit, both surfaces must be coated; when only one surface is coated, the whole constriction (or spreading) has to still take place in the other uncoated material.

6.4.1 *Constriction Resistance in a Plated Contact*

The analytical model, proposed by Mikic and Carnasciali (1970) for a *single* plated contact, is shown in Fig. 6.2. Here b_1 is a hypothetical intermediate radius. Physically, πb_1^2 represents the area at $z = t$, which is effectively used to transfer heat from the plated material to the base. To determine b_1, it was noted that, for given boundary conditions, of

TABLE 6.3. Thermal contact conductance in the presence of screens.

Details	Gyorog, 1971	Fried and Costello, 1962
Substrate material	Stainless Steel 304	Aluminum 2024-T3
Conductivity	15	206
Hardness	2550	1600
Roughness	0.075–0.150	0.150–0.200
Flatness	0.500–0.625	112.5
Screen material	Stainless Steel	Copper
Conductivity	15	380
Hardness	2550	1350
Mesh number	a. 100 b. 10	a. 50 b. 30
Pressure	0.690–2.090	.069–.207
$h_{\text{bare,vac}}$	359–2243 (Average of several values at each pressure)	190–300
h_{screen}	a. 186–364 b. 40–73	a. 160–270 b. 175–256
$\dfrac{h_{\text{screen}}}{h_{\text{bare,vac}}}$	a. 0.518–0.161 b. 0.111–0.32	a. 0.842–0.900 b. 0.921–0.853

Note: Conductivity in (W/mK), hardness and pressure in (MPa). Surface roughness and flatness in (μm), and conductance in (W/m^2K).

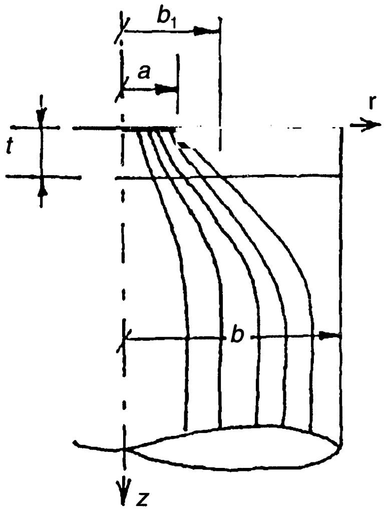

FIGURE 6.2. Single-plated contact.

all possible resistances which may be obtained by choice of flow distributions, the actual resistance is the one that gives the minimum value. Hence, for a fixed geometry and given thermal conductivities, the choice for b_1 for which the resistance is minimum, will yield the approximate (actually, an upper bound) constriction resistance.

Let

$$R_t = \text{resistance of the plated channel}$$

$$R = \text{resistance of the unplated channel}$$

Then

$$R_t = (1/4k_2a)[(16/\pi C)\phi(t/a, a/b_1)] + (1/4k_2b_1)F(b_1/b) \tag{6.3a}$$

$$R = (1/4k_2a)F(a/b) \tag{6.3b}$$

where

k_1 = thermal conductivity of the plating material
k_2 = thermal conductivity of the base metal
$C = k_1/k_2$
F = the appropriate constriction alleviation factor (See Eqs. 2.24 to 2.27)
ϕ = the contact resistance factor determined according to the above procedure

The contact resistance factor would depend on the boundary condition, isothermal or constant flux, applied over the contact spot.

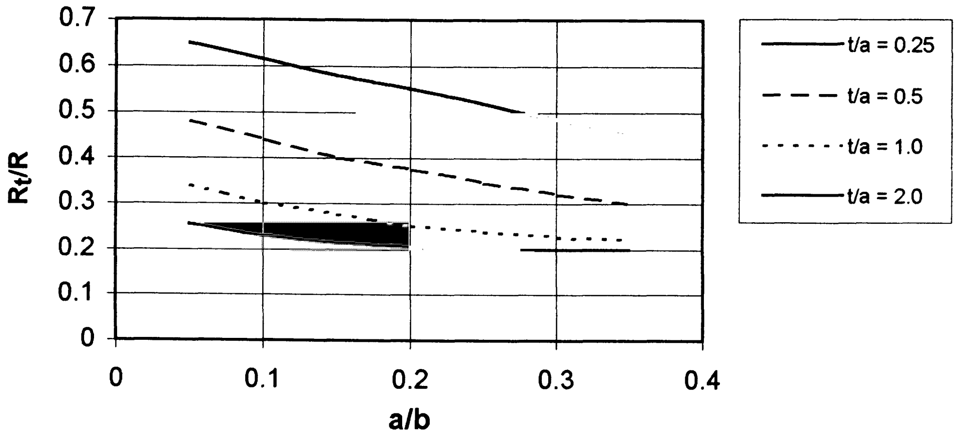

FIGURE 6.3. Reduction of resistance due to plating (based on the results of Mikic and Carnasciali, 1970).

From the above equations, it is noted that

$$R_t/R = F(a/b, t/a, C) \tag{6.4}$$

A typical result is shown plotted in Fig. 6.3 for the conductivity ratio, $C = 5.0$. It can be seen that considerable reduction in resistance can be obtained with sufficiently thick platings, $(t/a) > 2$.

For nominally flat surfaces, or, in general, when the microscopic resistance is predominant, the effect of plating in reducing the TCR could be very significant. Mikic and Carnasciali noted that, for wavy surfaces in contact, the contour area would be much too large to be affected by plating.

The analysis of Kharitonov et al. (1974) also confirmed that the TCR of a flat rough surface could be noticeably changed when the thickness of the coating is greater than the average contact spot radius, that is, $t > a$. Since $a \cong 30\,\mu$m, they concluded that coatings of a few tens of microns thick would cause a significant change. Kharitonov et al. considered not only conducting coatings but also insulating coatings such as oxide films. An open form solution was presented for the resistance.

For the limiting case when $(b/a) \to \infty$, the following approximate expression was given:

$$(R_t/R) = [1 + (1/C)\tanh(t/ma)]/[1 + C\tanh(t/ma)];$$

$$\begin{cases} m = 1 \text{ for } k_1 < k_2 \\ m = 1.5 \text{ for } k_1 > k_2 \end{cases} \tag{6.5}$$

Another theoretical analysis of a coated constriction in half space was that due to Dryden (1983). In this analysis, the heat flux distribution over the contact spot was assumed to be given by

$$f(r) = -Q/[2k_1\pi(a^2 - r^2)^{0.5}]$$

As seen in Chapter 2, this corresponds to an isothermal constriction.

The heat conduction equation was solved using Hankel transform of order zero. It was shown that the constriction resistance could be approximated by the following expressions:

Thin coatings, $(t/a) < 2$: $R_t = (1/4k_2 a) + (1/\pi k_1 a)(t/a)[1 - C^2]$ (6.6a)

Thick coatings, $(t/a) > 2$: $R_t = (1/4k_1 a) - (1/2\pi k_1 a)(a/t)$

$$\cdot \ln[2/(1 + C)] \qquad (6.6)$$

The theoretical analysis of Negus et al. (1988) also deals with coated constrictions in half space. As a result of this analysis, the following correlation was proposed for the isothermal constriction parameter for resistive layers $(0.01 < C < 1)$:

$$\psi_a = (0.12368 - 0.12309C - 0.00085C^2)\tanh(0.28479 + 1.3337B + 0.06864B^2) + 0.12325 + 0.14328C - 0.01657C^2 \qquad (6.7)$$

where

$B = \log_{10}(t/a)$

The constriction parameter in this case was defined by

$$F_a = k_1 a R_t$$

The disc constriction resistance of the unplated solid is

$$R = 1/(4ak_2)$$

Hence

$$R_t/R = 4aF_a/C$$

Negus et al. observed that no convenient expression could be found for conductive layers $(1 < C < 100)$.

For the elastic contact of a sphere with a coated flat surface, Fisher and Yovanovich (1989) presented an approximate analysis for estimating the contact spot radius, a. They noted that, for *thin* layers, the contact is effectively between the sphere and the substrate material. In such a case, the Hertzian contact radius is:

$$a_s = [(3/4)(W\rho/E_s)]^{1/3} \qquad (6.8)$$

where

W = mechanical load
ρ = radius of the spherical indenter
$1/E_s = (1 - \nu_1^2)/E_1 + (1 - \nu_2^2)/E_2$
E = Modulus of elasticity
ν = Poisson's ratio

and the subscripts 1 and 2 refer to the sphere and the flat substrate, respectively.

For *thick* layers, the situation is similar except that the flat surface is assumed to be composed of the coating material. In this case, the contact radius is:

$$a_L = [(3/4)(W\rho/E_L)]^{1/3} \tag{6.9}$$

where $1/E_L = (1 - \nu_1^2)/E_1 + (1 - \nu_c^2)/E_c$, and the subscript, c, refers to the coating material.

If $\alpha = a_L/a_s$, it is seen that $\alpha = \gamma^{-1/3}$ where $\gamma = E_L/E_s$. For common metallic materials, $0.2 \leq \gamma \leq 5$, so that, $1.7 \geq \alpha \geq 0.6$. In other words, the bounding radii do not vary a great deal. Hence the authors proposed that the arithmetic mean of the two bounds be taken as a good estimate of the contact radius. This radius is then used in conjunction with Dryden's (1983) analysis to obtain the constriction resistance.

6.4.2 Thermal Contact Conductance of Coated Surfaces

The discussion, so far, in this section refers to the constriction of a *single* contact spot on a coated surface. Analytical and experimental studies exist also of the TCC of *whole* coated surfaces. Some of these studies are described in this section.

In the theoretical part of the analysis of Antonetti (1983), and Antonetti and Yovanovich (1985), the coated metallic interface (soft metallic layer on a harder substrate) was reduced to an equivalent uncoated surface using concepts of effective hardness, H', and effective thermal conductivity, k'.

The effective microhardness was determined on the basis of experimental observations. It was noted that, when coating is thin, the hardness is mainly controlled by that of the substrate whereas, for thick coatings, the hardness of the coating is the controlling factor. The following relations were deduced:

$$H' = H_s[(1 - (t/d)] + 1.81H_c(t/d) \quad (t/d) < 1 \tag{6.10a}$$

$$H' = 1.81H_c - 0.208H_c[(t/d) - 1] \quad 1 \leq (t/d) \leq 4.9 \tag{6.10b}$$

in which the subscripts, s and c, refer to the substrate and the coating material respectively, t, is the thickness of coating and, d, is the equivalent indentation depth of the harder contacting surface obtained from a Vickers microhardness test. It should be emphasized that the above relations were obtained for vapor deposited silver on Nickel 200 specimens. The results can, therefore, be applied only to that coating/substrate combination. The results are not general. In any case, the determination of the effective hardness, as defined above, would involve a series of microhardness tests.

The effective thermal conductivity was defined as

$$k' = 2k_\alpha k_\beta/[C_\alpha k_\beta + C_\beta k_\alpha] \tag{6.11}$$

where α and β refer to the two sides of the contact and C is the constriction parameter correction factor, which must be determined by the thermal analyses of a surface with a layer and the surface without a layer.

With these definitions, the following relationship was derived between the contact conductance and the contact pressure:

$$h\sigma/(k' \tan\theta) = 1.25(P/H')^{0.95} \tag{6.12}$$

The experimental data of Peterson and Fletcher (1990) on anodized aluminum coatings, varying in thickness from 60.9 to 168.3 μm, in contact with an uncoated aluminum 6061-T6 surface, yielded the correlation

$$(ht/k)(t/\sigma)^{-0.25} = 0.83(10^{-2})(P/H) + 0.11(10^{-4}) \tag{6.13}$$

It is noted that any variation of surface thermophysical properties, due to anodization, was not reflected in the above correlation; also, only one of the interfaces was anodized.

An experimental study of the effect of metallic coatings on the TCC of turned surfaces was reported by Kang et al. (1990). Tests using coatings of tin, indium, and lead, four different thicknesses in each case, on bare aluminum 6061-T6 surfaces indicated that, for each coating material/surface combination, there existed an optimum thickness, which yielded the maximum conductance. The optimum thickness was found to be in the range 0.2–0.5 μm for tin, 2–3 μm for indium, and 1.5–2.5 μm for lead.

It may be recalled that the correlation proposed by Antonetti and Yovanovich (1985) was applicable only to *flat* nickel surfaces coated with silver and also required experimental and theoretical determination of the effective hardness and effective thermal conductivity. In order to derive a general, usable correlation, Lambert and Fletcher

(1993) analyzed 654 individual data points obtained from tests on 99 joints by nine different investigators and obtained the relation:

$$(h\sigma/k' \tan\theta) = 0.00977(P/H')^{0.520} \tag{6.14}$$

Since engineering surfaces are typically nonflat and wavy, the data for optically flat surfaces were excluded in a subsequent analysis. The remaining 579 data points, from 85 joints, yielded the correlation:

$$(h\sigma/k' \tan\theta) = 0.00503(P/H')^{0.455} \tag{6.15}$$

In cases where the combined mean slope, $\tan\theta$, of the surfaces was not furnished in the source investigation, it was estimated from the correlation:

$$\tan\theta = \sqrt{(\sigma/100)} \tag{6.16}$$

In either case, it could be seen that the slope of the conductance versus pressure graph is significantly smaller than the slope of 0.95 obtained for flat surfaces. This indicates that non-flat, or wavy surfaces are less sensitive to contact pressure variation than are flat surfaces. Table 6.4 summarizes the results of some experimental investigations on coated surfaces.

A new type of surface coating, the transitional buffering interface (TBI), was used in the studies of Chung et al. (1992, 1993a, 1993b) and Sheffield and Chung (1992). This process involved plasma-enhanced deposition of a thin coating of a two-phase mixture of either copper and carbon or silver and carbon. In each case, the relative ratio (Cu to C or Ag to C) could be altered by changing the deposition parameters, thus giving the desired chemical gradient through the coatings. This process is said to offer excellent characteristics of adhesion of the coating to a wide range of base materials as well as close control of coating thickness and surface roughness. In all of the experiments to be discussed in this section, the base material was aluminum 6061-T651.

Very thin coatings ($<0.4\,\mu$m) of silver or silver–carbon showed no consistent improvement in the TCC over that of the bare surfaces (Williams and Sherbrooke, 1992). It was concluded that such thin films did not significantly affect the real contact configuration.

Chung et al. (1993a) found that the silver–carbon coatings produced stronger adhesion than pure silver coatings. It was noted that, for both smooth and rough surfaces, the enhancement in conductance produced by coatings of silver and copper were significantly greater than those produced by silver–carbon and copper–carbon, respectively (see also, Sheffield and Chung, 1992). Sheffield and Chung noted

TABLE 6.4. Thermal contact conductance of coated surfaces.

Details	Antonetti and Yovanovich, 1985	Kang, Peterson, and Fletcher, 1990	Marotta et al., 1994	Lambert and Fletcher, 1992	Lambert and Fletcher, 1993
Substrate material	Nickel 200	Aluminum 6061-T6	Aluminum 6101-T6	Aluminum A351-T6[2]	Aluminum A351-T6[2]
Conductivity	77	179	207	151	151
Hardness	2750	980	410	980	980
Roughness	a. 1.27 b. 4.27 c. 8.32	1.00 (0.98–1.04)	0.87 (average)	0.45 (average)	0.45 (average)
Coating material	Silver	a. Tin b. Indium c. Lead	a. Titanium Nitride b. Beryllium Oxide	a. Gold b. Silver	Silver
Method of coating	Vapor deposited	Vapor deposited	Physical vapor deposited	Vapor deposited	a. Electroplated b. Flame sprayed
Conductivity	425	a. 65.8 b. 81.7 c. 37.0	a. 24 b.	a. 315 b. 427	427
Hardness	390	a. 49 b. 9.8 c. 39.2	a. 2600 b. 4900	a. 1250 b. 1250	1250
Thickness	a. 1.2; 6.3 b. 0.81; 1.4; 39.5 c. 2.4; 7.2; 18.0	a. 0.25; 0.76; 1.82 b. 0.28; 2.54; 3.71 c. 0.25; 1.8; 5.0	a. 3 b. 3	a. 1; 3 b. 1; 3	a. 13; 51 b. 13; 76
Pressure	500–3700 kPa	75–1600 kPa	170–700 kPa[4]	170–860 kPa	170–860 kPa
$h_{\text{bare,vac}}$	a. 2600–12000 b. 1100–8000 c. 1000–5400	1000–10500[2]	3500–8800	700–2000	700–2000
h_{coated}	a. 12000–58000 20000–70000[1] b. 2200–12000 4000–23000 11000–95000 c. 2200–14000 5200–33000 9500–58000	a. 170–12800 b. 1920–33370 c. 1990–22460	a. 2200–7900 b. 3000–9200	a. 1300–3000; 600–1800; b. 550–2500; 1200–4000	a. 1900–4500; 800–2100 b. 420–1250; 400–900
h_c/h_{bv}	a. 4.61–4.83; 7.69–8.75 b. 2–1.5; 3.64–2.88; 10–11.88 c. 2.2–2.59; 5.2–6.11; 9.5–10.74	a. 1.7–1.22; 0.85–0.75; 0.35–0.50 b. 2.6–1.9; 7.0–2.8; 2.3–1.8 c. 1.5–1.2; 4.2–2.2; 2.0–1.2	a. 0.65–0.90 b. 0.85–1.05	a. 1.86–1.5; 0.86–0.9 b. 0.78–1.25; 1.70–2.00	a. 2.7–2.25; 1.15–1.05 b. 0.6–0.62; 0.57–0.45

[1] At 1800 kPa; the corresponding bare joint conductance was 8000 W/m^2 K.
[2] Average for 12 pairs of surfaces.
[3] The other surface, common to all contacts, was electroless nickel-plated copper.
[4] Range for which the enhancement is reported.
Note: Units, except for pressure, as in Table 6.3.

that improvements in conductance of the order of 100% were observed when both surfaces were coated compared to the case when only one surface was coated, thus confirming the observation of Mikic and Carnasciali (1970).

Experimental results for the TCC of a ceramic (Al_2O_3) coated with thin (typically 0.2 to 0.3 μm) aluminum, copper, and iron carbide have been reported by Chung et al. (1993b). As expected, an enhancement of conductance was noted with aluminum or copper coatings, but TCC was reduced when the iron carbide coating was used.

6.5 Insulating Interstitial Materials

In applications such as isolation of spacecraft equipment, cryogenic storage tanks, and, in general, wherever strong insulating supports are required, it is necessary to increase the TCR. The use of wire screens as a means of increasing the TCR has already been noted in this chapter. Another method of achieving thermal isolation is by the introduction of low conductance interstitial materials in the interface.

The works of Fletcher et al. (1969), Smuda and Gyorog (1969), Gyorog (1970), Fletcher and Miller (1973), and Fletcher et al. (1976) are just some examples of the experimental investigations into the effect of thermal isolation materials on the TCR. Carbon paper, ceramic paper, WR-X-AQ felt, and T-30LR laminate were found to be good materials for increasing the resistance. Typically, the TCC values for aluminum 2024-T4 junctions reduced from 1000 to between 1 and 10 BTU/hr.ft.^{2} °F (from 5680 to between 5.68 and 56.8 W/m^2 K) in the pressure range 100 to 300 psi (0.69 to 2.07 MPa) and the temperature range -100 to 200 °F (-73 to 93 °C). It was noted by Fletcher et al. (1969) that Teflon, because of its comparatively high thermal conductivity, produced a relatively small reduction in the TCC. Gyorog (1970) observed that dusting of surfaces with powders such as manganese oxide or rutile produced noticeable reductions in the conductance, but the results were somewhat unpredictable and difficult to control.

The results of Fletcher and Miller for gasket materials for spacecraft joints indicated that elastomers were suitable for thermal control, producing an order of magnitude (or better) reduction in TCC. In particular, the silicone elastomers could be used over a large temperature range: -130 to 500 °F (-90 to 260 °C). By contrast, polyethelene materials, although effective in providing isolation, could be used only over a narrow temperature range, typically -60 to 150 °F (-51 to 66 °C) (see Table 6.5).

TABLE 6.5. Thermal contact conductance with insulating interstitial materials.

Details	Fletcher et al., 1969	Gyorog, 1971	Fletcher and Miller, 1973
Substrate material	Aluminium 2024-T4	Stainless Steel AISI304	Aluminium 2024-T4
Conductivity	210	15	210
Hardness		2550	
Roughness	0.076–0.152	0.076–0.152	0.381
Interstitial material	a. WRP-AX-AQ Felt b. Mica c. Teflon	a. WRP-AX-AQ Felt b. Mica c. Teflon	a. Carbon black filled fluorocarbon elastomer b. Neoprene c. Silver coated copper powder filled silicone elastomer
Conductivity	a. 0.069 b. 0.363 c. 2.34	a. 0.069 b. 0.363 c. 2.34	
Density, kg/m^3	a. 288 b. 208 c. 160	a. 288 b. 208 c. 160	a. 1875 b. 645 c. 3650
Thickness, mm	a. 4.47 b. 0.05 c. 0.05	a. 4.65 b. 0.076 c. 1.57	a. 2.1 b. 2.9 c. 0.71
Pressure	690–2070	690–2070	690–2070
$h_{bare,vac}$	7100–15000	360–2240	4300–6900
h_{insul}	a. 5–9 b. 280–730 c. 1730–2310	a. 3–5 b. 150–300 c. 16.5–17.5	a. 90–135 b. 125–190 c. 1470–1730
$\frac{h_{insul}}{h_{bare,vac}}$	a. 0.0007–0.0006 b. 0.039–0.049 c. 0.244–0.154	a. 0.008–0.002 b. 0.217–0.134 c. 0.046–0.008	a. 0.021–0.019 b. 0.029–0.028 c. 0.342–0.251

6.6 Lubricant Films and Greases

It is to be expected that, when the interface is charged with a grease, the conductance would be noticeably increased due to the establishment of better thermal bridges across the interstitial gaps. Cunnington (1964) conducted tests in vacuum at contact pressures ranging from 40 to 80 psi (276 to 551 kPa) and observed that the conductance of an aluminum joint increased by more than an order of magnitude when the contact surfaces were coated with DC-340 grease. In fact, the improvement in conductance was much greater than that obtained by the insertion of an indium foil, which is one of the most effective materials for enhancing the TCC. The use of a silicone grease was less effective although it produced enhancements of similar magnitudes to that produced by the indium foil. The reason was that the conductivity of the silicone grease was estimated to be only half the conductivity of the DC-340 grease. It was further noticed that the results for grease would be applicable to much wider range of joint configurations because of the ability of the grease to flow and fill the interstitial spaces at relatively low contact pressures. In other words, grease-filled joints would be less sensitive to changes in roughness and flatness of surfaces.

Experimental results for stainless steel surfaces treated with four different types of lubricant films, namely, silicone spray, Molykote, lithium and graphite greases, have been reported by Sauer et al. (1971) and Sauer (1992). All four lubricants provided enhancement, 8- to 70-fold, compared to vacuum conductance of the bare joint and 0 to 60% compared to the bare joint conductance in air. It was noted, however, that the lithium grease was the most effective and the graphite lubricant the least effective. The mean junction temperature of the tests was about 90 °C.

When the use of grease is considered for conductance enhancement, it may be noted that their thermal performance may deteriorate with time due to the loss of the volatile constituents in the grease.

6.7 Other Interstitial Materials

A variety of other fillers have been tested from time to time, the objective, in most cases, being the enhancement of the TCC. For example, Sauer (1992) tested the use of silica cement, epoxy resin, and thermosetting rubber in stainless steel–stainless steel, aluminum–aluminum, and copper–copper joints. The results, however, were not conclusive in that the insertion of such materials did not always increase the conductance compared to the bare joint conductance in air. It appears, however, that the thickness of the bond has to be small, of the order of 0.10 mm, for enhancement to occur.

In electronic packaging, heat generating components are typically mounted on printed circuit boards, which must be removed from the housing or rack for periodic maintenance. Thus the heat generated must pass through multiple mechanical interfaces before being absorbed by a remote cooling medium. A novel concept for reducing the TCR, using a low melting point interstitial material, at these interfaces was proposed by Cook et al. (1982). At room temperature, the alloy is in solid state to facilitate ease of handling during assembly and disassembly. During operation, heat transferred to the joint raises the interface temperature causing the alloy to change phase into the liquid state. Thus a continuous metallic heat transfer path is provided, significantly reducing the TCR. The authors proposed three ways in which the low melting point material may be inserted between the contacting surfaces:

1. As a thin sheet by itself.
2. As a filler in a thin porous metal structure.
3. As coatings on both sides of a thin solid metal sheet.

Also in relation to thermal management of electronic packages, Ochterbeck et al. (1990) observed that the enhancement of the TCC, while simultaneously insulating electrically, could be difficult. Only Isostrate, which is a Kapton MT coating (DuPont polyimide film) provided an increase in the TCC while all other electrically insulating films caused decrease in the TCC.

References

Al-Astrabadi, F.R., O'Callaghan, P.W., Probert, S.D., and Jones, A.M. (1977). Thermal Resistances Resulting from Commonly Used Inserts Between Stainless Steel Static Bearing Surfaces. Wear, 40(3):339–350.

Antonetti, V.W. (1983). On the Use of Metallic Coatings to Enhance Thermal Contact Conductance. Ph.D. Thesis, University of Waterloo, Canada.

Antonetti, V.W., and Yovanovich, M.M. (1985). Enhancement of Thermal Contact Conductance by Metallic Coatings: Theory and Experiment. Trans ASME, J Heat Transfer, 107:513–517.

Chung, K.C., Sheffield, J.W., and Sauer, Jr., H.J. (1992). Thermal Constriction Resistance of Phase-Mixed Metallic Coatings. Trans ASME, J Heat Transfer, 114:811–818.

Chung, K.C., Sheffield, J.W., Sauer, Jr., H.J., and O'Keefe, T.J. (1993a). Thermal Contact Conductance of a Phase Mixed Coating by Transitional Buffering Interface. J Thermophys Heat Transfer, 7(2):326–333.

Chung, K.C., Benson, H.K., and Sheffield, J.W. (1993b). Thermal Contact Conductance of Coated Junctions within Microelectronic Packages. AIAA Paper 93-2774, AIAA 28th Thermophys Conf. American Institute of Aeronautics and Astronautics. Washington, DC.

Cividino, S., and Yovanovich, M.M. (1975). A Model for Predicting the Joint Conductance of a Woven Wire Screen Contacting Two Solids. Prog Astro Aero, 39:111–128.

Cook, R.S., Token, K.H., and Calkins, R.L. (1982). A Novel Concept for Reducing Thermal Contact Resistance. AIAA/ASME Joint Conf. St. Louis. American Institute of Aeronautics and Astronautics, New York.

Cunnington, G.R., Jr. (1964). Thermal Conductance of Filled Aluminium and Magnesium Joints in a Vacuum Environment. ASME Paper 64-WA/HT-40. American Society of Mechanical Engineers, New York.

Dryden, J.R. (1983). The Effect of a Surface Coating on the Constriction Resistance of a Spot on an Infinite Half Space. Trans ASME, J Heat Transfer, 105:408–410.

Fisher, N.J., and Yovanovich, M.M. (1989). Thermal Constriction Resistance of Sphere/Layered Flat Contacts: Theory and Experiment. Trans ASME, J Heat Transfer, 109:249–256.

Fletcher, L.S. (1972). A Review of Thermal Control Materials for Metallic Junctions. J Spacecraft Rockets, 849–950.

Fletcher, L.S., and Gyorog, D.A. (1971). Prediction of Thermal Contact Conductance Between Similar Metal Surfaces. Prog Astro Aero, 24:273–288.

Fletcher, L.S., and Miller, R.G. (1973). Thermal Conductance of Gasket Materials for Spacecraft Joints. Prog Astro Aero, 35:335–349.

Fletcher, L.S., Smuda, P.A., and Gyorog, D.A. (1969). Thermal Contact Resistance of Selected Low-Conductance Interstitial Materials. AIAA J, 7(7):1302–1309.

Fletcher, L.S., Cerza, M.R., and Boysen, R.L. (1976). Thermal Conductance and Thermal Conductivity of Selected Polyethylene Materials. Prog Astro Aero, 49: 371–480.

Fried, E., and Costello, F.A. (1962). Interface Thermal Contact Resistance Problem in Space Vehicles. ARSJ, 237–243.

Gyorog, D.A. (1971). Investigation of Thermal Isolation Materials for Contacting Surfaces. Prog Astro Aero, 24:310–336.

Kang, T.K., Peterson, G.P., and Fletcher, L.S. (1990). Effect of Metallic Coatings on Thermal Contact Conductance of Turned Surfaces. Trans ASME, J Heat Transfer, 112:864–871.

Kharitonov, V.V., Kokorev, L.S., and Tyurin, Yu.A. (1974). Effect of Thermal Conductivity of Surface Layer on Contact Thermal Resistance. Atomnaya Energiya, 36(4):308–310.

Koh, B., and John, J.E. (1965). The Effect of Foils on Thermal Contact Resistance. Paper 65-HT-44, ASME-AIChE Heat Transfer Conf. American Society of Mechanical Engineers, New York.

Lambert, M.A., and Fletcher, L.S. (1992). A Review of Thermal Contact Conductance of Junctions With Metallic Coatings and Films. AIAA Paper 92-0709, AIAA 30th Aerospace Meeting, Reno, NV.

Lambert, M.A., and Fletcher, L.S. (1993). A Correlation for the Thermal Contact Conductance of Metallic Coated Metals. AIIA 28th Thermophys Conf, Paper AIAA 93-2778. American Institute of Aeronautics and Astronautics, Washington, DC.

Madhusudana, C.V. (1994). Control of Thermal Contact Conductance—Some Practical Considerations. In: Heat and Mass Transfer, Balakrishnan, A.R. and Srinivasa Murthy, S. (eds.). Tata McGraw-Hill, New Delhi, pp. 183–188.

Madhusudana, C.V., and L.S. Fletcher (1986). Contact Heat Transfer—The Last Decade. AIAA J, 24(3):510–523.

Marotta, E.E., Lambert, M.A., and Fletcher, L.S. (1994). Thermal Enhancement Coatings and Films for Microelectronic Systems. Proc 10th Int Heat Transfer Conf, Paper 15-CI-15. Institution of Chemical Engineers, Rugby, UK.

Mikic, B., and Carnasciali, G. (1970). The Effect of Thermal Conductivity of Plating Material on Thermal Contact Resistance. Trans ASME, J Heat Transfer, 92:475–482.

Negus, K.J., Yovanovich, M.M., and Thompson, J.C. (1988). Constriction Resistance of Circular Contacts on Coated Surfaces: Effect of Boundary Conditions. J Thremophys, 2:158–164.

O'Callaghan, P.W., and Probert, S.D. (1988). Reducing the Thermal Resistance of a Pressed Contact. Appl Energy, 30:53–60.

O'Callaghan, P.W., Snaith, B., and Probert, S.D. (1983). Prediction of Interfacial Filler Thickness for Minimum Thermal Contact Resistance. AIAA J, 21(9):1325–1329.

Ochterbeck, J.M., Fletcher, L.S., and Peterson, G.P. (1990). Evaluation of Thermal Enhancement Films for Electronic Packages. Paper 17-Cd-05, 9th Int Heat Transfer Conf, Jerusalem. Hemisphere, New York, pp. 445–450.

Peterson, G.P., and Fletcher, L.S. (1988). Thermal Contact Conductance in the Presence of Thin Metal Foils. AIAA Paper 88-0466. American Institute of Aeronautics and Astronautics, Washington, DC.

Peterson, G.P., and Fletcher, L.S. (1990). Measurement of Thermal Contact Conductance and Thermal Conductivity. Trans ASME, J Heat Transfer, 112:579–585.

Sauer, H.J., Jr. (1992). Comparative Enhancement of Thermal Contact Conductance of Various Classes of Interstitial Materials. NSF/DITAC Workshop, Melbourne, Monash University, Victoria, Australia, pp. 103–115.

Sauer, H.J., Jr., Remington, C.R., Stewart, W.E., Jr., and Lin, J.T. (1971). Thermal Contact Conductance With Several Interstitial Materials. Proc Int Conf Therm Cond, 11:22–23.

Sauer, H.J., Jr., Remington, C.R., and Heizer, G. (1971). Thermal Contact Conductance of Lubricant Films. Proc Int Conf Therm Cond, 11:24–25.

Sheffield, J.W., and Chung, K.C. (1992). Thermal Contact Conductance of Metal to Metal and Metal to Ceramic Joints. NSF/DITAC Workshop, Melbourne, Monash University, Victoria, Australia, pp. 13–18.

Smuda, P.A., and Gyorog, D.A. (1969). Thermal Isolation With Low Conductance Interstitial Materials Under Compressive Loads. AIAA Paper 69-25. American Institute of Aeronautics and Astronautics, New York.

Snaith, B., O'Callaghan, P.W., and Probert, S.D. (1984). Interstitial Materials for Controlling Thermal Conductances Across Pressed Metallic Contacts. Appl Energy, 16:175–191.

Williams, A., and Sherbrooke, P. (1992). Thermal Conductance of Aluminium Contacts Having Transitional Buffering Interface (TBI) Coatings. NSF/DITAC Collaborative Workshop on Thermal Conductance Enhancement in Microelectronics, Monash University, Australia, pp. 87–91.

Yovanovich, M.M. (1972). Effect of Foils Upon Joint Resistance: Evidence of Optimum Thickness. Prog Astro Aero, 31:227–245.

7
Special Topics in Thermal Contact Conductance

The discussion, so far, has been concerned basically with the general nature of contact heat transfer. In this chapter, some specific problems in thermal contact conductance will be considered. These include special contact configurations, such as bolted or riveted joints, and cylindrical joints. The effect of the direction of heat flow and the loading history will be considered next in separate sections. This is followed by a discussion of packed beds and stacks of laminations. In these applications, the contact resistance plays a major role in controlling their effectiveness as insulators. Finally, in view of their particular significance, contact heat transfer in specific materials, such as nuclear fuel elements and other specific materials, and the contact conductance in the presence of oxide films, will be considered in some detail.

Unlike the previous chapters, the sections of the present chapter are substantially independent of each other and each section can, therefore, be read without reference to another. The references for this chapter are also grouped under the appropriate headings.

7.1 Bolted or Riveted Joints

Bolted and riveted joints represent some of the most commonly used connections in engineering practice. It has been well known for a long time that when two plates are joined together by a central bolt, the contact area is limited to a relatively small annulus around the bolt hole (Rötscher, 1927). This area will be called the "contact zone" in the following discussion. As will be described in the next section, recent theoretical and experimental analyses have indeed confirmed that the contact pressure decreases from a maximum near the edge of the bolt hole to nearly zero within a short radial distance (see Fig. 7.1). In Figure 7.1, c and α define a conical envelope in which most of the

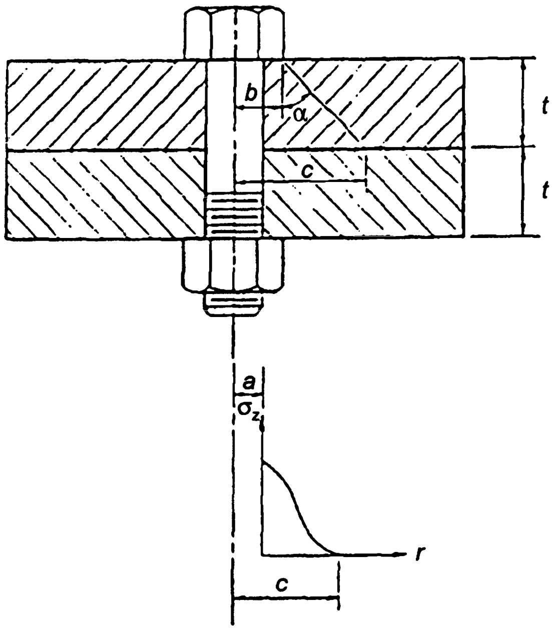

FIGURE 7.1. Interfacial stress in a bolted joint.

variation in stress takes place and, therefore, α is sometimes called the cone dispersion angle. It is clear, therefore, that the total resistance to the axial heat flow through a bolted joint must consist of two parts:

a. A "macroscopic" resistance resulting from the constriction and spreading of the heat flow lines through the contact zone (Fig. 7.2), and
b. A "microscopic" resistance associated with the individual contact spots located within the contact zone.

It would thus appear that the extent of the contact zone, that is, the outer radius of the annulus should first be estimated before a thermal analysis is undertaken to determine the overall thermal resistance of a bolted or riveted joint. In other words, the stress distribution at the interface of the joint must first be determined.

7.1.1 Stress Distribution at the Bolted Joint Interface

As an introduction to this problem, the simpler problem of a solid plate subjected to a uniform pressure over a central circular area will be considered first. The actual problem of two plates with central

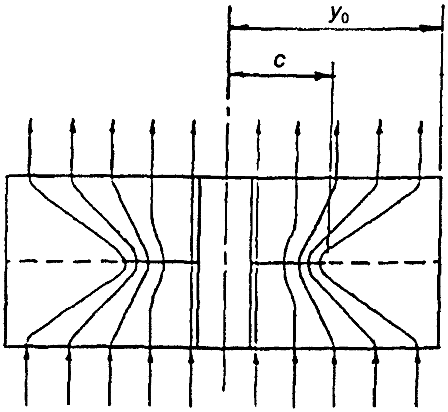

FIGURE 7.2. Heat flow through a bolted joint.

holes subjected to pressure over an annular area will be considered next.

One of the first mathematical investigations related to this problem was that described by Sneddon (1946). In this analysis, the stress distribution at different planes of a semi-infinite elastic medium subjected to a uniform pressure on parts of the boundary was considered. The solution to the biharmonic differential equation in cylindrical coordinates was obtained using Hankel transforms. The axial stress distribution at mid-plane ($z = 0$) for uniform pressure, p, applied over a circular area of radius, a, is shown in Fig. 7.3.

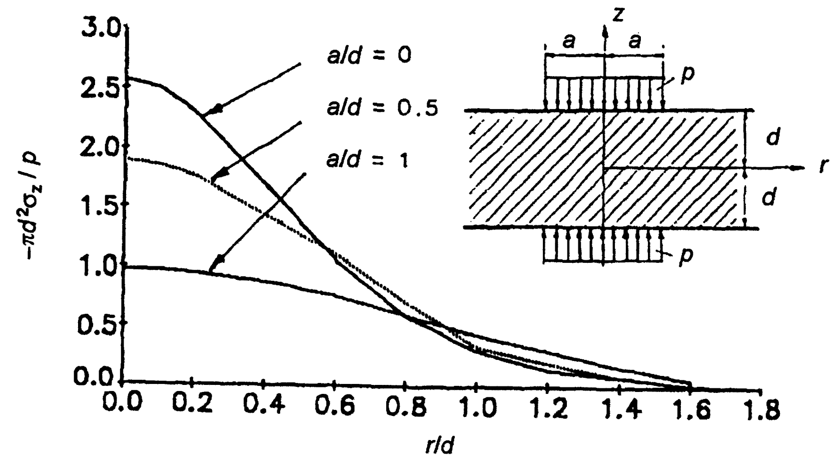

FIGURE 7.3. Axial stress distribution at the mid-plane of a thick plate (Sneddon, 1946).

Sneddon also proved that the axial stress, σ_z, was independent of the Poisson's ratio, ν, although the radial and circumferential stresses were slightly affected by the value of ν. These latter stresses, however, are not of significance to the present problem.

It was also shown that the result for the mid-plane of the thick plate could be used to determine the interface pressure distribution between the two plates of a bolted joint, provided the two plates were of equal thickness and made of the same material. Greenwood (1964) discussed the accuracy of Sneddon's solution and pointed out that they were accurate to values of r/d up to 0.6. In particular, he presented a table (see Table 7.1) for obtaining a good approximation of the radius of the contact circle: Thus, for $(a/d) > 0.5$, it is seen that

$$c \cong a + d \tag{7.1}$$

Lardner (1965) calculated the stresses as well as vertical displacements in a thick plate with axisymmetric loading and confirmed the result that two plates, of equal thickness, pushed together by forces opposite to each other, will separate when the vertical stress at the mid-plane of a single plate of twice the thickness becomes tensile. Thus the results for a single plate are applicable to two plates of equal thickness up to the radius at which the stress becomes positive.

In a bolted joint, the pressure would be applied over an annulus, rather than over a central circular area, on plates with a central hole. The solution to the problem of a single plate with a central hole subjected to a pressure applied over an annulus can be obtained by the method of superposition (Fernlund, 1961) (see Fig. 7.4).

Note that, in Fig. 7.4(c), although the pressure is applied over an annulus, the plate is still solid. To obtain the solution for the plate with a central hole (radius a), let

$$\begin{aligned} \sigma_r &= f_1(z) \\ \tau_{rz} &= f_2(z) \end{aligned} \tag{7.2}$$

at $r = a$. By further superimposing the normal stress, $-f_1(z)$ and the shearing stress, $-f_2(z)$ at $r = a$, we get a cylindrical surface of radius, a, that is stress free (Fig. 7.5). Thus the solution to the original problem

TABLE 7.1. Approximation of the radius of a contact circle.

a/d	0	0.5	1.0	1.5	2.0	2.5	3.0
c/d	1.566	1.693	2.028	2.471	2.949	3.438	3.933

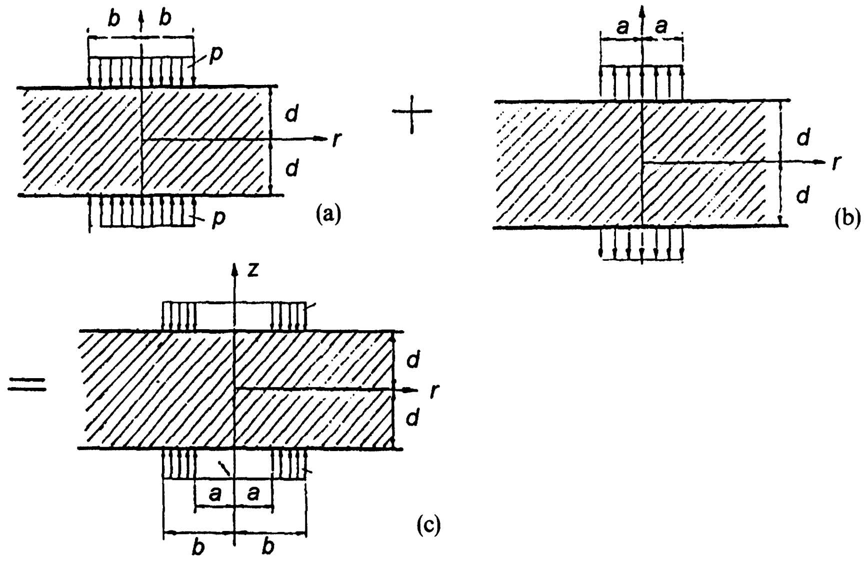

FIGURE 7.4. The method of superposition (Fernlund, 1961).

is obtained as

$$(\sigma_z)_{res} = \sigma_z + \sigma_z^* + \sigma_{z2} + \sigma_{z3} \tag{7.3}$$

in which

$(\sigma_z)_{res}$ is the resultant axial stress (contact pressure)
σ_z is due to pressure, p, applied over $0 < r < b$
σ_z^* is due to the tensile stress, p, applied over $0 < r < a$
σ_{z2} is due to the shearing stress $-\tau_{rz}$ applied at $r = a$
σ_{z3} is due to the normal stress $-\sigma_r$ applied at $r = a$

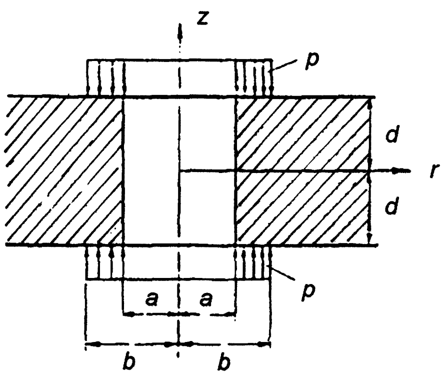

FIGURE 7.5. Fernlund's model of single plate with zero stress at $r = a$.

Bradley et al. (1971) noted that the above superposition technique requires additional normal stresses at the surface of the plates and, consequently, the plates no longer have uniform annular loading. Thus, Fernlund's solution is approximate. Bradley et al. determined the interface stress distribution and contact area by a three-dimensional photoelastic analysis using the stress freezing technique. Results were presented for smooth flat plates of equal thickness. The results for $(a/d) = 0.5$ and $(b/a) = 1.5$ showed good agreement with results for the mid-plane stress in a thick plate obtained by a finite element analysis. It was noted that Fernlund's solution overestimated the contact radius and underestimated the maximum interface pressure by some 20% (Fig. 7.6).

The theoretical analyses discussed so far have assumed that the bolted joint may be adequately modeled using the single plate model. The finite element and experimental analysis of Gould and Mikic (1972), however, showed that the single plate model yielded a contact zone that is larger than that obtained using a two-plate model, as shown in Table 7.2.

A series of papers dealing with the analytical solution of the problem of the thick plate with circular hole and axisymmetric loading was presented by Chandrashekhara and Muthanna (1977a, 1977b, 1978,

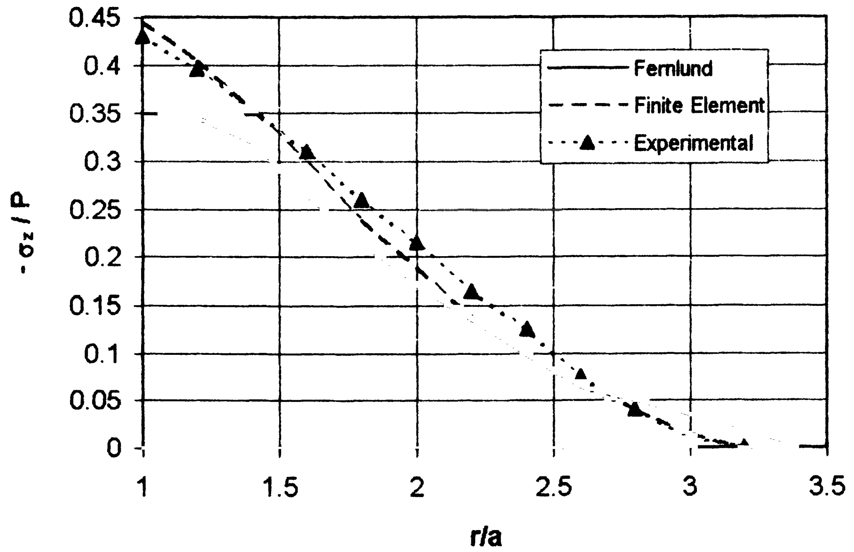

FIGURE 7.6. Comparison of solutions for the stress at the mid-plane of a single plate (after Bradley et al., 1971).

TABLE 7.2. Contact zone: Single-plate model vs. two-plate model.

		c/a		
a/d	b/a	Single-plate model	Two-plate model	% discrepancy between models
1	3.1	4.2	3.7	13.5
	2.2	3.3	2.7	22.2
	1.6	2.7	2.1	28.6
	1.3	2.4	1.7	41.7
0.75	3.1	4.5	3.8	18.5
	2.2	3.6	2.8	28.9
	1.6	3.0	2.2	36.4
	1.3	2.7	2.0	35.0
0.5	3.1	5.1	4.1	24.4
	2.2	4.2	3.2	31.3
	1.6	3.6	2.8	28.6
	1.3	3.3	2.5	32.0

1979). The solutions satisfied the exact boundary conditions rather than the approximate ones implied in Fernlund's superposition approach. The analytical results were expressed in terms of Fourier-Bessel series and integrals. Numerical computations showed that the results agreed well with those of Gould and Mikic for the single plate. Chandrashekhara and Muthanna (1978) also showed that the simpler two-dimensional solution for the semi-infinite strip gave results that were in substantial agreement with that for the more complex axisymmetric, three-dimensional problem for values of $(d/a) \leq 1$.

Motosh (1976) presented an approximate method for calculating the stress distribution, assuming that the bolt load dispersed in a conical or spheroidal envelope. The stress distribution was represented as a 4th degree polynomial (Eq. (7.4)), in which the constants were determined from the boundary and equilibrium conditions. The "boundary conditions" were based on the assumptions made by Fernlund and previous experimental results from photoelastic models. However, Chandrashekhara and Muthanna (1978) noted the solution thus obtained agreed reasonably with the exact analytical solution *only at the mid-plane*, and that, too, only for the conical envelope. Hence the conditions given below refer only to the mid-plane with load dispersed in a conical envelope. Inasmuch as we are interested only in the interface pressure distribution for the purpose of calculating the joint heat transfer, these results should be still useful in the present context.

$$\sigma = Ar^4 + Br^3 + Cr^2 + Dr + E \tag{7.4}$$

Equilibrium:

$$\int 2\pi\sigma r\, dr = \text{total joint load}$$

Boundary Conditions:

$$r = a: \quad \partial\sigma/\partial r = 0$$

$$r = c: \quad \sigma = 0,\ \partial\sigma/\partial r = 0 \text{ and } \partial^2\sigma/\partial r^2 = 0$$

Also, for the conical envelope (see Fig. 7.1),

$$c = b + d\tan\alpha$$

The recommended values for α are:

d/a	α (deg)
<2	≤40
2 to 4	45
≥4	≥50

Effect of Other Parameters

All of the above theoretical analyses have assumed that the interface is perfectly smooth. When the plate surfaces are rough, the width of the gap beyond the contact zone may be smaller than the surface asperities of either surface. This will cause compression of the interfering asperities, leading to an increase in the contact zone (Roca and Mikic, 1972). This, in turn, will result in a change in the interface pressure distribution as illustrated in Fig. 7.7. These facts were confirmed by Ito et al. (1979), who experimentally determined the pressure distributions for lapped and ground surfaces by means of ultrasonic waves.

Minakuchi et al. (1983) supported their theoretical work on bolted joints (two plate model) by an experimental technique in which the interface pressure distribution was measured by means of pressure-sensitive pins. The effects of using different materials and also different thicknesses of plates were investigated. The results for the cone dispersion angles are presented in Table 7.3 (in all cases b/a was equal to 1.5):

From an inspection of table 7.3, it is evident that:

1. The relative thicknesses of the plates can have a pronounced effect on the extent of the contact zone, and

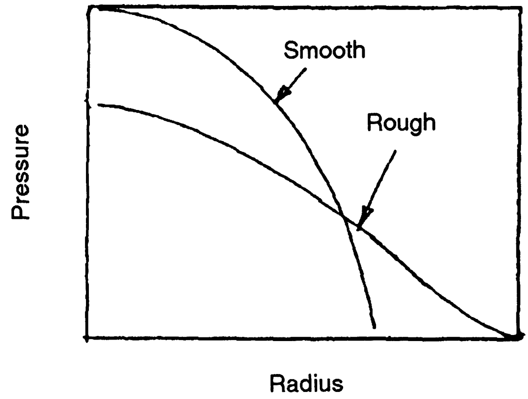

FIGURE 7.7. Effect of surface roughness on contact zone.

2. The contact zone is not significantly affected by the use of different materials unless the two moduli of elasticity are vastly different.

The second of the above conclusions is important when soft gaskets are used in the bolted joint. Minakuchi (1984), in fact, confirmed that the contact area is much larger and the stress distribution "more gentle" when a soft metallic gasket is used.

The majority of the theoretical analyses assume that the loading, p, is uniform. Curti et al. (1985), using the boundary element method, determined the stress distributions for different loading (uniform as well as linearly varying with respect to the radius) conditions on plates of equal thickness. Although the interface pressure distribution was found to depend on the loading profile, it was noted that any such effect disappeared for $(b - a)/d < 0.3$. In other words, the exact nature of the applied pressure distribution is immaterial for "thick" plates. This merely confirms the earlier observation made by Fernlund (1961) on the basis of St. Venant's principle.

TABLE 7.3. Summary of cone dispersion angle results.

$E_2/E_1 = 1; d_1/a = 3$			$d_2/d_1 = 1.5; d_1/a = 3$			$E_2/E_1 = 1; d_2/d_1 = 1$		
d_2/d_1	α_1 (deg)	α_2 (deg)	E_2/E_1	α_1 (deg)	α_2 (deg)	d_1/a	α_1 (deg)	α_2 (deg)
0.3	28	61	1.0	59	48	1	47	47
0.6	43	57	1.45	58	46	2	51	51
1.0	53	53	3.0	56	44	3	53	53
1.5	59	48	6.0	54	43	4.5	59	59
3.0	71	45	12.0	54	42	6	55	55

In their experimental study of bolted joint heat transfer, Oehler et al. (1979) noted that the axial tension in the bolt decreased with torquing cycles. Typically, about 10 cycles needed to be applied before a constant preload was reached. Oehler et al. also noticed that the interface pressure slightly increased at elevated temperatures due to the differential expansion between the bolt and the plates. Recent experimental and numerical analyses of Kumano et al. (1994) have shown that such increases could be very significant. Even for moderate temperature rises of the order of 100 to 200 °C, the corresponding increment in bolt tension could be greater than the initial preload.

7.1.2 Heat Transfer in Bolted Joints

As indicated at the beginning of this section, for axial heat flow through a bolted joint the total joint resistance is given by:

$$R_{\text{tot}} = R_{\text{micro}} + R_{\text{macro}} \tag{7.5}$$

Considering first the microscopic resistance, at first glance it would appear that this resistance must depend upon the interface pressure distribution within the contact zone. Yip (1972), indeed, considered three different stress distributions; namely, uniform, linear, and parabolic. Using the theoretical model for the contact conductance for nominally flat surfaces, he found that the three distributions yielded virtually the same resistance for any given load. Madhusudana et al. (1990) proved why this should be so as follows:

Let $p(r)$ be the arbitrary interface pressure distribution. Then, since the solid spot conductance for a given pair of flat surfaces is given by $h_s = kp^n$, where k is a constant, the total microscopic resistance for the joint is given by

$$h_{\text{tot}} = \int kp^n(2\pi r\, dr)$$

In the theoretical model for flat joints, n is nearly equal to 1 and, hence

$$h_{\text{tot}} = k \int p(2\pi r\, dr)$$

But

$$\int p(2\pi r\, dr) = \text{total mechanical load on the joint}$$

The total microscopic conductance or resistance for a given load must, therefore, remain the same irrespective of the pressure distribution.

Madhusudana et al. further pointed out that, if *experimental correlations* for the solid spot conductance is used, then, because of the flatness deviations and other surface irregularities inevitably present in practical surfaces, the value of n is smaller than unity (typically 0.6 to 0.7). In such a case, there may be a noticeable difference between the conductance values obtained using different stress distributions (Fig. 7.8). Again, this may not be significant for most applications. Referring to the same figure, it is important to note, however, that the microscopic conductance increases with the extent of the contact zone (defined by the radius, c). Inasmuch as the macroscopic conductance also increases with the radius, c, it is apparent that this radius is the single most important parameter defining the thermal conductance of a bolted joint for a given pair of surfaces. As seen during the discussion of the interface pressure distribution in the bolted joint, this radius itself is found to depend on the bolt hole radius, b, and the thickness, d, of the plates by means of an equation of the form:

$$c = b + (\text{constant})\, d$$

It is thus clear that the bolt hole radius and the plate thickness are two important parameters to be considered in the thermal design of a joint.

It may also be recalled that the presence of surface roughness tended to increase the radius, c. Although this would increase both the microscopic and macroscopic conductances, the roughness would also tend to increase the microscopic resistance. Hence Roca and

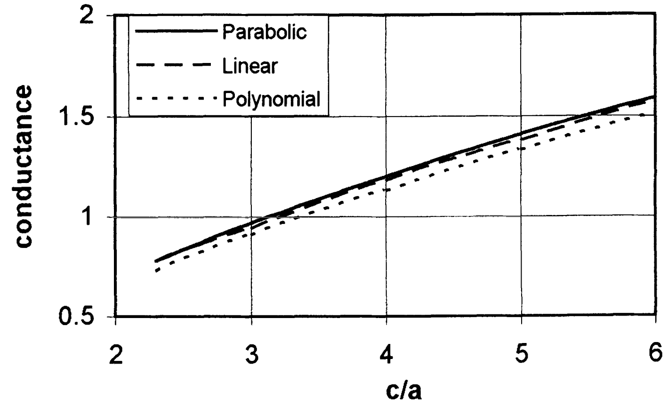

FIGURE 7.8. Effect of pressure distribution on microscopic conductance.

Mikic (1972) showed that it is possible to control the overall conductance by a suitable choice of roughness in relation to the other system parameters.

Once the contact zone radius has been determined, it is a straightforward matter to determine the macroscopic resistance associated with the contact zone. The macroscopic resistance of a bolted joint in vacuum, for example, may be simulated by a simple electrolytic tank analogue (Fletcher et al. 1990). The macroscopic resistance in a vacuum or in a conducting medium may be determined using a finite difference technique (Madhusudana, 1994). Figure 7.9 shows typical results obtained from the finite difference analysis. In this figure, x is the ratio of the conductivity of the fluid in the gap ($c < a < r_o$) to the conductivity of the material of the plates. The macroscopic resistance is nondimensionalized as:

$$R_N = (R - R_S)/R_S \tag{7.6}$$

in which

R = total resistance with the macroscopic constriction
R_S = total resistance without the constriction; i.e., the resistance of a hollow cylinder of inner radius, c, outer radius, r_o, and thickness equal to the sum of the thicknesses of the two plates

It is clear that the macroscopic resistance decreases with increase in both the thickness and the contact zone radius. In an actual joint, however, the thickness and the contact zone radius are not independent, as mentioned before. It is also seen that for $x \leq .0001$, the resistance is virtually the same as for vacuum ($x = 0$).

All of the above discussion refers to the situation where the heat transfer is parallel to the bolt axis. Heat flow across the joint may also be radial (Fig. 7.10). Whitehurst and Durbin (1970) stated that such a process may be analyzed by defining an effective thermal conductivity for the joint:

$$k_2 = (x_2/x_e)k$$

This method assumes one-dimensional heat flow without losses and requires temperature gradients be determined (experimentally) for the specific joints under consideration or, alternatively, a large number of models constructed and tested. Roca and Mikic (1972) presented the results of a numerical solution of a similar problem. Lee et al. (1993) described an analytical solution of the latter problem, assuming that the extent of the contact zone was known, and that perfect contact existed over this zone.

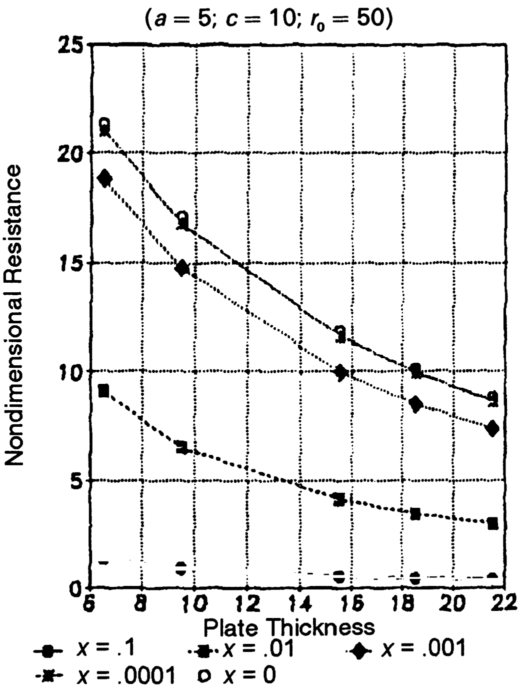

(a)

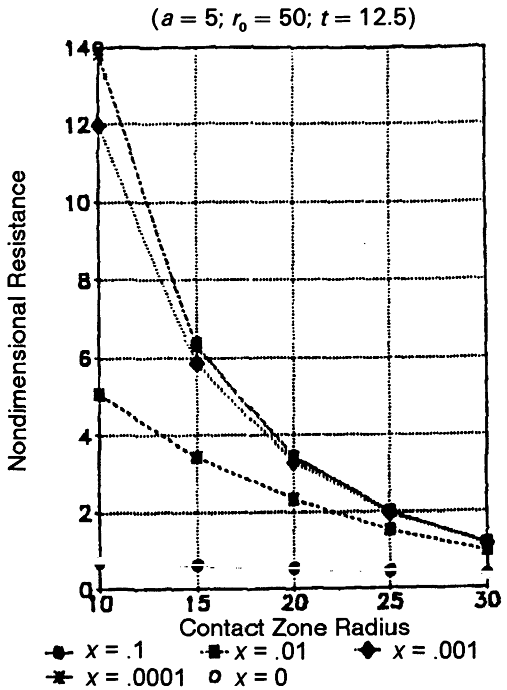

(b)

FIGURE 7.9. (a) Nondimensional resistance *vs.* plate thickness. (b) Nondimensional resistance *vs.* contact zone radius.

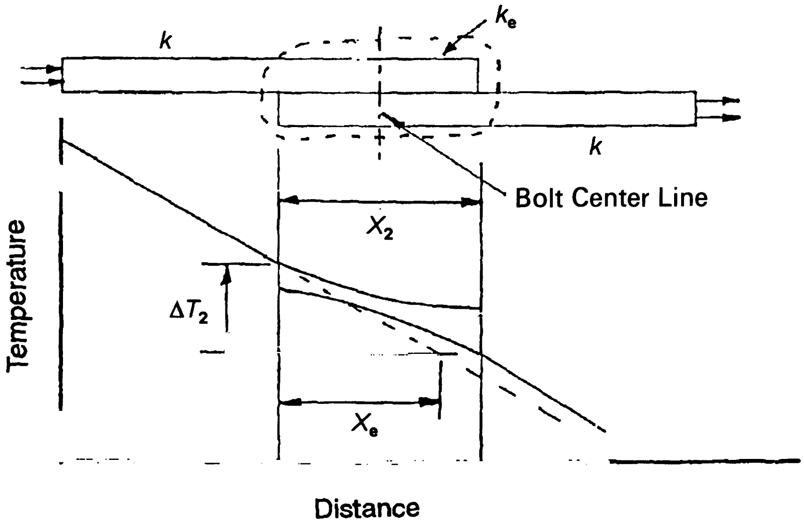

FIGURE 7.10. Transverse heat flow in a bolted joint.

There have been very few experimental studies dealing with the heat transfer in bolted joints. The representative ones are summarized in Table 7.4. All of these tests refer to alluminum alloy (Al6061-T6) plates bolted by a central bolt and placed in vacuum. Because of the differing loading conditions, surface texture, and the fact that some investigators reported only the total resistance rather than the additional resistance due to the presence of the joint, it is not possible to compare the results.

TABLE 7.4. Heat transfer in bolted joints; Parameters used in some representative studies.

Parameter	Aron and Colombo, 1963	Elliott, 1965	Veilleux and Mark, 1969	Oehler et al., 1979	Mittlebach et al., 1993
Plate thickness, t, mm	1.5	2.1	top: 1 bottom: 1.25	top: 29 bottom: 35.5	top: 25.4 bottom: 19.1
Bolt diameter, $2a$, mm	4.8	4.8	3.5	6.35	3.175
Loading radius, b, mm	5.5	5.5	3.4	≅6.35	4.77
Roughness (rms), μm	0.2 to 0.55	0.5 to 0.75	0.4 to 0.5	0.8	top: 0.64 bottom: 0.71
Bolt load, N	450 to 5800	900 to 5800	1600	6700	2000 to 6400 kPa

7.1.3 Summary

The following conclusions follow as a result of the discussion in this section.

1. The interface pressure distribution in a bolted joint is nonuniform, with the peak pressure near the edge of the bolt hole, rapidly decreasing to zero in a short radial distance.
2. The outer radius of the contact zone depends on the bolt hole radius and the plate thickness. It is independent of the axial bolt load.
3. The contact zone, as given by the two-plate analysis, is smaller than that obtained using a single-plate model.
4. The contact zone obtained for rough surfaces is larger than that obtained assuming the surfaces to be perfectly smooth.
5. For two plates made of different materials, the contact zone is not affected by the different moduli of elasticity, unless the two moduli are vastly different.
6. At elevated temperatures, the bolt load is increased due to differential expansion between the plates and the bolt.
7. Bolt preload decreases with the torquing cycles for the first few cycles before reaching a steady value.
8. The total resistance to heat flow in a bolted joint is the sum of the macroscopic resistance of the contact zone and the microscopic resistance associated with the individual solid contact spots within the contact zone.
9. Both the macroscopic and the microscopic resistances depend on the extent of the contact zone and hence the bolt hole radius and the thickness of the plates.
10. The exact nature of the interface pressure distribution is not important for estimating the microscopic resistance.

7.2 Cylindrical Joints

There are many applications in which the heat flow is radial across concentric, compound cylinders. Examples include plug and ring assemblies, shrink-fit cylinders, finned tube heat exchangers, and nuclear reactor fuel elements. The experimental and theoretical investigations in each of these categories usually deal with specific applications. For example, the works of Sheffield et al. (1984, 1985, 1987, 1989) deal with mechanically expanded copper tubes with aluminum fins. A detailed review of thermal conductance of cylindrical joints was presented by Madhusudana et al. (1990). In what follows, some significant aspects of this problem will be discussed.

In a flat joint, the contact pressure is usually explicitly known. It is, therefore, chosen both in theory and experiment, as the independent variable controlling the conductance of a given joint. In a cylindrical joint, however, the contact pressure is a function of the differential expansion between the two cylinders. According to classical thermoelastic analysis, this expansion, in turn, is a function of the heat flux across the two cylinders. Thus, the heat flux, rather than the indirectly estimated contact pressure, becomes the logical independent variable in the analysis of cylindrical joint thermal conductance.

Among the finned tube heat exchangers whose performance is affected by thermal contact resistance, three primary types may be identified (Fig. 7.11). Often, the liner tube is made from corrosion resistant material such as stainless steel and the outer finned tube made from high conductivity materials such as aluminum or copper.

The works of Dart (1959) and Gardner and Carnavos (1960) represent early investigations of the heat transfer performance of interference fitted tubes. Gardner and Carnavos noted that, as the temperature increased, the fins expanded away from the tube wall. As the temperature further increased, a successively greater proportion of the heat was transferred through the gas gaps in the interface than through the actual metal-to-metal contact spots. Eventually, a point was reached where the gap between the fin base and the tube was opened to such an extent that the heat transferred through the solid spots was deemed to be zero and all of the heat was assumed to pass through the entrapped fluid. These observations were also supported by the calculations of Kulkarni and Young (1966).

The loss of contact sets a maximum limit for the operating temperature for specific types of heat exchangers. For example, Taborek (1987), while reviewing the status of bond resistance and design tem-

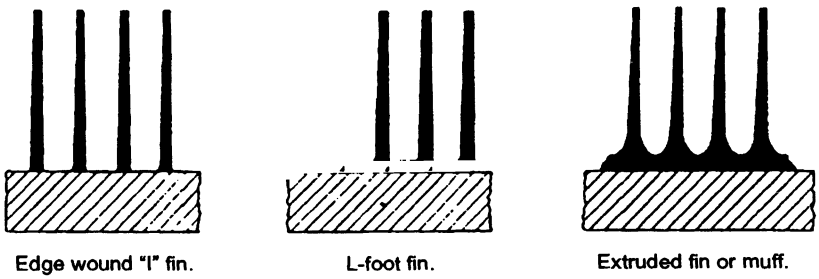

FIGURE 7.11. Examples of fins in bimetallic finned tubes.

TABLE 7.5. Maximum recommended bond temperatures.

	USA	Europe
L-footed tubes	176 °C (350 °F)	150 °C (300 °F)
Extruded fins	230 °C (450 °F)	250 °C (480 °F)

peratures for finned tubes, noted that the following maximum bond temperatures were recommended (see Table 7.5).

The fundamental studies of heat flow across cylindrical joints consider the general problem of radial flow in concentric cylinders, made from arbitrary materials, placed in either vacuum or in a conducting medium (Williams and Madhusudana, 1970; Hsu and Tam, 1979; Madhusudana, 1983, 1986; Lemczyk and Yovanovich, 1987). Williams and Madhusudana noted that the contact pressure developed depended on the interference existing between the two cylinders during operation. Hence the contact conductance depended on the interference, which consisted of the following components:

1. u_A: the differential expansion due to the temperature gradients caused by the flow of heat. This can be calculated using the well-known thermoelastic equations.
2. u_B: the differential expansion caused by the fact that, because of the contact resistance, the two surfaces at the interface will be at different temperatures.
3. u_C: the initial degree of fit.

Because the differential expansions, u_A and u_B depend on the heat flux, it is anticipated that the heat flux should be the primary variable controlling the conductance for a given pair of cylinders. In many subsequent works, the heat flux has, indeed, been used as the independent variable (Hsu and Tam, 1979; Egorov et al., 1989).

Consider first the differential expansion, u_A. The temperature drop in each cylinder will be inversely proportional to its thermal conductivity, so that the thermal strain would depend on α/k, where α is the coefficient of thermal expansion. Also, for radially outward flow, the outer surface of the inner cylinder would be in tension, whereas the inner surface of the outer cylinder would be in compression. Hence, for this situation, the interference would be reinforced, the exact amount of additional interference depending on several factors, including the ratio $\alpha_o k_i/(\alpha_i k_o)$, where the subscripts i and o refer to the inner and outer cylinder, respectively, and the ratio of inner to outer radius in each cylinder.

Now consider the differential expansion, u_B. In this case, both cylinders are subjected to tensile strain, but the temperature level of the outer cylinder would be less than that of the inner by an amount ΔT due to the contact resistance. Hence the interference may be strengthened or relaxed depending on whether the inner cylinder expands more or less than the outer cylinder by this mechanism. It must be emphasized that this differential expansion is also a function of the heat flux by virtue of the dependence of the interfacial temperature drop on the contact conductance.

The following theory applies to radially outward flow and makes use of the following simplifying assumptions:

1. The surfaces are rough but conforming; there are no large scale irregularities such as out-of-roundness or waviness.
2. The heat transfer rate across the gas gaps is constant; in other words, the variation of the effective thickness of the gap with heat flux is considered negligible.
3. Heat transfer by radiation is ignored.

Referring to Fig. 7.12, for a given interference, u, the shrink-fit pressure between two cylinders is (Ugural and Fenster, 1975):

$$u/b = (p/E_i)[C_1(C_2 + \nu_o) + (C_3 - \nu_i)] \tag{7.7}$$

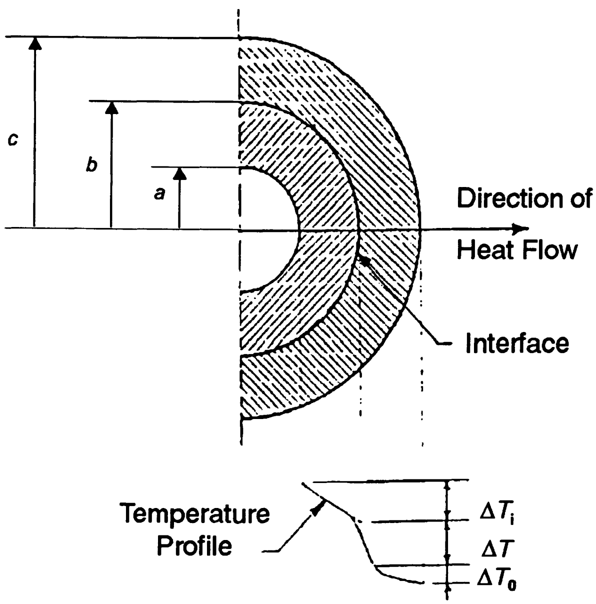

FIGURE 7.12. Heat conduction in a composite cylinder.

in which

$$u = u_A + u_B + u_C \tag{7.8}$$

$C_1 = E_i/E_o$; $C_2 = (c^2 + b^2)/(c^2 - b^2)$; $C_3 = (b^2 + a^2)/(b^2 - a^2)$

The heat flow is given by

$$Q = (2\pi l k_i)\Delta T_i/\ln(b/a) = (2\pi l k_o)\Delta T_o/\ln(c/b) \tag{7.9}$$

in which l is the length of the composite cylinder.

Hence,

$$\Delta T_o = (k_i/k_o)[\ln(c/b)/\ln(b/a)]\Delta T_i \tag{7.10}$$

By classical thermoelastic analysis (Timoshenko and Goodier, 1970), the radial displacements due to heat flow are,

$$u_{Ai} = b\alpha_i \Delta T_i\{1 - [2a^2/(b^2 - a^2)]\ln(b/a)\}/[2\ln(b/a)]$$

$$u_{Ao} = b\alpha_o \Delta T_o\{1 - [2c^2/(c^2 - b^2)]\ln(c/b)\}/[2\ln(c/b)]$$

Substituting for ΔT_o from Eq. (7.10),

$$\begin{aligned} u_{Ao} = {} & b\alpha_i \Delta T_i[\alpha_o k_i/(\alpha_i k_o)][\ln(c/b)/\ln(b/a)] \\ & \cdot\{1 - [2c^2/(c^2 - b^2)]\ln(c/b)\}/[2\ln(c/b)] \end{aligned}$$

Since,

$$u_A = u_{Ai} - u_{Ao}$$

we get

$$u_A = b\alpha_i \Delta T_i[C_4 - C_5 C_6 C_7] \tag{7.11}$$

in which

$C_4 = [1/[2\ln(b/a)]][1 - [2a^2/(b^2 - a^2)]\ln(b/a)]$
$C_5 = [1/[2\ln(c/b)]][1 - [2c^2/(c^2 - b^2)]\ln(c/b)]$
$C_6 = \ln(c/b)/\ln(b/a)$
$C_7 = \alpha_o k_i/(\alpha_i k_o)$
ΔT_i = temperature drop in the inner cylinder

The differential expansion due to the interface contact resistance is:

$$\begin{aligned} u_B &= u_{Bi} - u_{Bo} = b\alpha_i T_1 - b\alpha_o(T_1 - \Delta T) \\ &= b[T_1(\alpha_i - \alpha_o) + \alpha_o \Delta T] \end{aligned} \tag{7.12}$$

where

$T_1 = (T_a - \Delta T_i)$

T_a is the maximum temperature, i.e., the temperature at $r = a$

$\Delta T = q/h$

$$
\begin{aligned}
q = \text{heat flux at the interface} &= Q/A \\
&= 2\pi k_i l \Delta T_i / [(2\pi b l) \ln(b/a)] \\
&= k_i \Delta T_i / [b \ln(b/a)]
\end{aligned} \tag{7.13}
$$

and

$$h = h_s + h_g = 1.13 \tan\theta (k/\sigma)(P/H)^n + (k_g/\delta_{\mathrm{eff}})$$

In the above expression, n is nearly equal to 1 for theoretical flat surfaces. It is of the order of 0.6 to 0.7 for practical surfaces. Also, δ_{eff} is approximately equal to 3σ (Tsukizoe and Hisakado, 1965; Popov and Krasnoborod'ko, 1975). However, no numerical values need to be assumed in the derivation. We can thus write

$$h = C_9(k/\sigma)(P/H)^n + (k_g/C_{11}\sigma) = (k/\sigma)[C_9(P/H)^n + k_g/(C_{11}k)] \tag{7.14}$$

where

$$C_9 = 1.13 \tan\theta; \quad C_{11} = \delta_{\mathrm{eff}}/\sigma$$

In this expression, k is the harmonic mean of the solid conductivities.

Thus we see that, for a given pair of cylinders the differential expansion, u_B, depends both on the maximum temperature, T_a, and the heat flux as represented by the temperature drop, ΔT_i, in the inner cylinder.

Substituting for u_A and u_B in Eq. (7.8), the pressure, P, can be solved for any combination of the heat flux and the maximum temperature. The corresponding contact conductance may then be obtained by means of Eq. (7.14). When $\alpha_o > \alpha_i$, however, the differential expansion, u_B, may be negative. In this case, for each heat flux, there is a maximum temperature at which the interference is completely relaxed and, for all T_a values above this level, heat transfer takes place by gas gap conduction only.

Note that, for thin cylinders or tubes, both the thermal stress and the heat flux equations will be much simpler because linear approximations could be used for thin cylinders. As an example, Table 7.6 lists the inside surface temperature of the inner tube at which the interference is first reduced to zero for the following conditions:

Inner cylinder: Stainless steel; $E = 200\,\mathrm{GPa}$; $k = 16.5\,\mathrm{W/(m\,K)}$; $\alpha = 18(10^{-6})$; $(b/t) = 10$

Outer cylinder: Aluminum alloy; $E = 70\,\mathrm{GPa}$; $k = 200\,\mathrm{W/(m\,K)}$; $\alpha = 24(10^{-6})$; $(b/t) = 10$ (The thickness of each cylinder is t)

Interface medium: air; $k = 0.0298\,\mathrm{W/(m\,K)}$

TABLE 7.6. Temperature of the inner cylinder at which the interference is first reduced to zero.

ΔT_i(K)	T_a(C)
0	167
10	276
20	385
30	495
40	604

Surface properties: $(\sigma/b) = 10^{-4}$; $\theta = 5°$; $H = 1400\,\text{MPa}$
Initial interference: $(u_C/b) = 10^{-3}$

For the same conditions as Table 7.6, the variation of joint conductance with T_a, for radially outward flow from stainless steel to aluminum, is shown in Fig. 7.13a. (In Fig. 7.13, ΔT_i is the temperature drop in the inner cylinder and is, therefore, a measure of the heat flux). For this condition, it is clear that the joint conductance, at any given value of heat flux, continually decreases as the temperature of the inner surface of the inner cylinder increases, and is asymptotic to the gap conductance value as soon the temperature reaches the value given in the above table. By contrast, when the heat flow is from aluminum to stainless steel, the conductance continuously increases with the temperature for any given heat flux, as shown in Fig. 7.13b. According to the theory presented, if both cylinders are made from the same material, the conductance will not be affected by the temperature, T_a. There will be, of course, some variation if the change in material properties and radiation at higher temperatures are taken into account. In all cases of radially outward heat flow in similar materials, the conductance increases as the heat flux is increased.

7.3 Rectification

We have just seen that, for radial heat flow in cylindrical joints, the magnitude of the contact conductance depends on the direction of the flow, that is, whether from aluminum to stainless steel or vice versa. This dependence of conductance on the heat flow direction, which may be called rectification, has been found to exist for apparently plane joints as well. Since the heat flows primarily through the solid spots at moderate to high contact pressures and through the gas gaps

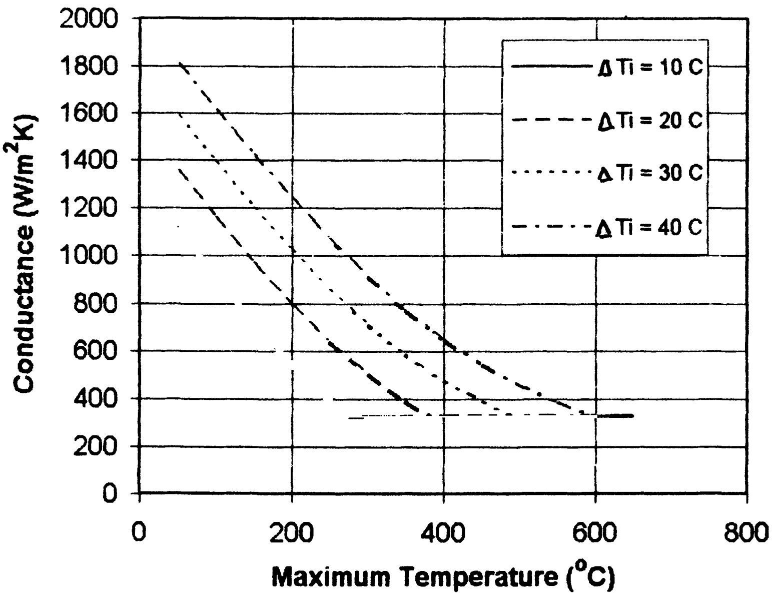

(a)

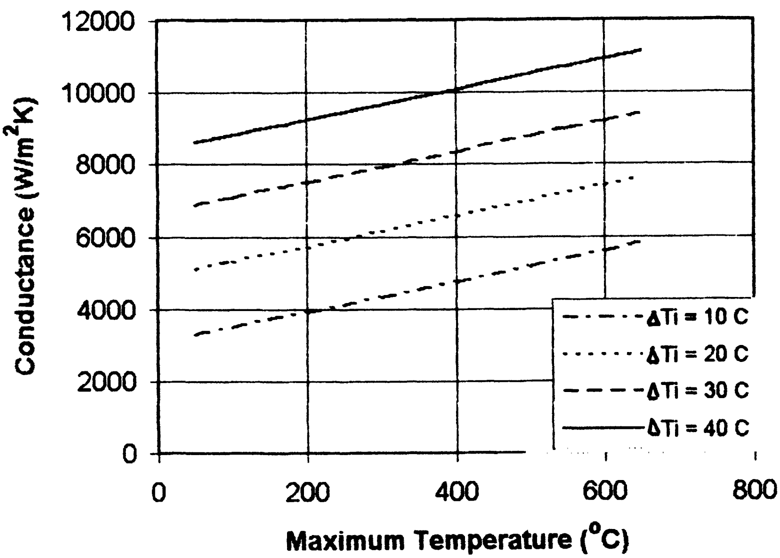

(b)

FIGURE 7.13. Conductance vs. maximum temperature for radially outward flow. (a) Stainless steel → aluminum. (b) aluminum → stainless steel.

at low contact pressures, we will consider the rectification in plane joints under two separate headings.

7.3.1 Rectification at Moderate to High Contact Pressures

Barzelay et al. (1954) and Rogers (1961) were some of the earliest investigators to observe experimentally the directional effect for nominally flat specimens. In both investigations, it was noted that the conductance for heat flow from aluminum to stainless steel was higher than for the opposite direction. Clausing's (1966) tests on "spherical cap" specimens, that is, both surfaces initially convex, however, showed that the conductance was the higher when heat flowed from stainless steel to aluminum. Powell et al. (1962) measured the heat transfer coefficient at the interface between a steel ball in contact, separately, with aluminum alloy, germanium, and soapstone ceramic. No rectification effect was observed in any of the three cases. The actual contact area in these tests, however, was very small ≈ 5.5 $(10^{-3})\,mm^2$. Hence, Powell et al. suggested that the direction effect was significant only when the contact area is large. It was also postulated that the rectification could be due to the distortion of the contact surface because of local temperature gradients. The tests of Lewis and Perkins (1968) showed that:

a. for flat, rough specimens (both flatness deviation and roughness of the order of $30\,\mu m$), the conductance was higher for the Al $\rightarrow$ SS direction.
b. for "spherical cap" specimens (flatness deviation 200 to $300\,\mu m$ compared to roughness of $5\,\mu m$), the conductance was higher for the SS $\rightarrow$ Al direction.

The experimental studies of Williams (1976) indicated that the contact elements need not be dissimilar to exhibit the rectification effect. He also found that the rectification effect was not permanent but tended to decrease with increasing number of heat flow reversals. More recently Stevenson et al. (1989) tested combinations of nominally flat stainless steel and nickel specimens in vacuum. Their experiments showed that while some rectification existed for contact between similar materials, it was not so significant as that exhibited by dissimilar metals in contact. The experiments of Williams, as well as those of Madhusudana (quoted in Williams, 1976), on Nilo 36 specimens showed that no rectification existed in this case. Since Nilo 36 is an alloy of very low thermal expansion coefficient, this confirms that thermal distortion of contacting surfaces is necessary for rectification to be present.

At present, there appears to be no single theory that can explain the rectification observed under all different conditions. However, on the basis of thermal distortions, explanations may be provided for some experimental observations.

7.3.2 *Specimens with Spherical Caps*

These typify plane ended specimens whose flatness deviations are large compared to the surface roughness. The theoretical model, first proposed by Clausing, is shown in Fig. 7.14. It is seen that the area of contact would be larger when heat flows from a material of high (α/k) to one of low (α/k). Thus the contact conductance for stainless steel to aluminum would be higher than for the opposite direction, confirming the experimental results for this type of contact.

We will prove the result for the spherical cap model in a more general form as follows (a somewhat different analysis was presented by Thomas and Probert, 1970):

Let r_1 and r_2 be the radii of curvature of the two surfaces in contact. Then for a given normal load, F, the Hertzian contact radius, a, is (Timoshenko and Goodier, 1970):

$$a = [(3/4)F\{(1 - \nu_1^2)/E_1 + (1 - \nu_2^2)/E_2\}\{r_1 r_2/(r_1 + r_2)\}]^{1/3}$$
$$= C\{r_1 r_2/(r_1 + r_2)\}^{1/3} = C\{(1/r_1) + (1/r_2)\}^{-1/3}$$

in which C depends upon the mechanical load.

Since the contact conductance is proportional to the contact spot radius, a, the conductances for opposite directions of heat flow may be compared by calculating this radius for each direction and then taking the ratio of the two radii.

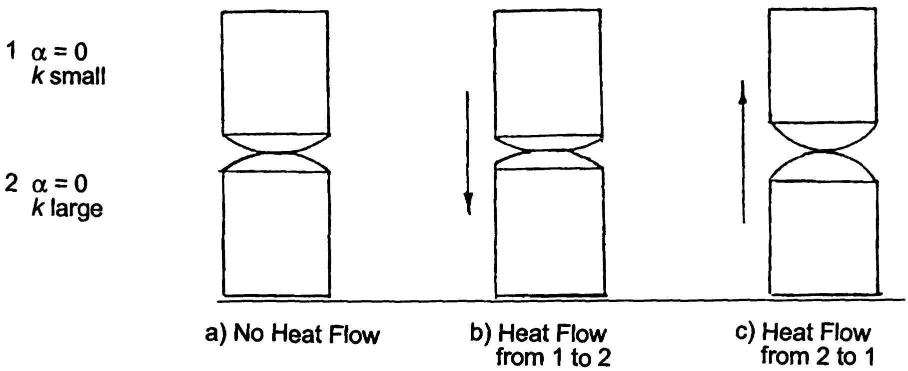

FIGURE 7.14. Effect of heat flow direction in surfaces with large flatness deviation (after Clausing, 1966).

If specimen 1 is heated and specimen 2 cooled, then r_1 is increased to $r_1 + \Delta r_1$ and r_2 is decreased to $r_2 - \Delta r_2$. Conversely, for the same heat flow in the opposite direction ($2 \to 1$), r_1 is decreased to $r_1 - \Delta r_1$ and r_2 is increased to $r_2 + \Delta r_2$. In other words, when heat flows *from* the surface of a sphere, the thermal strains cause the surface to become less convex, thus increasing the radius of curvature. On the other hand, when heat flows *into* the spherical surface, the convexity is increased, thus reducing the radius of curvature. Therefore

$$(a_{12}/a_{21})^3 = \{1/(r_1 - \Delta r_1) + 1/(r_2 + \Delta r_2)\}/\{1/(r_1 + \Delta r_1) + 1/(r_2 - \Delta r_2)\}$$

Now, $1/(r_1 - \Delta r_1) = (1/r_1)(1 - \Delta r_1/r_1)^{-1} \approx (1/r_1)(1 + \Delta r_1/r_1)$, by binomial expansion. We can express the other three terms similarly. Hence, after multiplying numerator and denominator through $r_1 r_2$, we get

$$(a_{12}/a_{21})^3 = \{r_2(1 + \Delta r_1/r_1) + r_1(1 - \Delta r_2/r_2)\}/\{r_2(1 - \Delta r_1/r_1) + r_1(1 + \Delta r_2/r_2)\} \tag{7.15}$$

Thus we see that specimens made of similar materials can indeed exhibit rectification so long as $r_1 \neq r_2$. Similar conclusions were reached by the independent investigations of Somers et al. (1987). This supports the experimental observations of Williams (1976).

From geometry (Fig. 7.15), the flatness deviation is related to the radius of curvature by

$$z \approx b^2/2r$$

Hence

$$\Delta z = -(b^2/2r^2)\Delta r \tag{7.16}$$

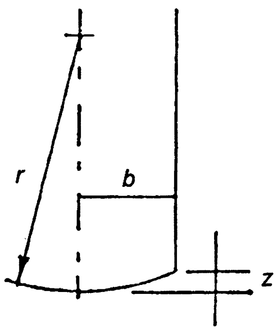

FIGURE 7.15. Relation between flatness deviation and the radius of curvature.

Also

$$\Delta z = [Q\alpha(1 + \nu)\ln(b/a)]/(2\pi k) \tag{7.17}$$

(see Barber, 1968). In this expression, Q is negative for heat flowing away from the spherical surface, so that Δr would be positive for heat flowing from the surface, as stated earlier.

In Clausing's model, $r_1 = r_2 = r$ and α_2 is taken to be zero so that Δr_2 will be zero by virtue of Equations (7.16) and (7.17). Hence, from Equation (7.15)

$$\begin{aligned}(a_{12}/a_{21})^3 &= \{r(1 + \Delta r_1/r) + r\}/\{r(1 - \Delta r_1/r) + r\}\\ &= (2 + \Delta r_1/r)/(2 - \Delta r_1/r)\end{aligned} \tag{7.18}$$

Since Δr_1 is positive, this ratio is greater than 1 and hence the conductance for the direction $1 \rightarrow 2$ will be greater than that for the opposite direction, as confirmed by the tests of Clausing (1966). Also, since the change in radius of curvature is dependent on the heat flux, we conclude that the contact conductance will be also dependent on heat flux.

7.3.3 Plane Ended Specimens

The explanation offered by Jones et al. (1974, 1975) is applicable to initially flat contacts and may be understood with reference to Fig. 7.16.

In a cylindrical specimen, the axial temperature gradient is constant, except in the vicinity of the disturbance represented by the contact interface. In the region of the constant temperature gradient, the two faces of a disc of radius, b, and small thickness, Δx, will suffer a relative radial displacement, $\Delta b = \varepsilon_T b = (\alpha \Delta T)b$. Because of this differential radial expansion, the initially flat surfaces assume a bowed configuration, the radius curvature, ρ, of which is, by geometry, given by:

$$(\Delta b/b) = (\Delta x/\rho)$$

Hence

$$(1/\rho) = (\alpha \Delta T/\Delta x) = \alpha q/k$$

where q is the heat flux.

Thus, the radius of curvature is inversely proportional to α/k. It is assumed that, if the resulting radius of curvature is appreciably larger than the length of the specimen, then the contact face will bend to the

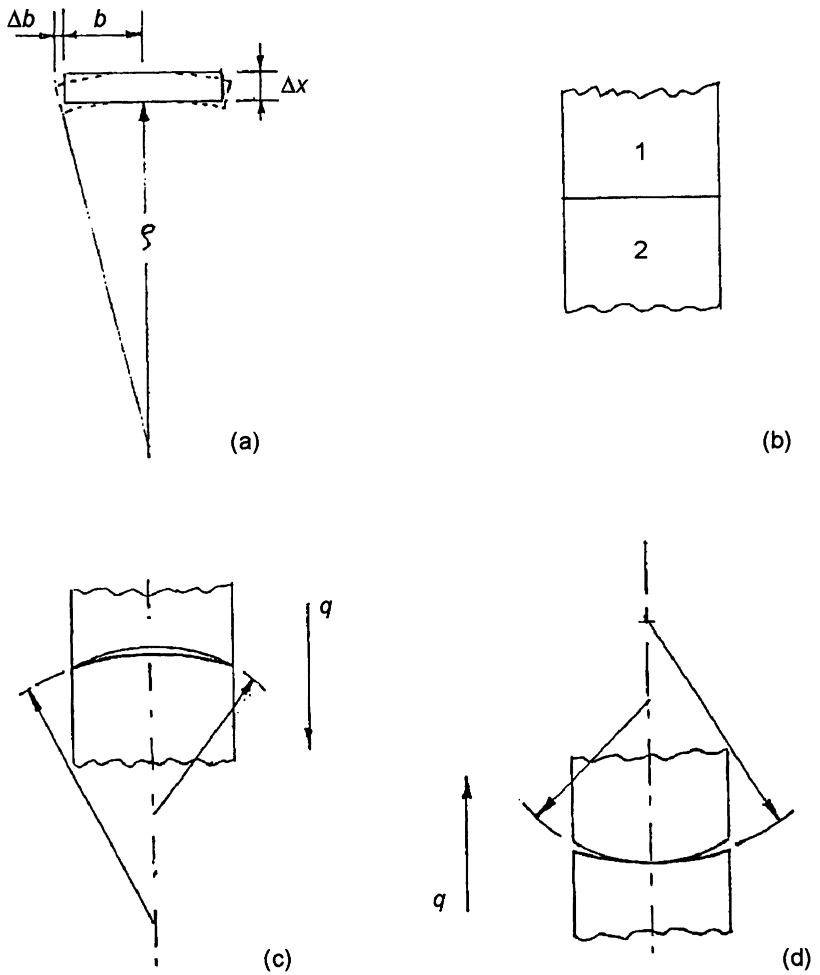

FIGURE 7.16. Rectification in plane ended specimens.

$$(\alpha_1/k_1) > (\alpha_2/k_2)$$

(a) Curvature induced due to axial temperature gradient. (b) No heat flow. (c) Heat flow from 1 to 2. (d) Heat flow from 2 to 1. (after Jones et al., 1974, 1975).

same curvature of the elemental disc. Hence, depending on the direction of heat flow, the contact may be peripheral or central. In particular, if $\alpha_1/k_1 > \alpha_2/k_2$, and the heat flow direction is $1 \rightarrow 2$, the contact would be peripheral, whereas the contact would be central for the $2 \rightarrow 1$ direction. It can be shown further that, for a given radial contact length, the peripheral contact would be less constrictive than the central contact. Thus we see that the conductance would be higher for the direction $1 \rightarrow 2$ in this case also. The theoretical analysis of Dundurs and Panek (1976) also indicated that the conductance is higher for the heat flowing from the material with the higher "distortivity" $\alpha(1 + \nu)/k$. For example, the conductance for SS → Cu direction would be higher than for the opposite direction.

Thus, none of the theories based on the macroscopic resistance changes due to thermal distortion support the experimental observations of the early investigators for flat specimens. Note, however, that in experimentally determining the direction effect, it is important to ensure that:

a. The mean interface temperature for the two directions is substantially the same.
b. The surfaces are not disturbed when the heat flow is reversed; thus the experimental setup should have facilities for heating and cooling at both ends of the column assembly so that the heat flow direction may be reversed without dismantling and reassembling the specimens.

It would appear that these precautions were not observed in some of the early investigations. For example, in the tests of conducted by Lewis and Perkins (1968), the mean interface temperature for the SS → Al direction ranged typically between 120 and 150 °F (50 to 65 °C), while for the opposite direction the range was from 215 to 250 °F (100 to 120 °C). Thus, at least some of the increased conductance observed for the Al → SS direction is attributable to the increased value of conductivity and decreased value of hardness at the higher temperatures obtained in this direction. This effect, however, will be small, typically 5%, compared to the 50 to 100% rectification observed by Lewis and Perkins.

7.3.4 Microscopic Resistance

The above theories consider only the macroscopic resistance. Veziroglu and Chandra (1970) observed that both microscopic and macroscopic resistances need to be taken into account in order to explain rectification, especially if the flatness deviations produced by thermal distortions are less than the order of magnitude of the surface roughness. Stevenson et al. (1989), however, found experimentally that the surface roughness had a secondary effect; it was the material properties that controlled the rectification. It has also been noted that (Somers et al. 1987) that the thermal rectification would be less if microscopic resistances are included because then the change in thermal resistance due to directional bias is a smaller percentage of the total resistance of the junction. In other words, Somers et al. attribute the directional bias to the changes in the macroscopic constriction only.

7.3.5 Rectification at Low Contact Pressures

The experimental results of Jeevanashankara et al. (1990) showed a pronounced rectification effect with the conductance for the Al → SS direction being much higher than for the SS → Al direction (see Fig. 7.17). This is contrary to the trend observed by most of the other investigators. Three relevant features of these experiments must, however, be noted:

a. The tests were conducted at low contact pressures (<0.5 MPa).
b. The tests were conducted in air, not in vacuum.
c. The mean interface temperature for the Al → SS direction was about 200 °C, whereas for the opposite direction it was about 120 °C.

Analyzing the heat flow at low contact pressures in general, Madhusudana (1993) observed first, that gas gap conductance predominates at these pressures. Second, the thermal conductivity of gases is very sensitive to temperature changes; for example, the conductivity of air increases by about 31% over the temperature range 0 to 100 °C, whereas the conductivity of aluminum over the same tem-

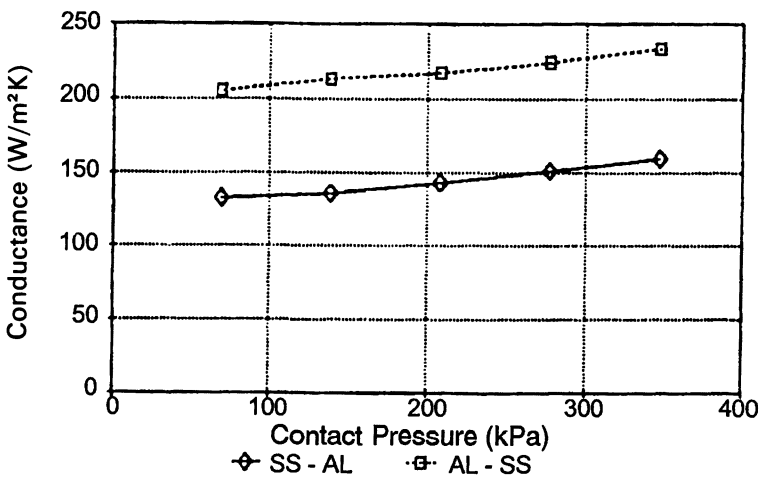

FIGURE 7.17. Rectification at low contact pressure; joint in air.

perature range increases by less than 2%, and that of stainless steel by just 4%. In view of the above factors, it was indeed to be expected that the conductance would be greater for the Al → SS direction in the tests of Jeevanashankara et al.

7.3.6 Summary

The following conclusions follow as a result of the discussion in this section.

1. At high contact pressures or for vacuum conditions, where the solid spot conduction is the predominant mode of heat transfer, the conductance would be greater when heat flows from the material of the higher distortivity, $\alpha(1 + \nu)/k$.
2. The materials need not be dissimilar to exhibit rectification effect, provided the initial convexities of the contacting surfaces are different.
3. At present, there appears to be no satisfactory explanation for the rectification observed for flat, rough surfaces in vacuum.
4. At low contact pressures when the gas gap conduction is important, rectification may be explained by means of the sensitivity of the thermal conductivity of the gas to variations in the mean junction temperature.

7.4 Hysteresis

When a joint is loaded progressively and then unloaded, the values of thermal contact conductance during unloading are often found to be higher than the corresponding values during the first loading. For example, see the experimental results of Madhusudana and Williams (1973) (Fig. 7.18 a,b,c) for mild steel/mild steel, zircaloy-2/zircaloy-2, and Nilo/uranium dioxide joints. In all cases a "hysteresis" loop may be seen to exist for the load–unload cycle. From the figures it may also be deduced that:

a. Hysteresis effect is more striking for coarse surfaces than for relatively smooth surfaces.
b. The hysteresis effect decreases with increasing number of cycles.
c. The conductance values eventually appear to settle down to values higher than those obtained during first loading.

The experimental results of Howells et al. (1969) had also indicated that the hysteresis effect became less significant in successive load

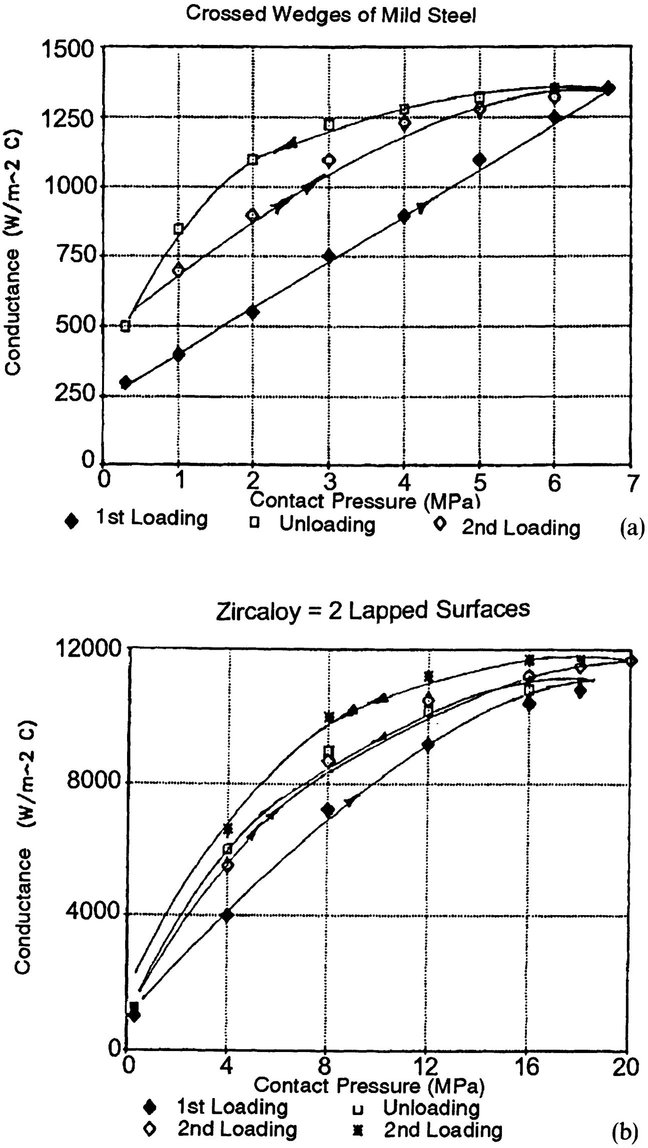

FIGURE 7.18. Effect of load cycling on thermal contact conductance for three different joints (Madhusudana and Williams, 1973).

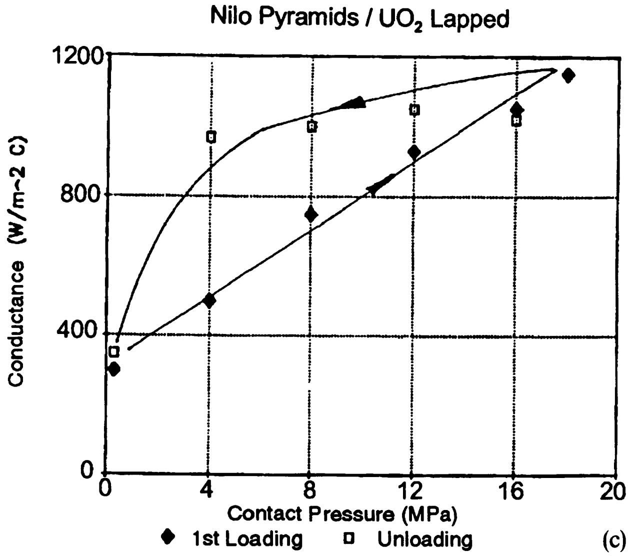

FIGURE 7.18 (cont.)

cycles provided the load was never reduced to zero. This is roughly in accordance with two of the three observations above.

Hysteresis is usually assumed to be caused by one or more of the following factors:

a. Cold welding.
b. Effect of contact duration.
c. Different surface deformation behavior during loading and unloading.

Cold welding requires the establishment of true metal-to-metal contact at room temperatures. For cold welding to occur, therefore, the contact must occur between perfectly clean surfaces. However, in many tests, especially those conducted in air, the surfaces are likely to be contaminated with oxide films, and so forth. Furthermore, as we have just seen, significant hysteresis has been observed for the contact between a metallic alloy (Nilo) and a ceramic (uranium dioxide). Hence it is unlikely that cold welding alone could be the cause of hysteresis.

The conductance may be expected to increase with contact duration due to the decrease of surface hardness of the specimens and hence an increase in contact area and conductance during subsequent unloading. For significant reductions in hardness to occur, the interface temperature must be well above the room temperature (Borzdyka, 1965). Significant hysteresis effects were noticed by Fenech and Rohsenow (1963) at temperatures less than 150 °C, and by Williamson and Majumdar (1992) at temperatures well below 80 °C. At these levels, the effect of contact duration will be quite small and we can conclude that this factor will not be the main reason for hysteresis to occur.

It may thus be concluded that hysteresis is primarily due to the difference in actual areas of contact between the first and subsequent loadings of the joint. The theoretical study of Mikic (1971) assumed that during first loading the surface asperities deform plastically. For a reduction in load and subsequent increase (up to the maximum load obtained in the first loading), the asperities are expected to deform elastically, giving, as an overall effect, a higher contact area for the same contact pressure. For Gaussian distribution of asperity heights, it was found that:

a. During first loading, the actual area of contact is proportional to the pressure, p.
b. For moderate pressure reduction, $0.5 < p/p_{\max} < 1$, the contact area decreases in proportion to $p^{2/3}$.

Thus the actual contact area would be larger during unloading than during the first loading. The analysis also showed that the number of contacts during unloading will be substantially higher in descending loading. Both of these effects result in higher values of conductance during unloading.

It may be noted that Mikic's analysis applies to nominally flat, rough surfaces in vacuum. The deformation of the bulk material was not considered in his analysis. Figure 7.18 shows, however, that when the load is fully reduced to the starting value, the contact conductance approaches the initial value at first loading. It would appear that, although the individual asperities might have suffered permanent damage due to plastic deformation, the contact area nevertheless approaches zero as the load is fully removed and the bulk sublayers recover elastically causing the contact surfaces to spring back and break the contact spots.

The experiments of Williamson and Majumdar (1992) on aluminum/stainless steel specimens showed that, when both surfaces were smooth ($\sigma_{\mathrm{Al}} = 0.47\,\mu$m; $\sigma_{\mathrm{ss}} = 0.27\,\mu$m), there was no significant hysteresis effect. On the other hand, when the aluminum surface was rough ($\sigma_{\mathrm{Al}} = 8.71\,\mu$m; $\sigma_{\mathrm{ss}} = 0.40\,\mu$m), there was a very noticeable, typically 100%, hysteresis effect. Hence it was concluded that when the surfaces are smooth, the deformation is predominantly elastic. Furthermore, in those cases where hysteresis did exist, subsequent loading and unloading curves essentially followed the first unloading curve. This is in agreement with the results of Madhusudana and Williams (1973) and of Howells et al. (1969). This suggests that the hysteresis effect may be used to advantage in obtaining enhancement of conductance in practice. The contact surface should be preloaded beyond the maximum load likely to be encountered in a given application. Subsequent unloading and reloading will yield a value of conductance, which would be higher than that which would be expected if the contact was not preloaded. A similar recommendation has recently been made by McWaid and Marschall (1992).

7.5 Effective Thermal Conductivity of Packed Beds

Packed beds of spherical particles are found in powder thermal insulation systems, chemical catalysts, automotive catalytic converters, sphere-pac reactor fuels, granular beds, naturally occurring soils and rocks, and so forth. In these applications, the spherical components react thermally with each other and with flat, convex, or concave bounding surfaces.

In general, conduction, natural convection, and radiation all contribute to energy transfer. Natural convection may be neglected unless very high temperature gradients and large pore sizes are involved. Radiation would be significant at high temperature especially if the conductivity of the particles is low. For example, at 1100 °C, 35% of heat is transferred by radiation in packed beds of silicon carbide grains; this figure rises to 85% in packed beds of glass beads (Chen and Churchill, 1963).

At low to moderate temperatures, the effective conductivity is the sum of the contact conductivity and the gas/solid conductivity. It may be noted that the model of Zehner and Schlunder (1970) assumes *point contact* between the adjacent spherical particles. Hsu et al. (1994) have recently shown that the Zehner-Schlunder model underpredicts the effective thermal conductivity of the packed sphere bed especially at high solid/fluid thermal conductivity ratios. The model based on *area contact* yields better agreement with experimental data. In vacuum, the heat is mainly conducted through the contact interface. The following discussion is based mainly on the analytical work of Chan and Tien (1973).

It is assumed that the radius of the contact area (Fig. 7.19) is given by the Hertzian relation

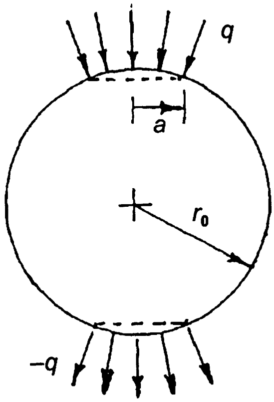

FIGURE 7.19. Constriction resistance in a spherical particle.

$$a = [(3/4)(1 - \nu^2)Fr_o/E]^{1/3}$$

in which F is the force between the two smooth particles.

For different packing patterns, the contact force is related to the external pressure, P, by:

$$F = S_F P/N_a$$

where N_a is the number of particles per unit area and S_F depends on the packing pattern.

For the simple cubic arrangment of spheres, there is a pair of diametrically opposite contact regions. Assuming that each contact surface is subjected to uniform heat flux, the constriction resistance associated with the solid sphere of Fig. 7.19 was shown to be

$$R_1 = 0.53/(ka), \quad (a/r_o < 0.1)$$

It may be noted that this is very nearly equal to twice the disc constriction resistance, $0.27/(ka)$, for uniform heat flux.

If the packing pattern is not simple cubic, a modified constriction resistance is defined as:

$$R = S_R R'$$

in which S_R depends on the contact radius and the wall thickness.

Again, for the solid sphere,

$$R_1' = 0.64/(ka), \quad (a/r_o < 0.1)$$

The thermal conductance of packed spheres depends on the packing pattern. The thermal resistance of a regular packed arrangement may be considered as a group of resistances, each composed of a series of the resistances of a single particle. Thus the conductance of the bed would be

$$h_{ij} = (N_a/N_t)(1/R_{ij})$$

in which R_{ij} is the constriction resistance of a single particle; subscript i refers to the type of solid ($i = 1$ for solid, $i = 2$ for hollow); subscript j refers to packing pattern ($j = 1$ for simple cubic, $j = 2$ for body centered cubic, and $j = 3$ for face centered cubic); N_a is the number of particles per unit area; N_t is the number of particles per unit length.

For small (a/r_o),

$$R_{ij} = S_R S_j R'_1$$

where S_R is given in Table 7.7 for solid and hollow spheres.

The values of S_j are 1, $\frac{1}{4}$ and $\frac{1}{3}$ for j equal to 1, 2, and 3, respectively. The expression for the conductance can then be written as

$$h_{ij} = S_p k[(1 - v^2)P/E]^{-1/3}$$

where S_p depends only on the packing pattern:

$$S_p = [1.56/(S_R S_j)](N_a/N_t)(0.75 S_F r_o/N_a)^{1/3}$$

When there is no external load, the force at each contact is equal to the weight of the particles above it. The contact resistance, therefore, decreases with increasing depth from the top surface. In this case, the conductance can be shown to be

$$h_{ij} = S_N k[(1 - v^2)\rho VL/(Er_0^2)]^{1/3}$$

where

TABLE 7.7. Values of S_R for hollow and solid spheres (Chan and Tien, 1973).

	t/r_o						
a/r_o	0.001	0.005	0.01	0.05	0.10	0.20	1 (Solid)
0.001	0.9384	0.8726	0.8479	0.8230	0.8201	0.8191	0.8252
0.002	0.9549	0.8955	0.8569	0.8071	0.8030	0.7984	0.8193
0.004	0.9582	0.9263	0.8831	0.8171	0.8489	0.8447	0.8207
0.006	0.9569	0.9380	0.9081	0.8664	0.8532	0.8236	0.8334
0.008	0.9554	0.9431	0.9192	0.8732	0.8339	0.8395	0.8280
0.010	0.9538	0.9433	0.9256	0.8588	0.8372	0.8415	0.8331

TABLE 7.8. Parameters for different packing patterns (Chan and Tien, 1973).

Parameter	Simple cubic	Body-centered cubic	Face-centered cubic
N_t	$1/(2r_0)$	$\sqrt{3}/(2r_0)$	$\sqrt{3}/(2\sqrt{2}r_0)$
N_a	$1/(4r_0^2)$	$3/(16r_0^2)$	$1/(2\sqrt{3}r_0^2)$
δ	0.524	0.680	0.74
S_j	1	1/4	1/3
S_F	1	$\sqrt{3}/4$	$1/\sqrt{6}$
S_P	1.36	1.96	2.72
S_N	0.452	0.713	1.02

$$S_N = 1.143(N_a N_t^{2/3})(S_F^{1/3}/S_j)r_o^{4/3}$$

ρ is the mass density, V is the volume of the sphere, and L is the thickness of the bed. The values of the other parameters required to calculate the conductance are listed in Table 7.8.

If the gas gap conductance is significant, then it may be added to the contact conductance (see, e.g., Yovanovich, 1973; Ogniewicz and Yovanovich, 1977) to get the total effective conductance. The effective conductivity is obtained by multiplying the effective conductance by the thickness of the packed bed.

Hadley (1986) derived the following semiempirical relation for the effective conductivity, k_e, of packed metal powders:

$$\begin{aligned} k_e/k_f = {} & (1-\alpha)[\phi f_o + \kappa(1-\phi f_o)]/[1-\phi(1-f_o)+\kappa\phi(1-\phi f_o)] \\ & + \alpha[2\kappa^2(1-\phi)+(1+2\phi)\kappa]/[(2+\phi)\kappa+(1-\phi)] \end{aligned} \tag{7.19}$$

In this expression,

k_f is the fluid thermal conductivity,
κ is the ratio of the solid of fluid thermal conductivity, k/k_f,
ϕ is the volume fraction or porosity (fractional theoretical density, $\delta = 1 - \phi$), and α allows for the contact between particles and depends on the degree of consolidation.

Ideally, α is determined from experiments in vacuum for randomly packed spheres. The variation of α with δ for metallic particles, as determined by Hadley, is shown in Fig. 7.20. If the contact conductance can be neglected, then α and, hence, the second term would be zero in Eq. (7.19). On the other hand, for evacuated powders, it is found that

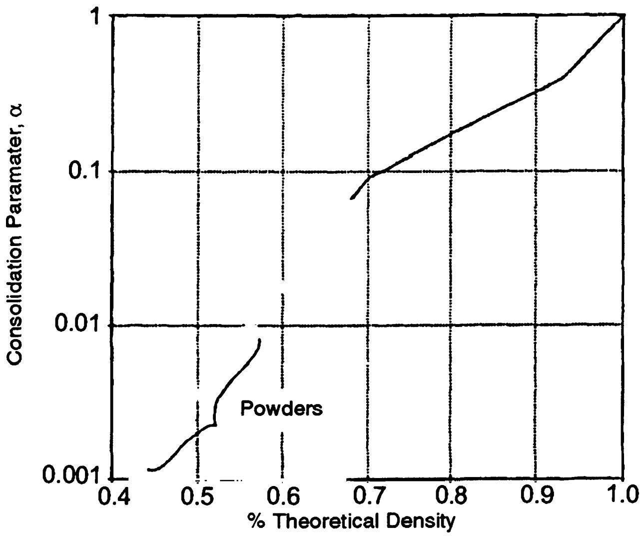

FIGURE 7.20. Curve representing experimentally determined values of α (after Hadley, 1986).

$$k_{e(\mathrm{vac})}/k = 2\alpha(1 - \phi)/(2 + \phi)$$

The parameter, f_o, is determined from measurements made using a high conductivity fluid, such as water. Hadley found that f_o ranged from 0.8 for (spherical) stainless steel particles to 0.9 for (angular) brass particles.

There are other empirical relations available for calculating the effective thermal conductivity of packed beds; see, for example, Kamiuto et al. (1989).

An experimental investigation of effective thermal conductivities of alumina-air, aluminum-air, and glass-air randomly packed beds has been reported by Nasr et al. (1994). The temperature range of the tests

TABLE 7.9. Temperature at which the radiation and conduction contributions became equal for alumina-air packed beds (Data from Nasr et al., 1994).

Particle diameter (mm)	Tempeature (K)
2.77	1300
6.64	860
9.61	650

was from 350 K to 1300 K and the diameter of the particles ranged from 2.5 mm to 13.5 mm. The porosity in all cases was approximately 38%. It was found that the effective thermal conductivity increased with particle size and bed temperature. At low temperatures, the heat transfer by conduction was the predominant mode; at high temperatures heat transfer by radiation became more significant. For alumina-air packed beds, the approximate values of the cross-over temperatures, that is, the temperatures at which the radiation and conduction contributions became equal are indicated in Table 7.9.

7.6 Stacks of Laminations

Stacks of thin layers will provide effective thermal insulation due to the resistance to heat flow at each interface. These resistances, being in series, add up to provide an overall high thermal resistance. Stacks of metallic laminations can be used in the design of mechanically strong, insulating containers or supports. Mikesell and Scott (1956), in particular, explored the use of stacks of stainless steel and monel plates in the design of large vacuum insulated containers for the storage of cryogenic fluids, such as liquid oxygen, nitrogen, and hydrogen. These containers need to be capable of withstanding shock and vibration during transportation by different types of carriers. Their experiments indicated that, at any given contact pressure, the contact resistance increased linearly with the number of laminations in the stack. It was also found that the resistance per unit length of the stack varied as the inverse square root of individual plate thickness. From the insulating point of view, the best assembly was a stack of stainless steel plates (type AISI 302), each 0.0008″ (0.02 mm) thick. Such an assembly, when supporting a load of 1000 psi (6.89 MPa), was found to have an effective conductivity of only 2% of a solid conductor of the same dimensions. The number of laminations in the stacks ranged from 148 to 315. Mikesell and Scott also observed that lightly dusting the plates with manganese dioxide more than doubled the resistance at all but the lowest contact pressures.

Stacks of enameled steel laminations are used in the construction of stator cores of large turbogenerators and transformers. In this case, unlike the evacuated cryogenic supports, however, the fluid trapped between laminations is partly responsible for the heat transfer across each interface. Williams (1971), in fact, noted that the effective conductivity of such laminations is sensitive to changes of environment. The contacts are influenced more by the fluid conductivity than by the conductivity of the materials of construction. A large hysteresis was observed in the contact pressure versus strain relationship for the first cycle of loading and unloading. Subsequent loadings and unloadings showed negligible hysteresis. Williams concluded that if the generator stator core is subjected to a succession of heating and cooling cycles, while clamped tightly, there will be a tendency for the laminations to "bed down"; provided the clamping pressure is maintained, the effective conductivity should improve.

The following correlation, based on the experimental results of six different investigators, was proposed by Al-Astrabadi et al. (1977) for the conductance for stacks of thin layers in *vacuum*:

$$h^* = 3.025\,(P^*)^{0.58}$$

where

$h^* = h_{LL}t/k$; $P^* = P/H$
h_{LL} = layer-to-layer conductance
t = thickness of each layer
k = conductivity of the stack material
H = hardness of the stack material

The total conductance of the stack would then be given by

$$1/h = \Sigma(1/h_{LL})$$

Babus 'Haq et al. (1991) tested the insulating performance of multilayer ceramic (alumina) sheets in vacuum. The sheets ranged in thickness from 0.65 to 1 mm. At a contact pressure of 1 MPa, the mean thermal resistance per interface was measured as 0.55 K/W; for example, the resistance of 5 plates was 2.6 K/W and that of 15 plates was 9 K/W, approximately. They also observed that hysteresis was present in all of the tests. It was also noted that the conductance variation at low loads is due mainly to layer flattening, that is, initially the load presses out any buckles in the individual layers. At high loads, the conductance decreases mainly as a result of asperity deformation.

The effect of the mean temperature was taken into account by Fletcher et al. (1993) in the correlation of their experimental data for multilayered aluminum alloy (3004, 5042, and 5182) sheets. For thick gauge samples (sheet thickness 2.896 to 3.056 mm), the correlation was

$$h_{LL}t/k = 40\,000\,(\alpha T)\,(P/H)^{1.15}$$

For thin gauge samples,

$$h_{LL}t/k = 2500\,(\alpha T)\,(P/H)^{0.97}$$

Since one single correlation could not be obtained to include both sets, it was suggested that consideration of another parameter, such as the surface roughness, was necessary.

7.7 Solid Spot Conductance of Specific Materials

7.7.1 Stainless Steel and Aluminum

Thomas and Probert (1972) collated 102 data points for stainless steel and 240 points for which one or both of the surfaces were aluminum alloys. These experimental results were obtained from thirteen different investigations. The correlations, together with estimates of errors, were as follows:

Stainless Steel Data

$$\ln C^* = (0.743 \pm 0.067) \ln W^* + (2.26 \pm 0.88) \tag{7.20a}$$

Aluminum Data

$$\ln C^* = (0.720 \pm 0.044) \ln W^* + (0.66 \pm 0.62) \tag{7.20b}$$

where

$C^* = C_s/(\sigma k)$
$W^* = W/(\sigma^2 H)$
W = Mechanical Load (N)
C = Thermal Conductance (W/K)

It is to be noted that the conductance and the load are expressed in their total values rather than in the usual, per-unit-area values, h_s and P. The range for W^* was from 10^4 to approximately 10^7, but there were comparatively small number of data points near the lower limit of the load. The relatively low values of the pressure exponents were attributed to the fact that the practical surfaces would contain some degree of waviness and would not be nominally flat. The correlation coefficients were 0.915 and 0.913 for the stainless steel and aluminum, respectively. Considering the number of different sources, these values indicate that the correlations can be called successful. No corrections, however, were applied for changes in the mean interface temperature, presumably because this information was not available in some of the experiments.

7.7.2 Zircaloy-2/Uranium Dioxide Interfaces

There is a large store of data available for this combination because of their importance to the nuclear power industry. Jacobs and Todreas (1973) considered a portion of the experimental data available and proposed a correlation whose constant term had to be adjusted to each set of data. Later on, Madhusudana and Fletcher (1983) collated data from five different sources* and proposed the correlation:

$$h_s\sigma/k = 12.29(10^{-3})(P/H)^{0.66} \tag{7.21}$$

This correlation was obtained after correcting the material properties for the different mean junction temperatures used by the various investigators. Also, in the final correlation Dean's (1962) data was omitted because, in this case, the solid spot conductances were deduced from tests in an argon environment and not direct measurements. A total of 78 data points fitted the above correlation with a correlation coefficient of 0.888 and a standard deviation of 6.78% (the graph is shown in Fig. 7.21).

7.7.3 Porous Materials

Porous materials find application in rocket motor nozzles, combustion afterburners, heat pipes, and so on. Miller and Fletcher (1973, 1975) obtained experimental results for the contact conductance of porous copper, nickel, stainless steel, and HCR (an iron-chromium-nickel-alloy) by using these as interstitial discs between 2024-T4 aluminum alloy end rods. The conductance of the interstitial material was determined by dividing the heat flux by the overall temperature drop across the insert. Hence the mechanical and surface properties of the end rods are likely to have some effect on the results obtained. The diameter of the discs was 1″ (25.4 mm) and the thickness, t, ranged from 0.026″ to 0.091″ (0.66 mm to 2.31 mm) while the porosity, ϕ, from 30% to 86%.

The results fitted the following correlation:

$$h_s t/k = 2.335\,[(P/H)(1-\phi)]^{0.72} \tag{7.22}$$

---

*Dean (1962), Ross and Stoute (1962), Cross and Fletcher (1978), Garnier and Begej (1979), and Madhusudana (1980).

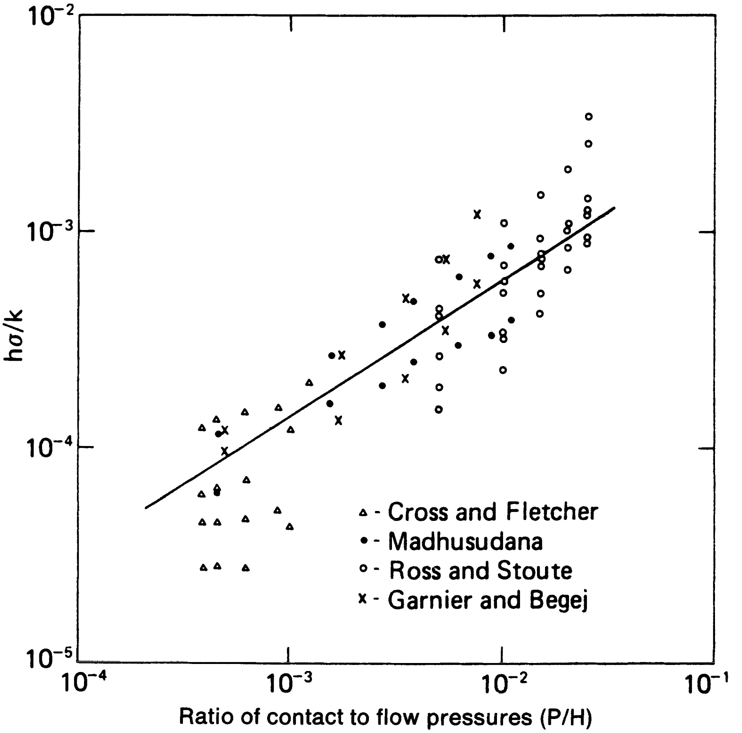

FIGURE 7.21. Correlation for zircaloy-2/uranium dioxide interfaces (Madhusudana and Fletcher, 1983). (Copyright 1983. Reprinted by permission from the American Nuclear Society, LaGrange Park, IL, USA).

in which

h_s = thermal contact conductance, BTU/(hr ft^2 °F)
k = thermal conductivity, BTU/(hr ft °F)
t = thickness, inch
P = contact pressure, psi
H = Vickers Hardness, psi

Since the true hardness of the porous material was not known, a harmonic mean of the hardnesses of the solid interstitial material and the parent material was used. Similarly, the conductivity was also the harmonic mean of the conductivities of the parent and the solid interstitial material. The expression, as given in Eq. (7.22) and plotted in Fig. 7.22, correlated the experimental data within an average overall deviation of 16%.

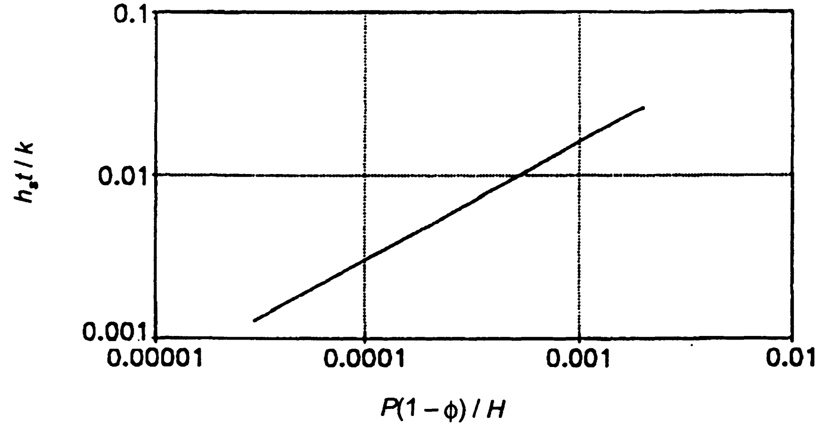

FIGURE 7.22. Correlation for porous materials (based on the data of Miller and Fletcher, 1975).

7.8 Thermal Contact Resistance in the Presence of Oxide Films

An oxide is, in general, harder (and less ductile) than its parent metal. The thermal conductivity of the oxide layer is also smaller by one or two orders of magnitude compared to that of the parent metal. For example, the hardness of mild steel EN3B is 1.67 GPa; that of iron oxide is 3.51 GPa. The thermal conductivity of EN3B is 47 W/m-K; that of the iron oxide is 0.875 W/m-K. Thus the formation of the oxide layer tends to reduce the TCC. However, the thickness of the oxide layer on metals in seldom more than 1 μm (Kharitonov et al., 1974). Indeed, Mian et al. (1979) listed twelve different types, depending on the time duration and, hence, the color of oxide film, of oxide layers on iron, and noted that the maximum thickness of the oxide layer ($Fe_2O_3 + Fe_3O_4$) was 0.118 μm. Hence, it is unlikely that the oxide films would have any effect on the TCC of practical surfaces which are non-flat and wavy.

The oxide films, however, might significantly affect the TCC of joints formed by *flat* surfaces. The experimental investigation of Mian et al. for oxide covered mild steel surfaces yielded the correlation:

$$R = 66\,P^{-0.945}\sigma^{-0.128}\chi^{0.0346} \tag{7.23}$$

in which

R = thermal contact resistance, m^2 K/W
P = contact pressure, Pa

σ = rms roughness, m
x = film thickness on each of the two contacting surfaces, m
X = total film thickness = $x_1 + x_2$.

Al-Astrabadi et al. (1980) developed a theory for oxide film covered flat surfaces based on several assumptions, including:

1. The surface heights are Gaussian and remain Gaussian when covered with the oxide layer.
2. Oxide film thickness is uniform.
3. Oxide films are thin and brittle so that metal-to-metal contact spots are formed at the mating asperities.
4. The microcontacts are of two types:
   a. metal-to-metal surrounded by annular area of oxide.
   b. oxide-to-oxide.

In calculating the resistance, R_1, of the metal-to-metal contact spots surrounded by oxide annuli, it was noted that the metal and oxide thermal circuits were in parallel and the effective conductivity was taken as the arithmetic mean. On the other hand, for calculating the oxide-to-oxide resistance, R_2, the metal and oxide were in series and the effective conductivity was taken as the harmonic mean. The total resistance was then

$$R_{tot}^{-1} = R_1^{-1} + R_2^{-1}.$$

It may be noted that this theory assumes that there is always either a metal-to-metal or an oxide-to-oxide contact; no gaps are postulated.

References

Bolted or Riveted Joints

Aron, W., and Colombo, G. (1963). Controlling Factors of Thermal Conductance Across Bolted Joints in a Vacuum Environment. ASME Paper 63-HT-196. American Society of Mechanical Engineers, New York.

Bradley, T.L., Lardner, T.J., and Mikic, B.B. (1971). Bolted Joint Interface Pressure for Thermal Contact Resistance. Trans ASME, J Appl Mech, 542–545.

Chandrashekhara, K., and Muthanna, S.K. (1977a). Stresses in a Thick Plate With a Circular Hole Under Axisymmetric Conditions. Int J Eng Sci, 15:135–146.

Chandrashekhara, K., and Muthanna, S.K. (1977b). Axisymmetric Stress Distribution in a Transversely Isotropic Thick Plate With a Circular Hole. ACTA Mechanica, 28:65–76.

Chandrashekhara, K., and Muthanna, S.K. (1978). Pressure Distribution in Bolted Connections. In: Advances in Reliability and Stress Analysis, ASME, Winter Meeting. American Society of Mechanical Engineers, New York.

Chandrashekhara, K., and Muthanna, S.K. (1979). Analysis of a Thick Plate With a Circular Hole Resting on a Smooth Rigid Bed and Subjected to Axisymmetric Normal Load. ACTA Mechanica, 33:33–44.

Curti, G., Raffa, F., and Strona, P. (1985). Analysis of Contact Area and Pressure Distribution in Bolted Plates by Boundary Element Method. Wire, 35:14–18.

Elliott, D.H. (1965). Thermal Conduction Across Aluminum Bolted Joints. ASME Paper 65-HT-53. American Society of Mechanical Engineers, New York.

Fletcher, L.S., Peterson, G.P., Madhusudana, C.V., and Groll, E. (1990). Constriction Resistance Through Bolted and Riveted Joints. Trans ASME, J Heat Trans, 112:857–863.

Fernlund, I. (1961). A Method to Calculate Pressure Between Bolted or Riveted Plates. Chalmers University of Technology, Gothenburg, Sweden, pp. 13–51.

Gould, H.H., and Mikic, B.B. (1972). Areas of Contact and Pressure Distribution in Bolted Joints. Trans ASME, J Eng Ind, 94:864–870.

Greenwood, J.A. (1964). The Elastic Stresses Produced in the Mid-Plane of a Slab by Pressure Applied Symmetrically at its Surface. Proc Cambridge Phil Soc, 60:159–169.

Ito, Y., Toyoda, J., and Negata, S. (1979). Interface Pressure Distribution in a Bolt-Flange Assembly. Trans ASME, J Mech Des, 101:330–337.

Kumano, H., Sawa, T., and Hirose, T. (1994). Mechanical Behaviour of Bolted Joints Under Steady Heat Conduction. Trans ASME, J Press Vess Technol, 116:42–48.

Lardner, T.J. (1965). Stresses in a Thick Plate With Axially Symmetric Loading. Trans ASME, J Appl Mech, 87:458–459.

Lee, S., Song, S., Moran, K.P., and Yovanovich, M.M. (1993). Analytical Modelling of Thermal Resistance in Bolted Joints. ASME, HTD, Enhanced Cooling Techniques for Electronic Applications, 263:115–122.

Madhusudana, C.V. (1994). Conduction of Heat Through Bolted Joints. In: Thermal Conductivity 22, Technomic Publishing, Lancaster, PA, pp. 701–711.

Madhusudana, C.V., Peterson, G.P., and Fletcher, L.S. (1990). Effect of Non-Uniform Pressures on the Thermal Conductance in Bolted and Riveted Joints. Trans ASME, J Energy Res Technol, 112:174–182.

Minakuchi, Y. (1984). Contact Stresses Between Two Thick Plates With a Circular Hole and a Sandwiched Solid Metal Gasket. Bulletin JSME, 27:17–23.

Minakuchi, Y., Koizima, T., Shibuya, T., and Yoshemine, K. (1983). Contact Stresses in Two Elastic Bodies (Elastic Bodies are Finite Hollow Cylinders). Bulletin JSME, 26:716–723.

Mittlebach, M., Vogd, C., Fletcher, L.S., and Peterson, G.P. (1992). The Interfacial Pressure Distribution and Thermal Conductance of Bolted Joints. ASME, HTD, Heat Transfer in Hazardous Waste Processing, 212:9–17.

Motosh, N. (1976). Determination of Joint Stiffness in Bolted Connections. Trans ASME, J Eng Ind, 91:858–861.

Oehler, S.A., McMordie, R.K., and Allerton, A.B. (1979). Thermal Contact Conductance Across a Bolted Joint in a Vacuum. AIAA Paper 79-1068. American Institute of Aeronautics and Astronautics, New York.

Roca, R.T., and Mikic, B.B. (1972). Thermal Conductance in a Bolted Joint. Prog Astro Aero, 31:193–207.

Rötscher, F. (1927). Die Maschinenelemente. Verlag Julius Springer, Berlin, pp. 230–236.

Sneddon, I.N. (1946). The Elastic Stresses Produced in a Thick Plate by the Application of Pressure to Its Free Surfaces. Proc Cambridge Phil Soc, 42:260–271.

Veilleux, E., and Mark, M. (1969). Thermal Resistance of Bolted or Screwed Sheet Metal Joints in a Vacuum. J Spacecraft, 6(3):339–342.

Whitehurst, C.A., and Durbin, W.T. (1970). A Study of Thermal Conductance of Bolted Joints. Report No. NASA-CR-102639, Louisiana State University, Baton Rouge.

Yip, F.C. (1972). Theory of Thermal Contact Resistance in Vacuum With an Application to Bolted Joints. Prog Astro Aero, 31:177–192.

Cylindrical Joints

Dart, D.M. (1959). Effect of Fin Bond on Heat Transfer. ASHRAE J, 1:67–71.

Egorov, E.D., Nekrasov, M.I., Pikus, V.Yu., and Daschyan, A.A. (1989). Investigation of Contact Heat Transfer Resistance in Two-Layer Finned Tubes. Soviet Energy Technol, 6(6):33–37.

Gardner, K.A., and Carnavos, T.C. (1960). Thermal Contact Resistance in Finned Tubing. Trans ASME, J Heat Transfer, 82:279–293.

Hsu, T.R., and Tam, W.K. (1979). On Thermal Contact Resistance of Compound Cylinders. AIAA 14th Thermophysics Conf, Paper 79-1069. American Institute of Aeronautics and Astronautics, New York.

Kulkarni, M.V., and Young, E.H. (1966). Bimetallic Finned Tubes. Chem Eng Prog, 62(7):68–71.

Lemczyk, T.F. and Yovanovich, M.M. (1987). New Models and Methodology for Predicting Thermal Contact Resistance in Compound Cylinders and Finned Tubes. Heat Transfer Eng, 8(2):35–48.

Madhusudana, C.V. (1983). Contact Heat Transfer Between Coaxial Cylinders of Similar or Dissimilar Materials. ASME-JSME Thermal Eng Joint Conf, 3:317–322.

Madhusudana, C.V. (1986). On Heat Flow Across Cylindrical Joints. 8th Int Heat Transfer Conf, 2:651–657.

Madhusudana, C.V., Fletcher, L., and Peterson, G.P. (1990). Thermal Conductance of Cylindrical Joints—A Critical Review. J Thermophys Heat Transfer, 4:204–211.

Popov, V.M., and Krasnoborod'ko, A.I. (1975). Thermal Contact Resistance in a Gaseous Medium. Inzhenerno-Fizicheski Zhurnal, 28(5):875–883.

Sheffield, J.W., Stafford, B.D., and Sauer, Jr., H.J. (1984). Finned Tube Contact Conductance: Investigation of Contacting Surfaces. ASHRAE Trans, 90:442–452.

Sheffield, J.W., Abu-Ebid, M., and Sauer, Jr., H.J. (1985). Finned Tube Contact Conductance: Empirical Correlation of Thermal Conductance. ASHRAE Trans, 91(2a): 100–117.

Sheffield, J.W., Sauer, Jr., H.J., and Wood, R.A. (1987). An Experimental Method for Measuring the Thermal Contact Resistance of Plate Finnned Tube Heat Exchangers. ASHRAE Trans, 93(2):776–785.

Sheffield, J.W., Wood, R.A., and Sauer, Jr., H.J. (1989). Experimental Investigation of Thermal Conductance of Finned Tube Contacts. Exp Therm Fluid Sci, 2:107–121.

Taborek, J. (1987). Bond Resistance and Design Temperatures for High-Finned Tubes—A Reappraisal. Heat Trans Eng, 8(2):26–34.

Timoshenko, S.P., and Goodier, J.N. (1970). Theory of Elasticity, 3d ed. McGraw-Hill, New York, pp. 443–452.

Tsukizoe, T., and Hisakado, T. (1965). On the Mechanism of Contact Between Metal Surfaces—The Penetrating Depth and the Average Clearance. Trans ASME, J Basic Eng, 87:666–674.

Ugural, A.C., and Fenster, S.K. (1975). Advanced Strength and Applied Elasticity. American Elsevier, New York, pp. 255–256.

Williams, A., and Madhusudana, C.V. (1970). Heat Flow Across Cylindrical Metallic Joints. 4th Int Heat Transfer Conf, Paper Cu 3.6. Elsevier, Amsterdam, The Netherlands.

Rectification

Barber, J.R. (1968). Comments on "Heat Transfer at the Interface of Dissimilar Metals—The Influence of Thermal Strain" by Clausing. Int J Heat Mass Transfer, 11:617–618.

Barzelay, M.E., Tong, K.N., and Hollo, C. (1954). Thermal Conductance of Contacts in Aircraft Joints, US Nat Adv Comm for Aeronautics, TN 3167. National Advisory Committee for Aeronautics, Washington, DC.

Clausing, A.M. (1966). Heat Transfer at the Interface of Dissimilar Metals—The Influence of Thermal Strain, Int J Heat Mass Transfer, 9:1371–1383.

Dundurs, J., and Panek, C. (1976). Heat Conduction Between Bodies With Wavy Surfaces. Int J Heat Mass Transfer, 19:731–736.

Jeevanashankara, Madhusudana, C.V., and Kulkarni, M.B. (1990). Thermal Contact Conductance of Metallic Contacts at Low Loads. Appl Energy, 35:151–164.

Jones, A.M., O'Callaghan, P.W., and Probert, S.D. (1974). Effect of Interfacial Distortions on the Thermal Contact Resistance of Coaxial Cylinders. AIAA Paper 74-689, AIAA/ASME Thermophys Heat Transfer Conf, Boston. American Institute of Aeronautics and Astronautics, New York.

Jones, A.M., O'Callaghan, P.W., and Probert, S.D. (1975). Thermal Rectification Due to Distortion Induced by Heat Fluxes Across Contact Between Smooth Surfaces. J Mech Eng Sci, 17(5):252–261.

Lewis, D.V., and Perkins, H.C. (1968). Heat Transfer at the Interface of Stainless Steel and Aluminum—The Influence of Surface Conditions on the Directional Effect. Int J Heat Mass Transfer, 11:1371–1383.

Madhusudana, C.V. (1993). Thermal Contact Conductance and Rectification at Low Joint Pressures. Int Comm Heat Mass Transfer, 20:123–132.

Powell, R.W., Tye, R.P., and Jolliffe, B.W. (1962). Heat Transfer at the Interface of Dissimilar Materials: Evidence of Thermal Comparator Experiments. Int J Heat Mass Transfer, 5:897–902.

Rogers, G.F.C. (1961). Heat Transfer at the Interface of Dissimilar Metals. Int J Heat Mass Transfer, 2:150–154.

Somers, II.R.R., Fletcher, L.S., and Flack, R.D. (1987). Explanation of Thermal Rectification. AIAA J, 25(4):620–621.

Stevenson, P.F., Peterson, G.P., and Fletcher, L.S. (1989). Thermal Rectification in Similar and Dissimilar Metal Contacts. ASME, Collected Papers in Heat Transfer, Htd, 123:126–132.

Thomas, T.R., and Probert, S.D. (1970). Thermal Contact Resistance: The Directional Effect and Other Problems. Int J Heat Mass Transfer, 13:789–807.

Timoshenko, S.P., and Goodier, J.N. (1970). Theory of Elasticity, 3d ed., McGraw-Hill, New York, pp. 409–413.

Veziroglu, T.N., and Chandra, S. (1970). Directional Effect in Thermal Contact Resistance. Heat Transfer, 1970, Vol. 1, Paper Cu 3-5. Elsevier, Amsterdam, The Netherlands.

Williams, A. (1976). Directional Effects of Heat Flow Across Metallic Contacts. Inst

Eng (Australia), Mech Eng Trans, Institution of Engineers (Australia), Canberra, pp. 1–5.

Hysteresis

Borzdyka, A.M. (1965). Elevated Temperature Testing of Metals. Israel Program for Scientific Translations, Jerusalem.

Fenech, H., and Rohsenow, W.M. (1963). Prediction of Thermal Conductance of Metallic Surfaces in Contact. Trans ASME, J Heat Transfer, 85:15–24.

Howells, R.I.L., Probert, S.D., and Jenkins J.H. (1969). Deformations of Stacks of Thin Layers Under Normal Compressive Loads. J Strain Anal, 4(2):115–120.

Madhusudana, C.V., and Williams, A. (1973). Heat Flow Through Metallic Contacts—The Influence of Cycling the Contact Pressure. 1st Australian Conf on Heat Mass Transfer, Sec 4.1, Monash University, Melbourne, Australia, pp. 33–40.

McWaid, T., and Marschall, E. (1992). Thermal Contact Resistance Across Pressed Metal Contacts in a Vacuum Environment. Int J Heat Mass Transfer, 35(11):2911–2920.

Mikic, B. (1971). Analytical Studies of Contact of Nominally Flat Surfaces Effect of Previous Loading. Trans ASME, J Lub Technol, 20:451–456.

Williamson, M., and Majumdar, A. (1992). Effect of Surface Deformations on Contact Conductance. Trans ASME, J Heat Transfer, 114:802–810.

Effective Thermal Conductivity of Packed Beds

Chan, C.K., and Tien, C.L. (1973). Conductance of Packed Spheres in Vacuum. Trans ASME, J Heat Transfer, 95:302–308.

Chen, J.C., and Churchill, S.W. (1963). Radiant Heat Transfer in Packed Beds. Am Inst Chem Eng., 9(1):35–41.

Hadley, G.R. (1986). Thermal Conductivity of Packed Metal Powders. Int J Heat Mass Transfer, 29:909–920.

Hsu, C.T., Cheng, P., and Wong, K.W. (1994). Modified Zehner-Schlunder Models for Stagnant Thermal Conductivity of Porous Media. Int J Heat Mass Transfer, 37:2751–2759.

Kamiuto, K., Nagumo, Y., and Iwamoto, M. (1989). Mean Effective Thermal Conductivity of Packed-Sphere Systems. Appl Energy, 34:213–221.

Nasr, K., Viskanta, R., and Ramadhyani, S. (1994). An Experimental Evaluation of the Effective Thermal Conductivity of Packed Beds at High Temperatures. Trans ASME, J Heat Transfer, 116:829–837.

Ogniewicz, Y., and Yovanovich, M.M. (1977). Effective Thermal Conductivity of Regularly Packed Spheres: Basic Cell Model With Constriction. AIAA Paper 77-188. American Institute of Aeronautics and Astonautics, New York.

Yovanovich, M.M. (1973). Apparent Conductivity of Glass Microspheres from Atmospheric Pressure to Vacuum. ASME Paper 73-HT-43. American Society of Mechanical Engineers, New York.

Zehner, P., and Schlunder, E.U. (1970). Thermal conductivity of Granular Materials at Moderate Temperatures (In German). Chemie Ingenieur Technik, 42:933–941.

Stacks of Laminations

Al-Astrabadi, F.R., O'Callaghan, P.W., Probert, S.D., and Jones, A.M. (1977). Thermal Contact Conductance Correlation for Stacks of Thin Layers in High Vacuum. Trans ASME, J Heat Transfer, 99:139–142.

Babbus'Haq, R.F., Gibson, C., O'Callaghan, P.W., and Probert, S.D. (1991). Multilayer Thermally Insulating Ceramic Contacts. J Thermophys Heat Transfer, 5(3): 429–434.

Fletcher, L.S., Blanchard, D.G., and Kinnear, K.P. (1993). Thermal Conductance of Multilayered Metallic Sheets. J Thermophys Heat Transfer, 7(1):120–126.

Mikesell, R.P., and Scott, R.B. (1956). Heat Conduction Through Insulating Supports in Very Low Temperature Equipment. J Res, US Natl Bureau of Standards, 57(6): 371–378.

Williams, A. (1971). Heat Flow Across Stacks of Steel Laminations. J Mech Eng Sci, 13(3):217–223.

Solid Spot Conductance of Specific Materials

Cross, R.W., and Fletcher, L.S. (1978). Thermal Contact Conductance of Uranium Dioxide-Zircaloy Interfaces. AIAA Paper 78-85. American Institute of Aeronautics and Astronautics, New York.

Dean, R.A. (1962). Thermal Contact Conductance Between UO_2 and Zircaloy-2. Westinghouse Electric Corporation, Report CVNA-127. Westinghouse, Pittsburgh, PA.

Garnier, J.E., and Begej, S. (1979). Ex-Reactor Determination of Thermal Gap Conductance Between Uranium Dioxide: Zircaloy-4 Interfaces. NUREG/CR-0330, PNL-2696, Battelle-Pacific Northwest Laboratories, 1979. US Nuclear Regulatory Commission, Washington, DC.

Jacobs, G., and Todreas, N. (1973). Thermal Contact Conductance in Reactor Fuel Elements. J Nucl Sci Eng, 50:283–306.

Madhusudana, C.V. (1980). Experiments on Heat Flow Through Zircaloy-2/Uranium Dioxide Surfaces in Contact. J Nuc Mater, 92:345–348.

Madhusudana, C.V., and Fletcher, L.S. (1983). Solid Spot Thermal Conductance of Zircaloy-2/Uranium Dioxide Interfaces. J Nucl Sci Eng, 83:327–332.

Miller, R.G., and Fletcher, L.S. (1973). Thermal Contact Conductance of Porous Materials in a Vacuum Environment. AIAA Paper 73-747. American Institute of Aeronautics and Astronautics, New York.

Miller, R.G., and Fletcher, L.S. (1975). Thermal Contact Conductance Correlation for Porous Metals. Prog Astro Aero, 39:81–92.

Ross, A.M., and Stoute, R.L. (1962). Heat Transfer Coefficient Between UO_2 and Zircaloy-2, Report CRFD-1075, Chalk River, Ontario, Canada.

Thomas, T.R., and Probert, S.D. (1972). Correlations for Thermal Contact Conductance in Vacuo. Trans ASME, J Heat Transfer, 94:276–281.

Thermal Contact Resistance in the Presence of Oxide Films

Al-Astrabadi, F.R., O'Callaghan, P.W., and Probert, S.D. (1980). Thermal Resistance of Contacts: Influence of Oxide Films. Prog Aero Astro, 78:266–284.

Kharitonov, V.V., Kokorev, L.S., and Tyurin, Yu.A. (1974). Effect of Thermal Conductivity of Surface Layer on Contact Thermal Resistance. Atomnaya Energiya, 36(4):308–310.

Mian, M.N., Al-Astrabadi, F.R., O'Callaghan, P.W., and Probert, S.D. (1979). Thermal Resistance of Pressed Contacts Between Steel Surfaces: Influence of Oxide Films. J Mech Eng Sci, 21:159–166.

8
Concluding Remarks

Having discussed the influence of various parameters, surface configurations and types of thermal and mechanical loading, it is now possible to review the means by which the TCC (or TCR) can be controlled to suit a given practical application. The first section of the present chapter summarizes the possible methods of control; for more specific details, reference may be made to the relevant sections in the earlier chapters.

A review of the preceding chapters indicates that, over the past fifty years, a great deal of research has been carried out into the general, *fundamental* aspects of contact heat transfer. Such research includes both theoretical and experimental work. On the more *applied* aspects, however, the review shows that there is still scope for further research. Hence the second section of this chapter lists recommendations for possible future research. This list, of course, can never be complete. As new materials and processes are developed and used in equipment which need to dissipate heat, new problems are likely to arise requiring further study.

8.1 Control of Thermal Contact Conductance

8.1.1 Bare Metallic Junctions

Equation (3.33), which governs the contact conductance of flat, rough surfaces may be rewritten as:

$$h\sigma/k = 1.13 \tan\theta \,(P/H)^{0.94} \tag{8.1}$$

Hence, it is immediately apparent that TCC may be enhanced by:

1. Using a material combination for which the ratio, k/H, of the harmonic mean conductivity to microhardness is high.

2. Use of high contact pressures, P,
3. Use of smoother surfaces (low value of σ).

Conversely, high values of TCR may be obtained by using material combinations for which k/H is low or using relatively small contact pressures or rough surfaces.

In many applications, however, the choice of materials and the surface finish are dictated by other considerations such as strength, durability, corrosion resistance, and economy. Likewise, the level of contact pressure may also be specified by design considerations other than heat transfer. In such instances, we need to consider other means of control than changing the characteristics of the bare junction.

Similarly, although theoretically it is possible to control the TCC by the use of a suitable interstitial gas, in practice, one has very little control over the environment in which the heat transfer takes place. For example, in nuclear reactors the gap between the fuel and the sheath may be occupied by fission gases. For spacecraft applications, the gas gap conductance is negligible.

In dealing with bare junctions, it is also necessary to note the effect of flatness deviation. Application of Hertzian elastic contact equations to the "spherical cap" model, it can be shown that, even minor degrees of flatness deviation can result in large values of the macroscopic constriction resistance. Therefore, if thermal enhancement is the criterion, attention must be focused on getting the surfaces flat to the same degree as the roughness; it is not sufficient to simply polish the surfaces without making sure that the surfaces are also flat.

8.1.2 Use of Interstitial Materials

The effect of interstitial materials is to fill the voids in the interface and thus provide a more continuous heat transfer path compared to that obtained in a bare junction. A joint, properly filled, is less sensitive to surface irregularities and to contact pressure variation. This means that the contact conductance is more predictable, thus contributing to reliability in thermal design. These factors make interstitial materials an attractive choice for thermal control.

Foils

Soft metallic foils of high thermal conductivity, for example, indium, are often used for TCC enhancement. Increases of an order of magnitude in conductance may be obtained compared to the bare junction conductance in vacuum; increases when compared to conductance in air will be somewhat less but it is possible, even in this case, to achieve significant enhancements (2 to 3 fold) by a suitable choice of the foil as indicated in Table 6.2 of Chapter 6. A very thin foil may not fill the voids completely. On the other hand, a very thick foil will result in an additional resistance in series. Thus there is usually an optimum thickness for a given surface finish beyond which the effectiveness of the foil as a conductance enhancer decreases. This optimum thickness is of the same order of magnitude as the rms surface roughness, that is, 0.48σ to 2σ, where the lower values apply for relatively harder foil materials.

In the use of foils, care should be taken to see that the foils are properly applied and remain so during operation. A wrinkled, folded, or torn foil obviously will not be as effective as one that uniformly covers the contact surface.

Metallic Coatings

Surfaces may be coated by vapor deposition, anodization, or other means. Compared to foils, coatings are more robust, uniform, and permanent. They are also likely to be more expensive. As with foils, soft metallic coatings, such as indium or tin, show maximum conductance enhancement. The enhancement also depends on the method of deposition. For example, on aluminum alloy surfaces ($\sigma = 1$ to $2\,\mu$m), electroplated silver coating of $12.7\,\mu$m thick, yielded a thermal enhancement of about 2.5 while a flame-sprayed silver coating of the same thickness on similar surfaces yielded an enhancement of only about 0.6 to 0.7 (Marotta et al., 1994). In general, anodized aluminum coatings as well as coatings of ceramics such as silicon nitride, boron nitride, and beryllium oxide tend to decrease the TCC and hence are useful for thermal isolation. Whether it is for the purpose of conductance enhancement or isolation, both surfaces need to be coated for best results.

Greases

Thermal conductance can be enhanced by the use of various greases and lubricants. Enhancement factors of around 10 can be obtained when the bare junction is in vacuum but the figure drops to between 1 and 2 for junctions in air (Sauer, 1992). Problems with greases include their tendency to run at elevated temperatures and their instability due to the loss of volatile fractions. Both of these factors tend to reduce their effectiveness as heat transfer enhancers.

Screens

Unless the screen material is very soft and conducting compared to the bare junction materials, wire screens are mainly used for increasing the TCR, that is, for thermal isolation. Thus, stainless steel wire screens have been found to be very effective for isolation; an order of magnitude reduction in TCC is obtainable with this type of screen. A relatively coarse mesh (small mesh number) should be used for maximum thermal isolation.

8.1.3 Load Cycling

The conductance values upon unloading and subsequent reloadings are found to be higher than at first loading (hysteresis). Hence if a joint is preloaded to a level higher than that expected in application and the load cycled two or three times, conductance values can be expected to be higher than would otherwise be obtained. Such a load cycling may also scour the contaminant films and establish more metal-to-metal contact points.

8.1.4 Heat Flow Direction

In many situations, the heat flow direction significantly controls the contact conductance. If a choice is possible, then for radially outward flow in cylindrical joints, heat flow should be in the direction from a material of higher α to one of lower α for thermal enhancement, and in the opposite direction for thermal isolation. Similarly for axial heat flow in surfaces with flatness deviation (convex surfaces) in contact, higher conductance values may be obtained by choosing the heat flow direction from the material of higher distortivity $\alpha(1 + \nu)/k$ to one of lower distortivity. On the other hand, for joints at low contact pressures in a conducting medium, heat flow from the material of higher thermal conductivity to one of lower thermal conductivity will result in higher values of conductance than for the opposite direction.

8.1.5 Stacks of Laminations

When a high degree of thermal isolation as well as mechanical strength is required, stacks of thin metal laminations provide one of the best answers. Thin stainless steel laminations, several hundred in number, may have an effective conductivity which is only 2% of that of a solid block of similar dimensions (Mikesell and Scott, 1956). The resistance may be further enhanced by lightly dusting the surfaces with an insulating powder, such as manganese dioxide.

8.2 Recommendations for Further Research

1. *Interstitial Materials.* There is a wealth of experimental data available on the effect of interstitial materials on TCC. Theoretical work needs to be done in order to be able to predict the behavior of filled or partially filled contacts. Further, more comprehensive correlations, taking into account all variables of significance, need to be derived.
2. *Bolted Joints.* Theoretical results are available for both the stress distribution at the interface and the heat transfer through a bolted joint. The effect of roughness and waviness on the stress distribution needs to be further explored. Very little experimental data on heat transfer through a bolted joint appears to exist in open literature. This situation needs to be remedied.
3. *Cylindrical Joints.* The situation here is similar to that for the bolted joint. There exists some theoretical work for cylindrical surfaces without macroscopic errors of form. Future theoretical work should, therefore, include effects of waviness, out-of-roundness, and so on. Further experimental work is also needed to substantiate existing theories.
4. *Rectification.* Currently, there appears to be no satisfactory theory that could explain the rectification behavior observed by early investigators, namely, that the measured conductance values, in vacuum, were higher when heat flowed from a material of higher conductivity to one of lower conductivity. Also, there is no satisfactory theory explaining the rectification observed for similar materials. Research in this area should also include the effect of microscopic irregularities.
5. *Packed Beds.* The theoretical results for contact and gap conductance, obtained by assuming suitable packing patterns, need to be verified by experimental results. Correlations, similar to those existing for metallic powders, need to be derived for insulating materials also.
6. *Microelectronics.* In view of the current trend toward microminiaturization of electronic circuits and consequent increased power densities, attention must be given to internal resistances in electronic packaging. This would include experimental determina-

tion of the thermal contact resistance of new mold compounds and epoxies.

7. *Manufacturing Processes.* Very little experimental or theoretical data exist for a variety of manufacturing processes including: metal casting, injection molding, metal forming, and chip removal.

References

Marotta, E.E., Lambert, M.A., and Fletcher, L.S. (1994). Thermal Enhancement Coatings and Films for Microelectronic Systems. Proc 10th Int Heat Transfer Conf, Paper 15-CI-15. Institution of Chemical Engineers, Rugby, UK.

Mikesell, R.P., and Scott, R.B. (1956). Heat Conduction Through Insulating Supports in Very Low Temperature Equipment. J Res, US Natl Bureau of Standards, 57(6): 371–378.

Sauer, H.J., Jr. (1992). Comparative Enhancement of Thermal Contact Conductance of Various Classes of Interstitial Materials. NSF/DITAC Workshop on Thermal Conductance Enhancement in Microelectronics, Melbourne, pp. 103–115.

Author Index

Subject Index

Laminar Viscous Flow
V.N. Constantinescu

Thermal Contact Conductance
C.V. Madhusudana